Design and synthesis of a photoaffinity labelling analogue of ivacaftor to probe its putative binding site on mutant CFTR

by

Christopher Michael Hamilton

B.Sc., University of Victoria, 2012

Thesis Submitted in Partial Fulfillment of the
Requirements for the Degree of
Master of Science

in the
Department of Chemistry
Faculty of Science

SIMON FRASER UNIVERSITY

Spring 2017

Approval

Name: **Christopher Michael Hamilton**

Degree: **Master of Science**

Title: ***Design and synthesis of a photoaffinity labelling analogue of ivacaftor to probe its putative binding site on mutant CFTR***

Examining Committee: **Chair:** Bingyun Sun
Assistant Professor

Robert Young
Senior Supervisor
Professor

Robert Britton
Supervisor
Professor

David Vocadlo
Supervisor
Professor

Peter Wilson
Internal Examiner
Associate Professor

Date Defended/Approved: March 6, 2017

Abstract

The cystic fibrosis (CF) therapeutic, ivacaftor, restores activity to certain cystic fibrosis transmembrane regulating protein (CFTR) mutations; however, the nature of ivacaftor's interaction with mutant CFTR is still under investigation. This study aimed to generate photoaffinity labelling (PAL) probes that will be used to elucidate putative ivacaftor binding sites on mutant CFTR.

Structure activity relationship studies indicated retention of ivacaftor's potentiating activity despite deletion of either of the *t*-butyl groups from the ivacaftor structure. These results initiated a synthesis program to prepare PAL probes incorporating a carbene-generating diazirine moiety in place of a *t*-butyl group on the ivacaftor scaffold.

Initial synthetic approaches towards creating the diazirine PAL probe were devised with the ability to afford diversification at a late stage in the synthesis to allow incorporation of reporter tags into the PAL probe. While these approaches were unsuccessful, ultimately a linear synthetic approach successfully afforded the target diazirine PAL probe.

Keywords: CFTR; Ivacaftor; mechanism of action; diazirine; photoaffinity labelling; synthesis

Dedication

For Rachel Fortier, Julie Bowers, Raymond Edwards, Eva Markvoort, and Joanie Brennan who are no longer with us.

Acknowledgements

There are many people to thank, firstly, Tracy Lee who was a constant source of encouragement and love.

To my immediate family who has always been there for me, and my extended family who have always been supportive.

To my many friends who continually inspire me, and who have kept me honest.

To all my coworkers who have helped me greatly throughout this process including Dr. Robert Young, Dr. Christine Bear, Dr. Russell Viirre, Dr. Zafar Qureshi, Maurita Hung, Dr. Krimo Toutah, Dr. Gang Chen, Dr. Manuel Lasalle, Dr. Sankar Mohan, Dr Marion Thévenin, Dr. Damien Bosc, Dr. Than Nguyen, Dr. Christophe Andre, Dr. Haibo Xie, Dr. Peter Clark, Dr Siva Krishnamoorthy, Dr. Suzana Kovacic, and John Thompson, Ph.D.

I want to acknowledge Cystic Fibrosis Canada, NSERC, and Simon Fraser University for funding and support.

Table of Contents

List of Tables

List of Figures

List of Acronyms

[o]	Oxidation
ABC	ATP-binding cassette protein
AcOH	Acetic acid
AGP	α_1-acid glycoprotein
ASL	Airway surface layer
ATP	Adenosine triphosphate
ATR	Attenuated total reflection spectroscopy
BnBr	Benzyl bromide
Boc	*tert*-Butyl carbonate
cAMP	cyclic adenosine monophosphate
$CDCl_3$	Chloroform-d
CF	Cystic Fibrosis
CFRD	CF related diabetes
CFTR	Cystic Fibrosis Transmembrane Conductance Regulator protein
cLogP	Partition coefficient between *n*-octanol and water
COPD	Chronic obstructive pulmonary disease
CRISPR	Clustered regularly interspaced palindromic repeats
CYP3A	Cytochrome P450 3A
DCM	Dichloromethane
DIPEA	*N,N*-diisopropylethylamine
DMAP	*N,N*-Dimethyl-4-aminopyridine
DMF	Dimethyformamide
DMP	Dess–Martin periodinane
DMSO	Dimethylsulfoxide
DMSO-d_6	Dimethyl sulfoxide-d_6 / deuterated DMSO
EC_{50}	concentration of a drug that gives half-maximal response
ECL	extracellular loops
ENaCs	Epithelial sodium channels
EOM	Ethoxymethyl ether
Equiv.	Equivalent
ER	endoplasmic reticulum

ERAD	ER-associated degradation process
Et_2O	Diethyl ether
EtOAc	Ethyl acetate
EtOH	Ethanol
FDA	Food and Drug Administration of the United States
FEV_1%	Percent predicted forced expiratory volume in 1 second
FRET	Fluorescence resonance energy transfer
FTIR	Fourier transform infrared spectroscopy
FVC	Forced vital capacity
G551D	Glycine residue 551 to aspartic acid mutation
$GABA_A$	γ-aminobutyric acid ligand-gated ion channel receptor
HATU	1-[*Bis*(dimethylamino)methylene]-1*H*-1,2,3-triazolo[4,5-*b*]pyridinium 3-oxid hexafluorophosphate
HBE	Human bronchial epithelial cells
HBTU	*N,N,N′,N′*-Tetramethyl-*O*-(1*H*-benzotriazol-1-yl)uronium hexafluorophosphate
hERG	Human ether-a-go-go cardiac potassium channel
Hex	Hexanes
HOBt	Hydroxybenzotriazole
HPLC	High-pressure liquid chromatography
HRMS	High-resolution mass spectrometry
HSA	Human serum albumin
HTS	High-throughput screening
HX	Hydrogen/deuterium exchange
ICL	intracellular loops
IV	Intravenous
kDa	kilo Daltons
K_i	Inhibition constant
LC-MS	Liquid chromatography-mass spectrometry
LHS	“left-hand side” of the ivacaftor scaffold
m.p.	Melting point
MeLi	Methyl lithium
MeOD	Methanol-d_4
MeOH	Methanol

MOM	Methoxymethyl ether
mRNA	messenger ribonucleic acid
MS	Mass spectrometry
MsCl	Mesyl chloride
MSD	Membrane spanning domains
MTBE	Methyl-*tert*-butyl ether
NBD	Nucleotide binding domains
n-BuLi	Butyl lithium
NMR	Nuclear magnetic resonance
PAL	photo-affinity labelling
Pd/C	10% palladium on carbon
PFT	Pulmonary function test
Pi	Inorganic phosphate
Piv	Pivaloyl
PKA	Protein kinase A
P_o	Open channel state probability
PTC	pre-mature termination codons
Pyr	Pyridine
Quant.	Quantitative
R	Regulatory domain
rf.	Retardation factor
RHS	“right-hand side” of the ivacaftor scaffold
rRNA	Ribosomal ribonucleic acid
SAR	Structure activity relationship
T3P	Propylphosphonic anhydride
TBAF	*tetra*-butyl ammonium fluoride
t-butyl	Tertiary butyl group
TFA	Trifluoroacetic acid
TFAA	Trifluoroacetic anhydride
THF	Tetrahydrofuran
TLC	Thin layer chromatography
TsCl	*p*-tosyl chloride
UPS	ubiquitin proteasome system

UV	Ultra violet
UV-Vis-NIR	UV-Vis near infrared spectroscopy
wt-CFTR	Wild-type CFTR
ΔF508-CFTR	Deletion of the 508 amino acid phenylalanine from CFTR

Chapter 1.

Introduction

1.1. Cystic fibrosis

Cystic fibrosis (CF) is the most common fatal genetic disease among Canadians affecting approximately 4100 people throughout Canada.[1,2] CF was first described in the medical literature in 1938,[3] and in 1989 the underlying cause of CF was found to result from mutations in the gene encoding the cystic fibrosis transmembrane regulator protein (CFTR).[4–6] As an autosomal monogenic recessive disorder, two non-functioning copies of the CFTR gene are required to develop CF.[2] Although more commonly described in peoples of European descent, cases have been described in populations worldwide.[7,8]

CF is a multi-organ disease affecting the hollow organs of the body, including the respiratory tract, pancreas, skin, stomach, liver, and testes.[9] The CFTR protein is a phosphorylation dependent channel primarily responsible for the efflux of chloride and bicarbonate across the apical membranes of epithelial tissues.[10] The chloride efflux activity of CFTR plays an important role in regulating the quantity and composition of epithelial fluids required for the normal function of many organs. Mutations causing loss of CFTR function lead to the development of Cystic Fibrosis. In the respiratory tract, CFTR activity maintains the airway surface layer (ASL) critical for proper lung function; loss of CFTR activity leads to depletion of the ASL causing persistent cycles of pulmonary obstruction, inflammation, infection, and scarring.[11,12] In the pancreas loss of CFTR activity leads to impaired transport of digestive enzymes leading to malnourishment. Although CF patients experience a myriad of symptoms and complications, the two primary endpoints for the disease are double-lung transplant or respiratory failure. Reduced CFTR activity has also been implicated in other respiratory disorders such as bronchitis and COPD, although the link to these diseases is still under investigation.[13,14]

To date, over 2000 CFTR mutations have been identified that are associated with loss of protein expression or loss of function. The clinical phenotypic presentation of CF is highly variable between patients, not only between patients with different mutations, but also between patients of the same genotype.[15,16] Despite a correlation between certain mutations and pancreatic symptom severity, as well as certain classes of CFTR mutations generally leading to a more severe disease state,[17] there are no clear correlations between specific mutations and clinical outcomes. Additionally, modifier loci have also been identified which correlate with a more severe CF disease state.[15] While the majority of CF patients present with multi-organ complications, approximately 10% of patients can present with very mild symptoms sometimes affecting a single organ, such as presenting with bilateral absence of the vas deferens.[18] While people who carry only one copy of a mutant CFTR allele (carriers) do not develop CF, there is evidence that carriers are less prone to secretory diarrhea caused by *Vibrio cholera.*[19]

Although historically thought of as a children's disease, improvements in disease management and diagnosis (including a newborn screening program in all Canadian provinces and territories, excluding Quebec)[20] have increased the median age of survival to over 50 years of age in Canada.[1,12,18,21] As of 2008 there are more adults than children affected by the disease in Canada.[2]

Until recently therapeutic options for CF were limited to those which managed the resulting symptoms; however, in 2012 the first small-molecule CF therapeutic, ivacaftor (**1**, Figure 1), was approved by the FDA which rescues the activity for certain classes of CFTR mutations.[22] Therapeutics that rescue CFTR activity are broadly termed as CFTR modulators and specifically, ivacaftor is termed a CFTR potentiator as it restores gating activity to mutant CFTR located at the apical membrane. Following the successful development of ivacaftor, other classes of CFTR modulators have been developed and evaluated in clinical trials. Although the current pipeline of potential therapeutics holds great promise in the long term management of CF, the mechanisms of these new CFTR modulators are not fully understood. In order to improve the understanding of the new CFTR modulators, particularly ivacaftor, there is a need to determine their binding sites on mutant CFTR as this information can be utilized to further optimize second generation therapeutics and possibly enable the discovery of novel classes of structures which modulate mutant CFTR.[23] Our goal is to utilize photo-affinity labelling (PAL)

techniques, including the installation of a photo-sensitive diazirine motif onto the ivacaftor scaffold (**2**), in order to elucidate the binding site on mutant CFTR.

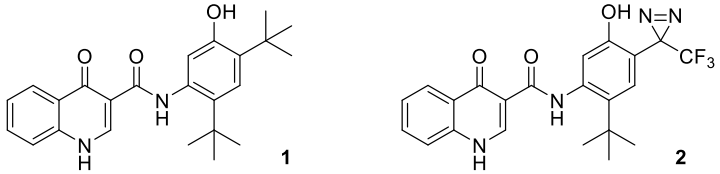

Figure 1 **Chemical structure of the CFTR potentiator ivacaftor (1), and target PAL probe (2).**

1.2. Cystic fibrosis transmembrane regulator protein (CFTR)

1.2.1. Pathophysiology

The activity of CFTR has been shown to play a crucial role in a variety of systems in the human body, with loss of CFTR activity leading to the development of CF.[12] The most widely accepted hypothesis on the implication of diminished CFTR activity in the lungs is termed the "low-volume" hypothesis.[5,24] This hypothesis states that decreased CFTR chloride efflux causes increased sodium adsorption by reducing CFTR-dependent inhibition of epithelial sodium channels (ENaCs). This unbalanced sodium adsorption/chloride efflux increases fluid transport into the epithelial tissue, depleting the airway surface layer (ASL). However, results from porcine CF models have shown that decreased bicarbonate secretion might also play a role in the pathophysiology of the disease by reducing airway surface pH, impairing bacterial defence mechanisms, as well as impacting mucous unfolding and rheology.[25]

Disruption to the ASL leads to decreased mucocilliary clearance of pathogens coupled with an exaggerated, neutrophil-driven inflammatory response that leads to scarring of the lung tissue.[12,24] Overall, decreased CFTR activity leads to chronic cycles of infection, inflammation, scarring, and bronchiectasis which eventually results in respiratory failure as the main outcome for the majority of patients.[12] The most common means of measuring a patient's respiratory health is by performing a pulmonary function test (PFT), which gives the measure of both the percent predicted forced expiratory volume in 1 second (FEV_1%) and the forced vital capacity (FVC). CF patients exhibit a slow decline in FEV_1% coupled with the progression of bronchiectasis and lung scarring.

Treatments for pulmonary symptoms have progressively evolved to include the use of steroids to reduce inflammation, mucolytics and hypertonic saline to aid in airway clearance, and the use of antibiotics to treat bacterial exacerbations. Although significant improvements in disease management have been made with these regimes, they do not correct the underlying defect and at best delay the progression of the disease.[11]

Exocrine pancreatic insufficiency is a major complication arising from CF.[9] In the pancreas, as a result of loss of CFTR activity, reduced bicarbonate and fluid secretion leads to retention of digestive proenzymes which are prematurely activated in the pancreatic ducts causing tissue and islet cell destruction, fibrosis, and reduced β-cell mass. Although approximately 10% of CF patients are pancreatic sufficient until adulthood, many of these patients become pancreatic insufficient later in life. Patients with pancreatic insufficiency are routinely prescribed oral pancreatic enzyme supplements, particularly lipases, amylases, and proteases. As CF patients experience difficulty absorbing nutrients, they are commonly prescribed a high salt and high fat/calorie diet.

As well, CF related diabetes (CFRD) has become the most common comorbidity in CF.[26] CFRD describes a spectrum of glucose tolerance abnormalities, ranging from an impaired glucose tolerance to CFRD with or without a fasting hyperglycemia. With features of both type 1 and 2 diabetes, CFRD is associated with both reduced insulin secretion and insulin resistance.[27] While CFRD is not commonly described in children with CF, 20% of adolescents and 40-50% of adults develop the disorder. In addition to complicating dietary management for CF patients, CFRD has also been associated with a reduced pulmonary function.[28]

In the sweat gland, malfunctioning CFTR prevents the reabsorption of chloride ions which subsequently leads to production of hypertonic sweat.[29] In fact, the main clinical diagnostic for CF is an elevated sweat chloride measurement (>60 mM), with more severe CFTR mutations being associated with a higher sweat chloride level.[18] Carriers of CFTR also have a slightly elevated sweat chloride compared to normal. One of the primary measures in clinical trials for evaluating efficacy of CFTR modulators is a reduction in sweat chloride.

Biliary tract disorders are found in a third of CF patients.[9] In these patients the bile-duct epithelium becomes hyperplastic with periductal inflammation and fibrosis; as well, in some patients, fatty infiltration can lead to cirrhosis. Up to 30% of CF patients also present with a

poorly functioning gallbladder and 10% present with gallstones. Although uncommon, liver transplants are required in some CF patients.

Up to 98% of CF males are infertile, presenting with aspermia resulting from either blocked or bilateral absence of the vas deferens. However, spermatogenesis is typically normal, allowing males to become fathers through techniques such as microscopic epididymal sperm aspiration and intracytoplasmatic sperm injection.[30] Although the reproductive systems of female CF patients are anatomically normal, many female patients experience difficulties conceiving due to what is presumed to be dehydrated cervical mucus.[31] Interestingly, there are anecdotal accounts of female CF patients previously diagnosed with fertility issues successfully conceiving after beginning treatments with the CFTR modulator ivacaftor.[32]

1.2.2. ABC proteins

CFTR is a member of the ATP-binding cassette (ABC) protein family of transporters.[6,33] ABC proteins are a ubiquitous class of active transporters which utilize the energy derived from ATP binding/hydrolysis to transport substrates across membranes.[34] ABC proteins more commonly function as exporters; however, ABC protein importers have been described in prokaryotes.[35] Members of the ABC family are responsible for the transport of a variety of substrates, including amino acids, sugars, ions, proteins, and small molecules. Human ABC proteins are classified into subfamilies ABC-A through ABC-G, with CFTR being a part of the ABC-C subfamily (ABC-C7). CFTR is unique in the ABC family as it is the only identified member that acts as an ion channel.[10,33]

1.2.3. CFTR/ABC protein domain organization, structure, and function

CFTR is multi-domain glyco-protein with 1480 amino acids and a molecular weight of ~170 kDa.[1,36,37] As with other ABC proteins, CFTR (Figure 2) is comprised of two membrane spanning domains (MSDs; each comprised of 6 transmembrane spanning helices) which form the channel core; as well as two intracellular nucleotide binding domains (NBDs) responsible for the binding and hydrolysis of ATP. CFTR is unique in the ABC family in that it also contains a regulatory domain (R), which requires multiple phosphorylation events by protein kinase A

(PKA) in order to activate the channel.[38,39] The domains of CFTR are arranged from the amino terminal to the carboxy-terminal in the following order: MSD1-NBD1-R-MSD2-NBD2.[40]

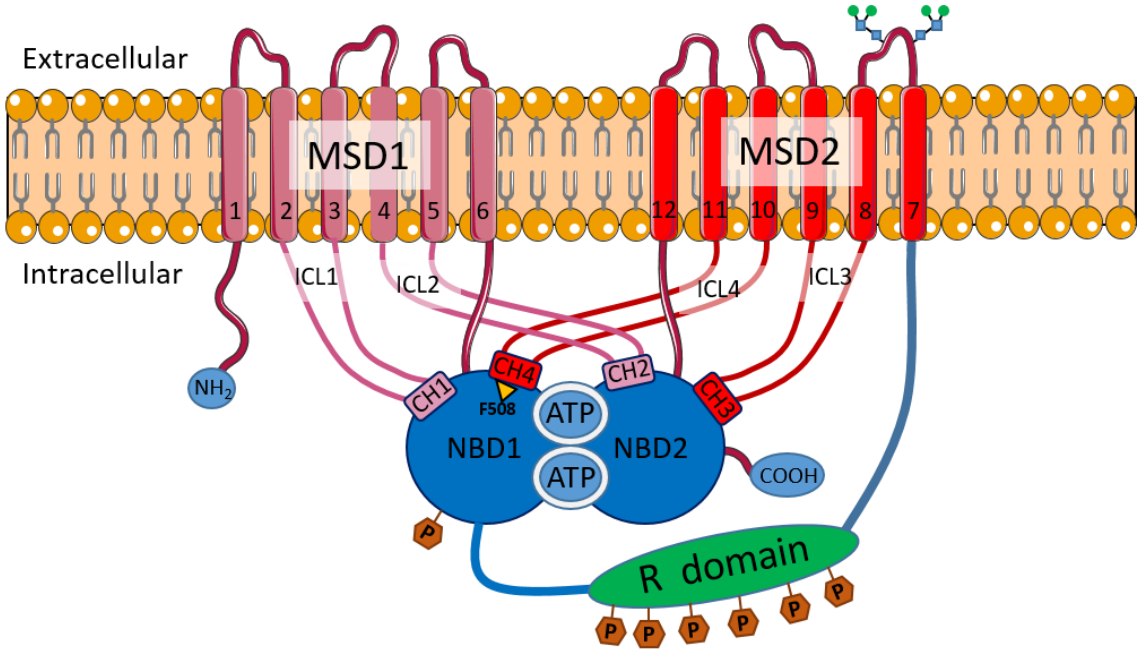

Figure 2 Schematic of the domain structure and organization of CFTR

Note: Representation of the CFTR domains and their organization at the cell membrane. MSD1 in pink, MSD2 in red, NBD1 and NBD2 in blue, R domain in green, phoshorylation events as orange hexagons, ATP a small blue ovals, the location of F508 as a yellow triangle, and glycosylation chains as small blue squares and small green circles.
Adapted from "Servier Medical Art" by Servier under CC BY 3.0 (https://creativecommons.org/licenses/by/3.0/).

To date, a high resolution x-ray crystal structure of whole CFTR protein has not been obtained; however, high-resolution crystal structures of isolated NBD1 domain constructs have been obtained enabling the generation of NBD dimer models (Figure 3).[41–43] Lower resolution structures such as NMR, and electron crystallography (9 Å resolution) structures of the complete CFTR protein have been obtained indicating that the channel adopts conformations akin to other ABC proteins.[44,45] In order to gain a better understanding of the CFTR gating cycle, homology models have been created for both open and closed states by combining the available CFTR structural data with that of other members of the ABC family (including full length ABC protein crystals structures).[23,35,45–52] While full protein high-resolution structures of a few members of the ABC family have been obtained; no single ABC protein has structural data

for each conformation in a complete gating cycle. The X-ray crystal structures of mouse P-glycoprotein (P-gp), and *Vibrio cholerae* MsbA, both ABC multi-drug exporters, are commonly used to generate homology models of the putative closed state of CFTR, as the NBDs for these structures are in an apo-state, with the MSDs having a large intracellular vestibule (inward facing).[53] While significant differences are expected as CFTR behaves as a channel rather than a transporter, these models seem to agree with the low-resolution X-ray data for CFTR. As well, the structural data from the *S. aureus* multi-drug exporter *Sav*1866 is similarly used as a template to generate models of the putative open-channel state, as the NBDs in this structure are in an ATP bound dimer-state with the MSDs in an outward facing conformation. While homology models of the intracellular components of CFTR, including ΔF508-CFTR-NBD1, have been successfully utilized in *in silico* screens to generate novel correctors,[54,55] the low sequence homology of the MSDs of CFTR to other members of the ABC family, as well as the unique presence of the R domain, diminish the accuracy of these models for *in silico* ligand-protein docking studies.[50,56,57] Despite this limitation, homology modelling has proven informative in describing the domain organization and gating cycle of CFTR.[40]

Similar to other eukaryotic ABC proteins, the NBDs of CFTR combine to form a “head-to-tail homo-dimer” upon binding two ATP molecules in binding sites located at the dimer interface (Figure 3). A canonical ATP binding site is comprised of a conserved motif associated with phosphate binding (Walker A sequence) from one NBD with a matching signature sequence important for ABC gating (LSGGQ) from the second NBD.[58] For ABC transporters typically both ATP binding sites exhibit ATPase activity and upon hydrolysis of both ATP molecules, the NBD dimer dissociates to release ADP and Pi.

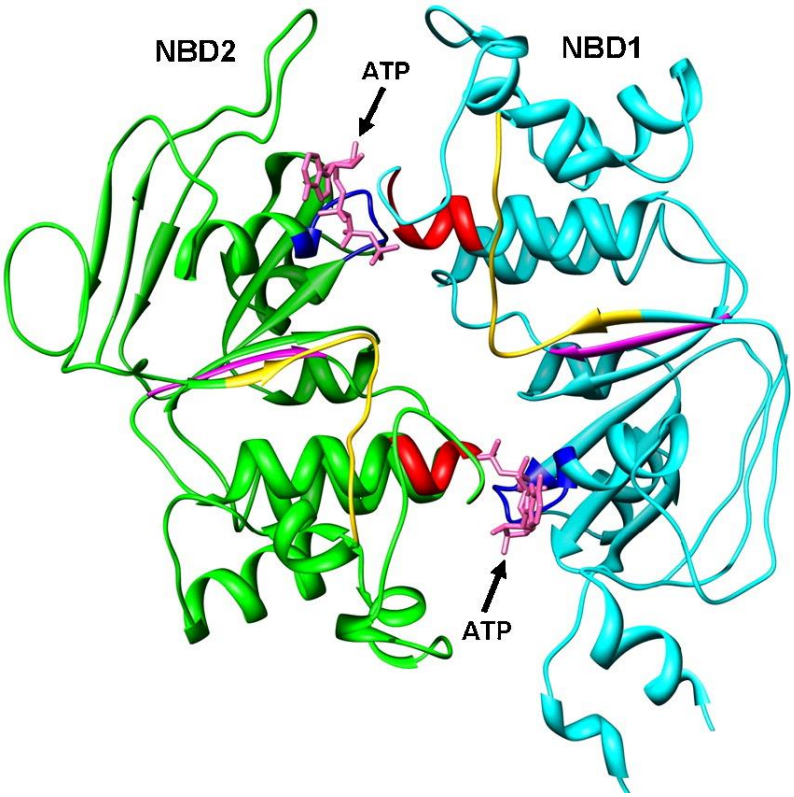

Figure 3 Molecular model of the human CFTR NBD1-NBD2 heterodimer (top view).

Note: NBD1 and NBD2 are represented by ribbons and colored cyan (NBD1) and green (NBD2). Also noted are the Walker A motif (blue), Walker B motif (magenta), signature sequence (red), Q-loop (important for ATP binding, yellow), and ATP molecules indicated in pink. In the figure the lower portion/binding site is the degenerate site exhibiting reduced ATPase activity (site 1), and the upper portion /binding site is the consensus binding site (site 2) exhibiting normal ATPase activity.
Reprinted from Journal of Molecular Graphics and Modelling, (27), Huang, S.; Bolser, D.; Liu, H.; Hwang, T.; Zou, X.; Molecular modeling of the heterodimer of human CFTR's nucleotide-binding domains using a protein–protein docking approach, p. 7, Copyright 2009, with permission from Elsevier.[43]

In CFTR and other members of the ABC-C subfamily, the ATP binding sites are asymmetric with only one site exhibiting normal ATPase activity (consensus site, site 2, lower). The other binding site (site 1, degenerate site) contains non-consensus sequences in the Walker A and B motif on NBD1, and in the corresponding signature sequence (LSHGH) on NBD2. The resulting binding site strongly binds ATP but exhibits limited ATPase activity. As a result of the limited ATPase activity, evidence has indicated site 1 remains occupied by ATP during the gating cycle, implying NBD dimer does not fully dissociate to release the hydrolyzed products from site 2.[43]

As with other ABC proteins, the six transmembrane spanning helices of each MSD combine to form the channel core. From the electron crystallography structure, the CFTR channel core appears to adopt an “hour-glass like” shape with a large intracellular vestibule and a small extracellular vestibule separated by a constriction closer to the extracellular end of the channel.[47,58] Evidence has shown that the anion selectivity of CFTR may be determined by the size of the constriction in the pore of the channel.[59] The transmembrane spanning helices are linked together by both intracellular loops (ICLs) and extracellular loops (ECLs). The ICLs each contain long helical portions extending from the membrane joined by a small helical segment (coupling helices). The coupling helices make crucial contacts with grooves on the NBDs (figure 1), which during the gating cycle of CFTR (and other ABC proteins), couple the NBD dimerization to the changes in channel configuration.[60] Homology modelling and molecular dynamics simulations suggest that the coupling helices act as a pivot point allowing twisting of the helical extensions and the transmembrane spanning helices.[46,60] In particular, evidence has shown that residue phenylalanine 508 is part of a crucial interaction between ICL4 and NBD1 in this process.[1,23,34,36,45–47,58,60] In ABC transporters, upon NBD dimerization the MSDs change from an inward facing conformation with a high substrate affinity to an outward facing state with low substrate affinity. For CFTR, the channel changes from a closed state with high substrate affinity in the inner vestibule to an anion selective open channel conformation upon NBD dimerization.[34] Evidence indicates that channel opening undergoes an “iris-like” mechanism with twisting of the spanning helices. Recent experiments introducing mutations near the pore restriction in certain ABC transporters can cause formation of a channel-like state permeable to chloride ions.[61]

The R domain is unique to CFTR and joins NBD1 to MSD2. Experimental data has indicated that the R domain is phosphorylated on multiple serine residues by PKA with cyclic adenosine monophosphate (cAMP) which activates CFTR with increasing phosphorylation events increasing channel activity.[38] Evidence suggests that in the un-phosphorylated (apo) state, the R domain adopts a loosely packed conformation residing between the NBDs. Phosphorylation of the R domain causes it to compact and dissociate from the NBDs activating the channel.[1]

1.2.4. CFTR/ABC Protein Gating mechanism

The classic gating cycle of ABC transporters is proposed to undergo an ATP switch model[62] (Figure 4) in which changes to MSD configuration is coupled to ATP binding/hydrolysis events.

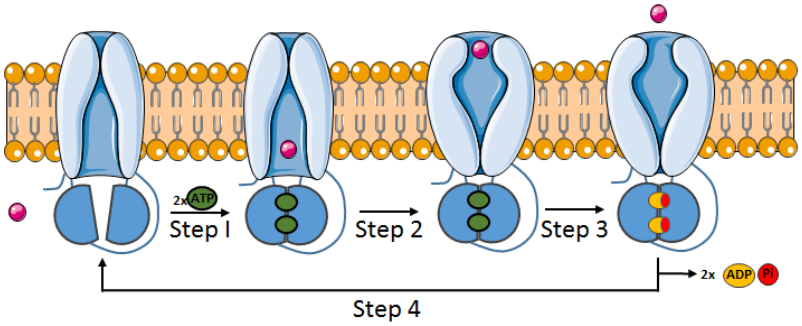

Figure 4 Gating cycle of ABC transporters.

Note: Representation of the different conformations of an ATP transporter during active transport at a cellular membrane. Portions overlaying the membrane represent the MSD region, with the blue semi-circles representing the NBD domains, pink circle representing the substrate to be transported, green ovals representing ATP, yellow ovals representing ADP and red circles representing inorganic phosphate (Pi).
Adapted from "Servier Medical Art" by Servier under CC BY 3.0 (https://creativecommons.org/licenses/by/3.0/).

At the start of the cycle the MSDs are inward facing conformation and the NBDs in a non-dimerized apo state.[47,63] The cycle is initiated when two ATP molecules bind to the NBD binding sites causing formation of the NBD dimer (it has been observed that some ABC transporters hydrolyze ATP without transporting substrate, suggesting substrate binding is not required to initiate the cycle). In the second step of the cycle, the conformational change from NBD dimerization is translated to the MSDs, driving the change to an outward facing conformation and release of substrate across the membrane. The third step of the cycle involves the hydrolysis of the ATP molecules to ADP and Pi, causing destabilization of the NBD dimer. In the final step the NBD dimer opens to release the inorganic products, causing the MSDs to revert the inward facing closed state to begin another cycle.[63]

The classical CFTR gating cycle (Figure 5) is similar to the ABC transporter cycle in that channel opening events are strictly coupled directly to ATP binding/hydrolysis events.[34,63] The gating cycle is initiated with phosphorylation of the R domain, allowing binding of one ATP molecule and formation of a partial NBD dimer. Upon binding of a second ATP molecule the

NBD fully dimerizes causing opening of the channel. Subsequent to the hydrolysis of ATP at the consensus site, the NBD dimer partially dissociates releasing ADP and Pi and causing the channel to close, ready to begin another cycle.

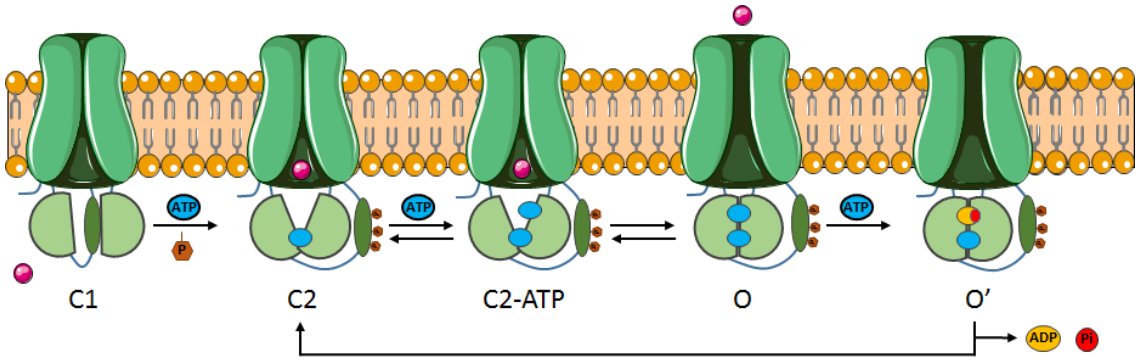

Figure 5 Representation of the classical CFTR gating cycle.

Note: Representation of the different conformations of CFTR during a gating cycle where gating is strictly coupled to ATP hydrolysis. Portions overlaying the membrane represent the MSD region where the gap between the regions represents the open/closed states of the channel. The green semi-circles represent the NBD domains as they progress through a non-dimerized state to a full heterodimer state bound to two ATP molecules. Pink circle represent the substrate of the channel, blue ovals represent ATP, yellow ovals representing ADP, orange hexagons representing phosphorylation events, and red circles representing inorganic phosphate (Pi).C1 represents a closed channel not bound to ATP with the R domain not phosphorylated; C2 represents a closed activated channel with the R domain phosphorylated and bound to one ATP molecule. C2-ATP represents a closed state with two ATP molecules to the NBD domains. O represents the open channel state where the NBD domains have formed the heterodimer bound to two ATP molecules, causing the channel to open; O' represents an open channel state where one of the ATP molecules bound in the NBD hetero-dimer has been hydrolyzed to ADP and Pi. The O'→C2 transition shows the partial cleavage of the NBD dimer with release of ADP and Pi and closing of the channel. Adapted from "Servier Medical Art" by Servier under CC BY 3.0 (https://creativecommons.org/licenses/by/3.0/).

CFTR activity can be measured through a variety of means, including the use of patch clamp assays, and more recently through the use of halide sensitive fluorescent dyes.[64] Through use of these assays in measuring the functional activity of various CFTR mutants, insight can be gained into the gating mechanism of CFTR. Patch clamp assays measure potential difference across a membrane, enabling the ability to measure the varying lengths and intensities of CFTR channel opening events. While the classic gating model mostly accounted for the normal gating events of wt.-CFTR, recent observations in studies of certain CFTR mutants, as well as mechanism-of-action studies of new CFTR modulators, have led to a gating model which takes into account observed channel opening events independent of ATP hydrolysis (Figure 6).[63] This model is designated as the energetic-coupling model which postulates that the ATP binding and NBD dimerization events promote an energetically

favourable pathway to channel opening, but that opening events can be decoupled from the ATP binding/hydrolysis events.[65] However, recent studies into gain-of-function mutations which observed NBD dimerization in the absence of ATP binding at site 2, suggest that channel opening may be strictly coupled NBD dimerization.[66]

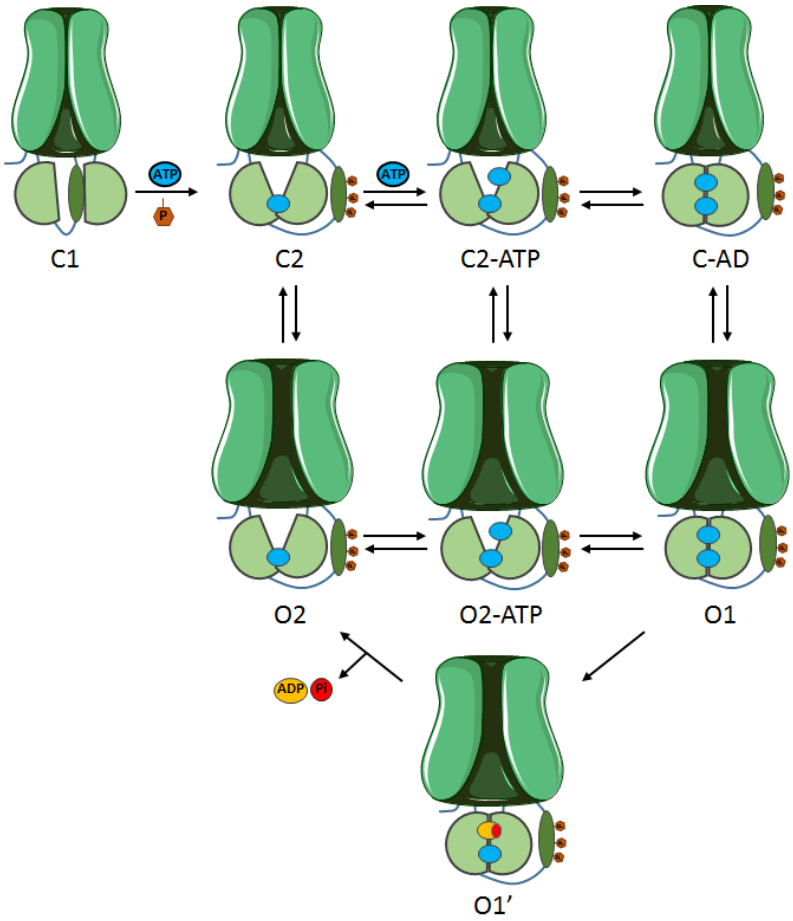

Figure 6 Energetic coupling model of CFTR gating

Note: Representation of the different conformations of CFTR during a gating cycle where the transitions between each conformation are regulated by rate constants and not strictly coupled to ATP hydrolysis. Open states begin with an O designation an closed states begin with a C designation. Portions overlaying the membrane represent the MSD region where the gap between the regions represents the open/closed states of the channel. The green semi-circles represent the NBD domains as they progress through a non-dimerized state to a full heterodimer state bound to two ATP molecules. Pink circle represent the substrate of the channel, blue ovals represent ATP, yellow ovals representing ADP, orange hexagons representing phosphorylation events, and red circles representing inorganic phosphate (Pi).

1.2.5. Biosynthesis

The biosynthesis of wild-type CFTR is a highly regulated process involving several control mechanisms in a variety of cellular compartments (Figure 7).[1,67,68] Starting with transcription in the nucleus, the mRNA is translated predominantly in the endoplasmic reticulum (ER) to give the nascent polypeptide. Protein maturation begins in the ER lipid bilayer and ER lumen with a series of complex folding processes mediated by chaperone proteins. CFTR folding proceeds in a modular fashion, beginning with MSD1; NBD1 is then synthesized and stabilized by chaperone proteins until the synthesis of the R domain is complete. MSD2 is then synthesized and inserted into the ER membrane where it forms the channel with MSD1, as well as making contacts between the ICLs of MSD2 to NBD1 which stabilize the protein, leading to dissociation of some of the chaperone proteins. Finally NBD2 is synthesized and interactions with the rest of the protein lead to a more stable tertiary structure. This initial folding process is surprisingly inefficient with misfolding occurring in over half of wild-type CFTR proteins.[37,69] The chaperone proteins monitor proper protein folding and coordinate with the quality control ER-associated degradation process (ERAD) which tags misfolded CFTR with ubiquitin for degradation in the ubiquitin proteasome system (UPS).

Following translation, CFTR is glycosylated with core N-linked glycosylation on the 4th ECL (Figure 7 and Figure 2 for location of glycosylation on CFTR) before being transferred by chaperone proteins to the Golgi apparatus via the cytoplasm. During transport to the Golgi apparatus, quality control processes involving the coat protein complex II assess proper cellular CFTR protein folding.[37,69]

Ensuing trafficking to the Golgi body, CFTR undergoes final processing and glycosylation from a mannose-enriched to a complex oligosaccharide side-chain. This complex oligosaccharide side-chain is thought to increase the stability of the mature protein at the plasma membrane. As well, the glycosylation state of CFTR is routinely used in Western blot analyses (particularly as a tool for measuring rescue of mutant CFTR protein by small molecules) to assess protein maturation with the lower molecular weight core N-glycosylated state referred to as band B, while the heavier complex glycosylated state is referred to as band C.[70,71]

Following glycosylation in the Golgi body, mature CFTR is shuttled to the apical membrane via clathrin-coated vesicles. Once at the apical membrane, wild-type CFTR undergoes a high turnover rate (similar to other membrane proteins) with a half-life between 12-24 hours. CFTR is internalized into endosomes where quality control processes assess protein function. The CFTR protein is then either recycled back to the apical membrane or removed for lysosomal degradation.[37,69]

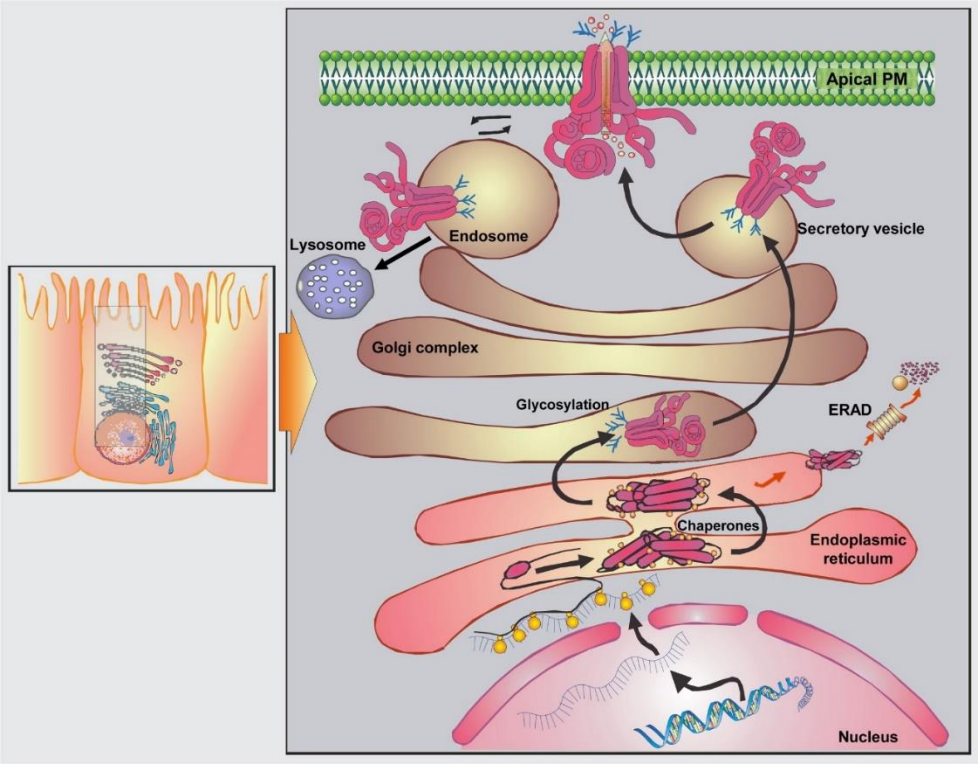

Figure 7 CFTR biosynthetic pathway overview

Note: Representation of the biosynthetic pathway of CFTR beginning with transcription in the nucleus, insertion into the ER during translation, where domain assembly and core-glycosylation occur, followed by transportation to the Golgi body for complex glycosylation then final trafficking to the cell membrane. Once at the cell membrane CFTR can be internalized into endosomes where it is either recycled to the cell membrane or sent for lysosomal degradation.
Reprinted from The International Journal of Biochemistry & Cell Biology, (52), Pranke, I.; Sermet-Gaudelus, I.; Biosynthesis of cystic fibrosis transmembrane conductance regulator, p. 13, Copyright 2014, with permission from Elsevier.[72]

1.2.6. CFTR Mutations

To date, over 2000 CFTR genetic variants have been identified, of which approximately 242 variants have been characterized as disease causing.[73–75] While the most common CF causing mutation, ΔF508-CFTR, appears in at least one allele of 90% of all CF patients, only approximately 20 other variants appear with a frequency above 0.1% worldwide.[76] Aside from ΔF508-CFTR, the next 4 most common mutations appear with a frequency between 1-3% worldwide.[77] The majority of CFTR mutations remain to be fully characterized and each accounts for less than 0.01% of observed mutations worldwide; however, in some populations certain less common mutations appear with significantly higher frequency. The characterized mutations are grouped into 5 classes (Figure 8) depending on the nature of how each mutation affects the activity or biosynthesis of CFTR.[76,78,79]

Class I mutations result in the absence of translated CFTR protein due to nonsense mutations, frame-shift mutations, and mRNA splicing defects. In particular, nonsense mutations (designated as a mutations ending in X), can introduce pre-mature termination codons (PTCs) resulting in a truncated mRNA and absence of CFTR protein translation.

Class II mutations give rise to misfolding, trafficking, and maturation defects causing the premature CFTR protein to be sent for proteosomal degradation. Class II mutations are exemplified by the most common CFTR variant ΔF508-CFTR. This mutation involves the deletion of a phenylalanine residue from NBD1 (F508). The deletion of F508 increases the energy required for proper folding as well as increasing the thermal instability of NBD1 which disrupts the folding and assembly of the whole protein.[41] As well, deletion of ΔF508-CFTR significantly alters the surface region that normally provides a stabilizing interaction at the interface between NBD1 and the coupling helices of ICL4 (Figure 2) important for proper protein folding and assembly.[72] While ΔF508-CFTR is successfully translated in the ER, misfolding prevents proper trafficking to the Golgi apparatus and leads to retention of the protein in the ER.[67] In ΔF508-CFTR expressing cell lines, incubation at 27 ^{o}C gives rise to fully glycosylated protein which is properly trafficked to the cell surface; however, while “temperature-rescued” ΔF508-CFTR protein displays diminished gating at the cell surface, (similar to a class III mutation) the protein is responsive to CFTR potentiators (such as the isoflavone genistein) which restore chloride conductance. Therapeutics which rescue the expression of trafficking mutations are generally referred to as correctors.

Class III mutants, classified as gating mutants, consist of substitutions to residues in either NBD which result in protein which exhibits defective channel function despite being properly translated and trafficked to the cell membrane. The most prevalent class III mutation is the G551D missense mutation found in at least one allele of ~3% of CF patients worldwide. The G551D-CFTR mutation involves replacing a neutral glycine residue located at the NBD dimer interface with a charged aspartic acid. Introduction of a negative charge at the dimer interface hinders the NBD dimerization process upon binding of a second nucleotide molecule, which renders the channel inactive. Although G551D-CFTR is clinically inactive, a limited burst-like channel activity was observed in patch-clamp assays of G551D-CFTR. The observation of this limited channel activity aided in the generation of the energetic-coupling gating mechanism (Figure 6), which postulated that G551D-CFTR could proceed to a normally short lived open-channel state O2, independent of NBD dimerization.[80,81] Patients with a G551D-CFTR mutation were the first approved cohort for the CFTR therapeutic ivacaftor. As a therapeutic aimed at restoring function to gating mutations, ivacaftor is referred to as a potentiator.

Class IV mutations result from mutations in the MSDs which leads to CFTR protein properly expressed at the cell membrane but exhibiting reduced chloride conductance.

Class V mutants, the least common class, give rise to functional CFTR protein; however at significantly reduced levels. In Class V mutations, either splicing defects lead to reduction in transcription of CFTR protein, or high turnover of protein at the cell membrane leads to a reduction of available CFTR protein.

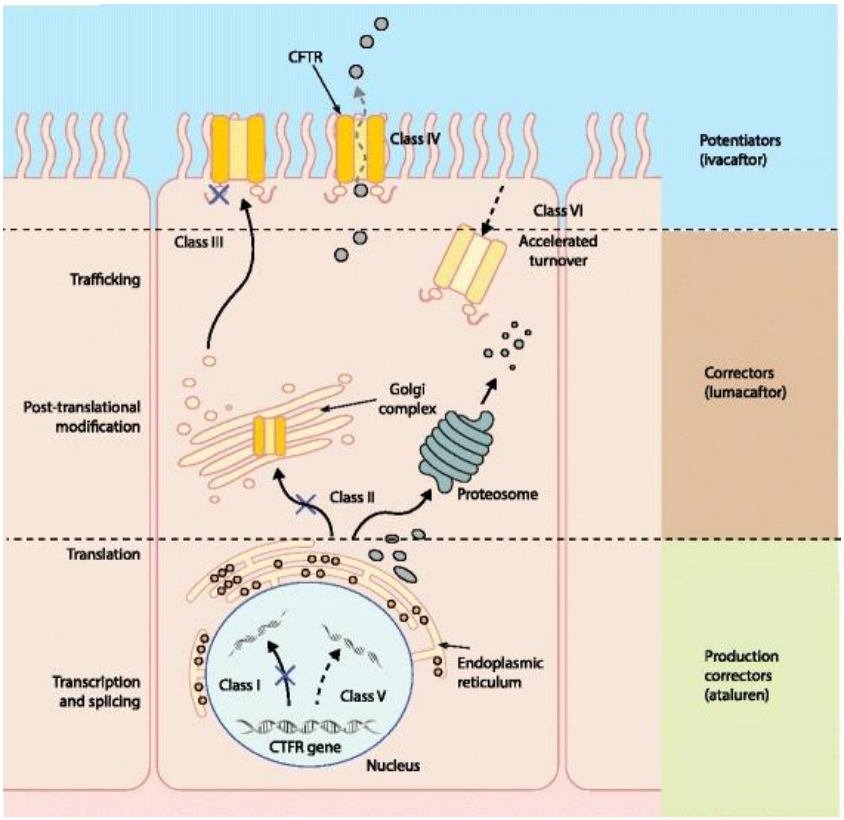

Figure 8 CFTR Mutation classifications and the mechanisms of CFTR modulators

Note: CFTR mutation classes I, II, V (and formally Class VI, now part of class V) cause an absence or reduced quantity of CFTR at the cell membrane. CFTR mutation classes III and IV affect the function of CFTR at the cell membrane. Correctors aim to increase the amount of mutant CFTR at the cell membrane, while potentiators restore function to mutant CFTR at the cell membrane.
Reprinted from Genome Medicine, (7), Brodlie, M.; Haq, I.; Roberts, K.; Elborn, J., p. 102, Copyright 2015, under CC BY 4.0 (http://creativecommons.org/licenses/by/4.0/).[82]

1.3. Correcting CFTR

Despite the improvements in clinical outcomes through management of disease symptoms, restoration of CFTR function is the most optimistic therapeutic strategy.[67,75,79,82–84] While this continues to be a challenge, clinical observations suggest that restoring 5-30% of CFTR function compared to wild-type may be enough to exhibit a clinical therapeutic benefit.[83] Towards this goal many strategies have been employed, including various gene therapy techniques and more recently small-molecule CFTR modulators targeting specific mutations derived from high-throughput functional assays which assess rescue of CFTR activity independent of mechanism-of-action. [12,71,85–89]

1.3.1. Gene therapy

Following the identification of the CFTR gene, a variety of gene therapy approaches utilizing both viral and non-viral methods to deliver copies a of functional CFTR gene have been attempted with limited success.[12,90–94]

Despite the majority of past clinical trials involving gene therapy not meeting their desired endpoints,[91,93] a recently completed phase IIb clinical trial conducted by UK CF Gene Therapy Consortium utilizing a non-viral CFTR gene/liposome complex delivery method was able to show a statistically significant halting of the decline of FEV_1% in treatment arm versus placebo.[92]

As well, research into the utility of other gene editing technologies including Zinc-finger nucleases and CRISPR/CAS9 have shown promise for delivering a functional CFTR gene.[94,95] In particular, the use of CRISPR/CAS9 as a delivery method was successful in restoring CFTR activity in primary intestinal stem cell organoids from patients homozygous for ΔF508-CFTR.[95,96]

1.3.2. Small-molecule CFTR Modulators

Recently efforts have been focused towards finding small-molecule CFTR modulators which can restore protein activity. Due to the varying nature in the types of malfunctions arising from the different CFTR mutations,[68] multiple classes of CFTR modulators have been described which affect protein trafficking and/or function including: potentiators,[70,78,81,97,98] correctors,[99] activators,[39,100] read-through agents,[85] and proteostatics,[101,102] and inhibitors.[103] Despite the success of potentiators, correctors, and read-through agents in showing efficacy in clinical application, many challenges remain in finding a cure or control for CF.[76,79,104–110]

In 2006,[111–114] the Cystic Fibrosis Trust (US based CF advocacy group) partnered with Vertex Pharmaceuticals to initiate a drug discovery effort to develop small-molecule modulators which restored mutant CFTR activity,[70] particularly for ΔF508-CFTR. Vertex developed two high-throughput screening (HTS) assays using fibroblast NIH/3T3 cells expressing ΔF508-CFTR;[115,116] the first measured the ability of compounds to rescue ΔF508-CFTR trafficking and expression (correctors), while the other measured the ability of compounds to rescue ΔF508-CFTR gating at the plasma membrane (potentiators).

Both of the HTS assays determined CFTR gating by monitoring changes in chloride conductance through measurement of fluorescence resonance energy transfer (FRET) between a membrane-soluble voltage sensitive dye and a plasma membrane-localized fluorescent coumarin-linked phospholipid. Stimulation of CFTR gating caused depolarization of the membrane leading to a decrease in FRET and an increase in the fluorescence signal from the coumarin linked phospholipid.[115]

In the ΔF508-CFTR corrector assay, compounds were screened for the ability to enable synthesis and trafficking of function ΔF508-CFTR protein to the membrane by incubating cells with compounds at 37 °C then measuring chloride conductance upon stimulation with genistein (CFTR potentiator) and forskolin (activates CFTR by increasing the concentration of the PKA substrate cAMP). By comparing the signal obtained from each compound relative to temperature rescued ΔF508-CFTR controls, a measure of the amount of functional protein rescued to the membrane could be established.[71,115,117,118]

In order to discover potentiators, a similar HTS assay was developed which measured the ability of compounds to increase conductance of temperature-rescued ΔF508-CFTR in NIH/3T3 cells. Following temperature rescue of ΔF508-CFTR to the plasma membrane, the cells were treated with test compounds and stimulated with forskolin to activate channel gating.[70,115] Following identification of active hits in the HTS assays confirmation of the CFTR modulating effects of the compounds were tested in a variety of functional assays. Significant medicinal chemistry efforts from initial hits generated compounds which eventually showed efficacy in clinical trials.[70,71] Importantly, the assays used to develop CFTR modulating compounds measured functional/trafficking rescue independent of any mechanistic data.

Read-through agents are being investigated for treating Class I mutations for their ability to allow ribosomes to “read-through” PTCs in mRNA of mutant CFTR. These compounds act by binding to the decoding site of rRNA interfering in the codon-anticodon binding process, allowing the incorporation of an amino acid in place of a PTC and enabling translation to continue[85]. The first examples of read-through agents were aminoglycosides such as gentamicin. Unfortunately, these compounds exhibited toxicity issues at the concentrations required to exhibit ribosomal read-through activity. The most important read-through agent is

ataluren, a non-aminoglycoside currently being evaluated in a phase III clinical trial in CF patients with a nonsense mutation (NCT02139306).

1.3.3. Lumacaftor

CFTR correctors are compounds which aid in repairing the processing and maturation of mutant CFTR. Correctors have been shown to act through enabling proper folding of the mutant protein by direct interactions, or through modulation of the quality control mechanisms assessing proper folding.[85,88,94,119] Lumacaftor (VX-809),[71,115] developed by Vertex Pharmaceuticals, was the first CFTR corrector to obtain FDA approval. Lumacaftor (Figure 9-B) was discovered following a medicinal chemistry effort on a hit from a HTS assays which assessed the correction of trafficking, maturation, and eventual conductance of ΔF508-CFTR.[71] 164K compounds were screened in the HTS Fret assay and hits were further tested using an immunoblot assay which assessed the maturation of ΔF508-CFTR from the core-*N* glycosylated to the complex glycosylated state (band B to band C).[115] One hit from this assay, VRT-768 (Figure 9-A), increased the maturation of ΔF508-CFTR by 2.5 ± 0.1 fold (EC_{50} 16 ± 6 μM; n = 4) as well as also displaying potentiating activity, increasing chloride transport (EC_{50} 7.9 ± 1.1 μM; n = 4) in Fischer rat thyroid cells expressing ΔF508-CFTR. Utilizing the pharmacophore of the central amide bond an extensive medicinal chemistry effort focused on independently varying the amine and acid moieties eventually led to the discovery of the clinical candidate VX-809 (Figure 9-B) which would later be named lumacaftor.

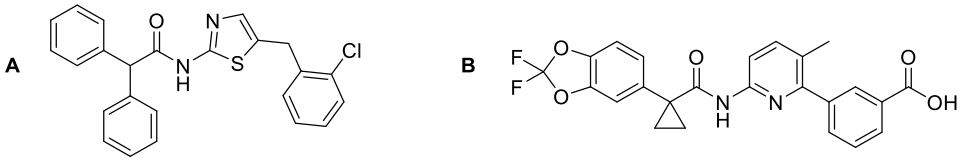

Figure 9 Structures of A) initial hit from HTS ΔF508-CFTR corrector assay VRT-768, and B) eventual clinical candidate VX-809

As lumacaftor was also partially active as a potentiator in ΔF508-CFTR functional assays, it was hoped that it could be administered as monotherapy in homozygous ΔF508-CFTR patients. However, when administered as a monotherapy in clinical trials for patients homozygous for ΔF508-CFTR, lumacaftor failed to display efficacy in improving FEV_1%. Previous studies had suggested that ΔF508-CFTR corrected by lumacaftor would be sensitive to combination therapies with other CFTR modulators,[104,120] particularly potentiators. This lead

to clinical testing of lumacaftor co-administered with the potentiator ivacaftor as a combination therapy. This combination therapy, later named Orkambi, gave a modest improvement in clinical endpoints for patients homozygous for ΔF508-CFTR. In 2015, the combination therapy, Orkambi, was approved for the treatment of patients homozygous for ΔF508-CFTR.[121]

While lumacaftor stabilizes the folding of ΔF508-CFTR in the ER, there is debate as to the location of the binding site on ΔF508-CFTR.[122] *In silico* screening experiments suggest that lumacaftor docks in a pocket at the NBD1-ICL4 interface, providing a favourable interaction normally absent due to the deletion of the Phe residue;[123] while competing evidence suggests that lumacaftor helps stabilize the folding of MSD1.[89,124] Most recently the second-generation corrector VX-661, based on the lumacaftor scaffold, is currently in a phase III clinical trial as a combination therapy with ivacaftor for patients both homozygous for ΔF508-CFTR, and heterozygous ΔF508-CFTR with certain mutations (NCT02565914).

Potentiators in the context of CFTR are compounds which restore gating activity to CFTR proteins at the cell membrane (typically Class III and IV mutants).[97,125] Although potentiators and activators both increase the gating of CFTR, recent definitions place activators as modulators which directly cause an increase in CFTR gating (usually by stimulating cAMP production),[126,127] whereas potentiators increase gating activity in response to cAMP signalling;[39,127] importantly some modulators display both activating and potentiating effects on mutant CFTR. Many compounds have been found which potentiate CFTR either *in vitro* or in animal models, including some natural products (*e.g.* capsaicin);[99] however only one compound, ivacaftor, has shown efficacy in clinical application.[128]

1.3.4. Ivacaftor

Approved in 2012 by the FDA, the drug ivacaftor (**1**, Figure 1) was the result of a medicinal chemistry effort improving on a hit from the high-throughput functional FRET screen (p.18) which measured potentiation of temperature rescued ΔF508-CFTR in NIH/3T3 cells.[70] As potentiators act on CFTR present at the cell membrane, Vertex also tested their compounds against gating (Class III) CFTR mutations such as G551D with the intent of finding a compound which could act on multiple forms of mutant CFTR including those rescued by correctors.[70]

The initial hit from the HTS assay **1a** (Figure 10) was found to potentiate chloride efflux with an EC_{50} = 2.1 ± 1.4 μM (a 4-fold improvement compared to the standard genistein (EC_{50} = 8.0 ± 2.0 μM)). The chloride efflux response to this initial hit was only observed following CFTR activation with forskolin, indicating that this hit acted as a potentiator. In order to confirm potentiating activity, the hit was tested in human bronchial epithelial (HBE) cells isolated from CF patients who were either homozygous ΔF508-CFTR or heterozygous G551D/ΔF508-CFTR. Compound **1a** potentiated chloride conductance in both cell types with EC_{50} values of 1.5 μM and 12.2 μM respectively. This result indicated that the hit could be active against multiple CFTR variants including Class III mutants. Based on these results, as well as the low molecular weight (368 $g \cdot mol^{-1}$) and cLogP of 2.9, this hit was chosen as the starting point to initiate a medicinal chemistry effort. Initially, Vertex pursued variation to the **1a** quinolinone moiety which tested whether activity existed for both the keto and enol forms. While a naphthol derivative was active, removal of the 4-oxo group, methylation of the quinolinone nitrogen, and truncation of the fused ring all lead to reduced activity. Of the variations attempted in this series, the 4-oxo quinolinone ring remained the most potent.

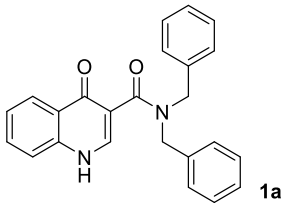

1a

Figure 10 Structure of the initial hit from HTS CFTR potentiator assay

Vertex next pursued many variations of the amine constituent, including primary, secondary, aliphatic, aromatic, and heterocyclic amines. Out of the more than 70 compounds tested the most potent compound incorporated an indolyl moiety **1b** (Figure 11) which had an EC_{50} = 0.1 μM, a 20-fold increase in potency versus **1a**. Compound **1b** was then tested in a lead profiling screen against important biological targets and was found to interact with a $GABA_A$ benzodiazepine receptor, a ligand-gated chloride channel, with an IC_{50} = ~0.1 μM. Further testing found showed that **1b** had a cLogP of 1.6, but low solubility, and low oral bioavailability in rats (11). As well as, **1b** displayed a short intravenous (IV) half-life ($t_{1/2}$ = 0.9 h) in dogs primarily due to clearance (17 $mL \cdot min^{-1} \cdot kg$).

Other compounds from this series indicated that a phenyl ring with alkyl substituents both *ortho* and *para* to the nitrogen were tolerated. Two of these analogues, **1d** and **1e**, in the

NIH/3T3 cell assay showed a 5 to 10-fold increase in potency from compound **1a**, each obtaining an EC_{50} = 0.2 μM. As well, the reduced version of **1b**, indoline **1c** also showed activity with an EC_{50} = 0.4 μM.

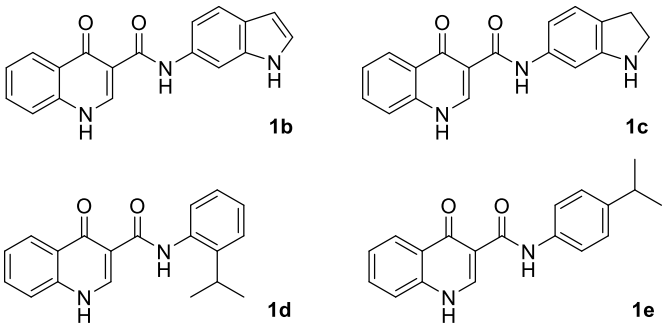

Figure 11 Important intermediate during the development of ivacaftor varying amine portion

From these results, Vertex pursued efforts to increase the solubility, bioavailability, and potency, while decreasing $GABA_A$ activity by following two approaches. The first pursued adding substituents to the 3 and 5 positions on the indole ring of compound **1b**. Of note from this series were structures **1f** and **1g** (Figure 12) which had 10-fold increases in potency to EC_{50} values of 0.009 μM and 0.011 μM respectively, showing tolerance for alkyl groups both small and bulky at these positions.

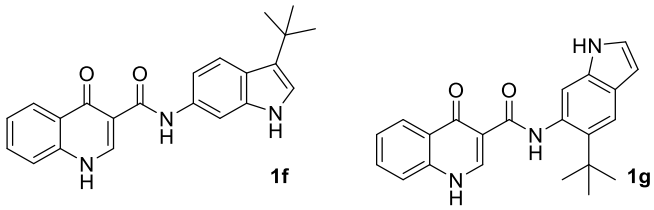

Figure 12 Important intermediate during the development of ivacaftor varying indole ring

The second approach based on the results of the indoline **1c** which indicated that a hydrogen bond donating group *meta* to the aniline moiety with an alkyl group *para* could show activity. This series focused on ring-opened anilines with various alkyl substituents. Although few of the structures from this series showed any dramatic increase in potency, introduction of a bulky *t*-butyl group as in compound **1h** retained activity compared to compound **1b**.

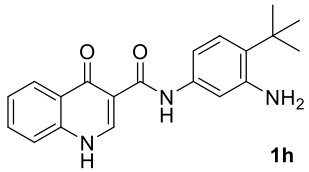

1h

Figure 13 Important intermediate during the development of ivacaftor with ring alkyl groups and an aniline moiety.

In order to explore the role of the aniline moiety from compound **1h** (Figure 13), substitutions which retained hydrogen bond donating character, as well as aniline bioisosteres were prepared. Of significant note from this series was the replacement of the aniline from **1h** with a phenol as in compound **1i**, giving a 40-fold increase in potency to an EC_{50} = 0.003 μM. Phenol **1i** (Figure 14) showed a potency of 5 nM in potentiating ΔF508-CFTR in HBE cells a 300-fold improvement from compound **1a**.

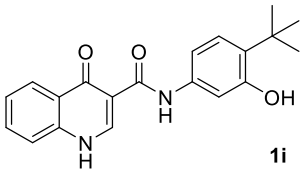

1i

Figure 14 Important intermediate during the development of ivacaftor resulting from exploring role of aniline.

Finally, following the observation of the effects of substituents at the 5-position on compound **1g** (Figure 12), the effects of alkyl substituents *para* to the phenol were tested, ranging from hydrogen to a *t*-butyl group. While none of those tested showed an increase in potency, they all were active. However, introduction of a *t*-butyl group to give compound **1** (Figure 1) lead to an improved pharmacokinetic profile in rats with a low clearance (CL = 5.5 $mL \cdot min^{-1} \cdot kg^{-1}$) and long half-life ($t_{1/2}$ = 9.5 h). Further profiling of compound **1** indicated an improved solubility, as well as no significant activity against $GABA_A$, CYP_{450}, or inhibition of the cardiac potassium channel hERG. Potentiating activity was confirmed in human bronchial epithelial cells (HBE) from CF patients heterozygous for the G551D CFTR mutation and showed an increase in chloride secretion with an EC_{50} of 0.0236 μM, as well as a maximum chloride secretion approximately 50% compared to HBE cells from healthy individuals[115].

Compound **1** (designated ivacaftor) was selected for clinical evaluation, and in a phase III clinical trial of patients heterozygous for the G551D-CFTR mutation[128,129], showed an overall 10.6% increase in FEV_1%, mean weight gain of 3.1 kg, as well as a 55% decrease in the rate of

pulmonary exacerbations, and a mean decrease in sweat chloride concentration[130,131] to 47.8 mmol/L, well below the diagnostic threshold of 60 mmol/L. In the study, ivacaftor showed few severe side effects, however, elevated hepatic enzyme levels lead to the discontinuation in one study subject. As well, ivacaftor was found to have good oral bioavailability, which was augmented when administered with a fat containing meal (20 g of fat). Peak plasma levels for ivacaftor were reached within 4 hours, and displayed a half-life $t_{1/2}$ = 12 hours. It was found that the majority of ivacaftor in the blood was bound (>97%) to the plasma proteins albumin and α_1-acid glycoprotein. The metabolism of ivacaftor is primarily mediated by CYP3A and the metabolites are cleared via feces. [112,129]

As part of ivacaftor's development it was also tested against other gating mutation constructs, and after receiving approval for the use in patients with a G551D mutation, ivacaftor received approval in 2014 for expanded use in treating 8 other gating mutations. Having shown that ivacaftor can potentiate corrected ΔF508-CFTR *in vivo*; ivacaftor was tested as a combination therapy with lumacaftor. A phase III clinical trial exploring the use of ivacaftor as part of a combination treatment with a ΔF508-CFTR corrector (lumacaftor) showed positive results in treating homozygous ΔF508-CFTR patients,[132] a group which constitutes approximately 70% of Canadian CF patients. Unfortunately, initial results of clinical studies in heterozygous ΔF508-CFTR were less promising and imply better therapies are needed for this cohort of patients.[133]

As these compounds were discovered using functional screens, there was no immediate evidence as to their exact molecular mechanism or binding sites on CFTR. Although determination of the binding site of ivacaftor was not critical for approval by the FDA, knowledge of the binding site location could help in the basic understanding of the disease as well as aid in the design of second-generation CFTR potentiators. Recent work suggests that ivacaftor acts directly with CFTR and potentiates gating activity by stabilizing a normally short lived open-channel state,[65,81] however, the exact mechanism remains unknown. Despite ivacaftor's' initial clinical success as a co-therapy with lumacaftor for homozygous ΔF508-CFTR patients, recent studies have shown that in cells,[107,110,134] chronic exposure to ivacaftor decreased the thermal stability of chemically rescued ΔF508-del CFTR, increasing the rate at which the protein is removed from the membrane. These results underscore the importance of determining the mechanism of action and the binding site (or sites) of ivacaftor on CFTR.

Currently, many groups are actively researching the mechanism of action of ivacaftor, particularly how ivacaftor affects the gating cycle of mutant CFTR. A study has shown that ivacaftor interacts directly with, and potentiates, both purified G551D- and ΔF508-CFTR constructs.[81] This study also showed ivacaftor did not alter the dose response for ATP-mediated halide flux over a range of ATP concentrations when wild-type-CFTR (wt.-CFTR) was pretreated with ivacaftor; this suggests ivacaftor does not compete for binding at the canonical ATP binding site.[81] Other evidence indicates that the binding site of ivacaftor is potentially located in the MSD of CFTR.[63,65,67,135,136] importantly, the development of ivacaftor focused on the G551D-CFTR mutation which lacks ATP hydrolysis activity in the canonical binding site. The G551D mutation contains mutations which preclude the formation of the NBD dimer, presumably due to the introduction of a charged Asp residue at the dimer interface. Studies have shown that while G551D can bind a second molecule of ATP, this has no impact on the gating activity of the channel. Importantly, the potentiating activity of ivacaftor is not affected by varying concentrations of ATP, implying that ivacaftor interacts with the MSDs.[65] The observation that ivacaftor promotes opening of the channel in a manner independent of NBD dimerization helped lead to the development of the energetic-coupling gating mechanism (Figure 6).[65,81] This gating model proposes that ivacaftor can shift the equilibrium of the C2 ↔ O2 transition, increasing the P_o in an ATP independent manner.[63,65,67,135,136]

Despite the advancements in understanding the effects on the gating of CFTR through mechanistic studies, determination of the binding sites(s) on CFTR will play an important part in understanding how potentiators function, and how to develop more efficacious ones in the future.

1.4. Binding site determination

Determination of the binding site of a drug/natural product on its target protein is critical to understanding its mechanism of action, as well as in the development of molecular probes and second generation therapeutics.[137,138] Many techniques have been developed to enable binding site identification, including hydrogen/deuterium exchange,[139–141] *in silico* docking experiments,[142] NMR spectroscopy,[142,143] and photo-affinity labelling.[137,144–148]

While solution NMR spectroscopy is a powerful tool for elucidating protein-small molecule interactions, it is still generally utilized in the analysis of smaller proteins.[143]

Hydrogen/deuterium exchange mass spectrometry (HX MS), (as well as HX NMR spectrometry) utilizes the rate of exchange based on solvent accessibility of peptide backbone hydrogen atoms with deuterium atoms. HX MS has been successfully utilized to measure protein folding/dynamics, protein-protein interactions, as well as small-molecule-protein interactions.[140,141] Recently, HX MS was successfully applied to model the conformations of a bacterial multi-drug ABC transporter,[149] implying the potential to utilize HX MS to evaluate CFTR. However, transmembrane proteins remain a challenging task for HX MS due to the difficulty of digesting the large hydrophobic membrane spanning regions and removal of the lipid components.[141]

In silico docking experiments generally require high resolution crystal structures, or homology models with >50% sequence homology to similar proteins with crystal structures. Although modelling structures with >30% sequence homology can still inform on the "druggability" of a protein, lower (<30% sequence homology) homology models become speculative.[138] While *in silico* modelling has proven successful in generating CFTR correctors which interact with NBDs,[55] the low sequence homology of the MSDs of CFTR to other ABC transporters hinder the utility of this strategy for whole protein CFTR, especially with the assumption that the binding site for ivacaftor is located on the MSDs.[50]

1.4.1. Photo-affinity labelling

Photo-affinity labelling (PAL) is a common technique used in medicinal chemistry and drug design to determine the interactions between small molecules and their target proteins.[137,148] PAL probes incorporate photo-reactive chemical groups into the small molecule of interest, which upon activation bind the probe irreversibly to the residues lining the binding pocket of the target protein. Another component commonly incorporated into a PAL probe is a reporter tag containing an identification or purification handle; such as an alkyne enabling cross-linking to biotin via "click-chemistry", or a dansyl group to enable FRET analysis.

When designing a PAL probe, it is important to identify a site on the parent compound which can tolerate a diverse range of substituents and does not disrupt the binding and activity.

While this typically means that PAL probes require optimization with a variety of analogues and photo-reactive groups, this can be made easier if a structure activity relationship (SAR) from a set of analogues of the parent compound is already known.[137]

In choosing a photo-reactive group to incorporate into the PAL probe, several traits require consideration.[137,147] Firstly, the photo-reactive group should have structural similarity to the substituents of the parent small-molecule. The activation wavelength of the photo-reactive group should not also damage biological molecules, and the probe should be stable to a range of pH's and reaction conditions. As well, the half-life of the generated reactive species should be shorter than the dissociation rate of the ligand/protein complex. The most commonly used photo-reactive groups for PAL are benzoquinones, azides, and diazirines (Figure 15),[137] which upon photo-activation produce a diradical, a nitrene and a carbene respectively.

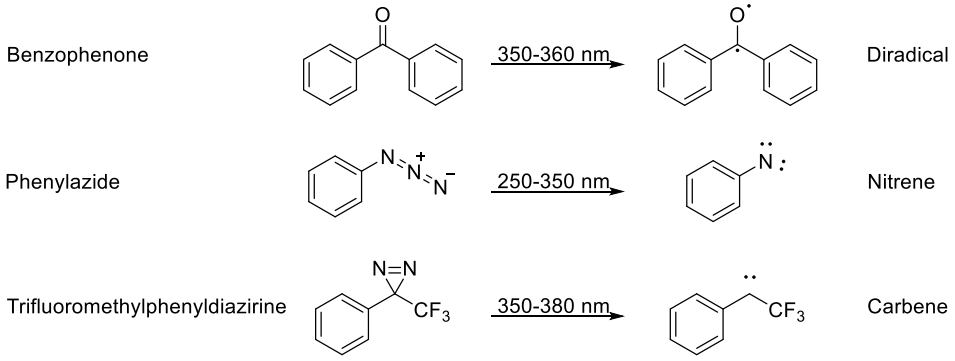

Figure 15 Common classes of photo reactive groups used in PAL and the reactive species they produce

Benzophenones are commonly utilized in PAL probes as they are activated by a long wavelength, are easy to prepare, and are stable in many solvents. Despite these advantages, benzophenones are large substituents and often require long irradiation periods; both of these factors if not accounted for can lead to increased nonspecific labelling.

Phenylazides are advantageous in that they are easy to synthesize and many are commercially available. However, phenylazides have several disadvantages in that they require shorter wavelength light which can damage biological molecules. As well, the reactive nitrene intermediate produced is less reactive than carbenes, can rearrange to form benzazirines and other side products, and can also be reduced to amines by thiols under alkaline conditions. As

well, nitrenes generated from azides are known to undergo undesired intramolecular cyclizations with *ortho* substituents.[137,150]

1.4.2. Diazirines

Phenyldiazirines, particularly trifluoromethylphenyldiazirines, have come to be the most commonly used photoreactive group in PAL probes.[137,145–148,151] Trifluoromethylphenyldiazirines have many desirable traits; they are a relatively small and lipophilic functional group, they are stable to a variety of reagents (*i.e.* nitrating and iodinating reagents),[145,152] temperatures, nucleophiles, acidic and basic conditions, as well as oxidizing and reducing agents. As well, the long wavelength required to produce the reactive carbene species reduces the potential damage to biological molecules. Upon irradiation, pyrolysis or ultrasonification,[147] phenyldiazirines produce a singlet carbene. One drawback to the phenyldiazirine is that up to ~30% can convert to a diazo species which can participate in dark reactions which is not favoured in photolabelling experiments; however, this species will itself slowly convert to a singlet carbine. The use of the trifluoromethylphenyldiazrine analogue promotes and stabilizes the formation of a singlet carbene reducing the rate of intramolecular rearrangements.[147,151] The carbene species generated from photolysis of a diazirine is well suited to photo-labelling as it is very reactive with a short half-life compared to the off-rate of most ligand-protein complexes, and readily inserts into the N-H, O-H and C-H bonds of peptide residues and backbones (Figure 16). Indeed, this reactivity be can utilized to characterize diazirines by performing photolysis in an alcohol solution (*e.g.* methanol or phenol),[151] to produce an ether photo-adduct. As carbenes readily react with water to produce an alcohol, the chance of nonspecific binding in cell-based experiments is minimized.[145]

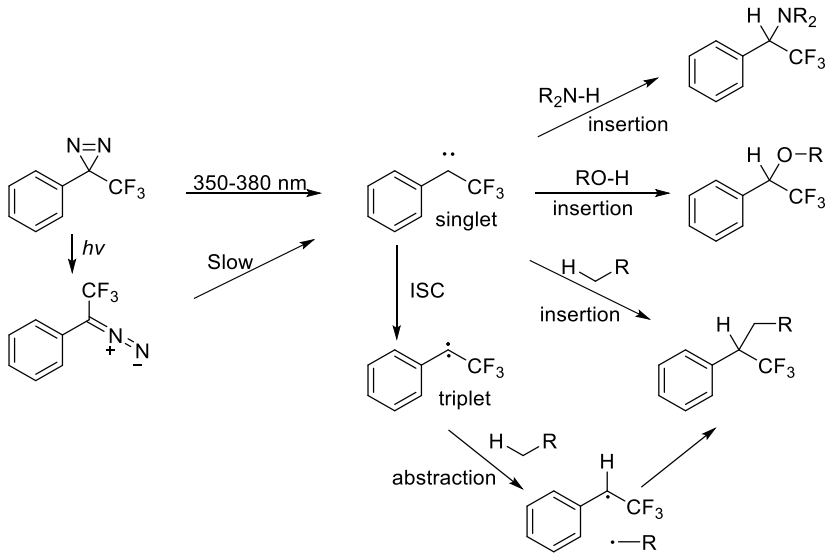

Figure 16 Photolytic products of a diazirine

While many synthetic routes to generate a diazirine have been developed,[146,153] the first and most commonly utilized route to synthesize the diazirine moiety proceeds from a trifluoromethylketone.[151] The trifluoromethylketone is converted to an oxime upon reaction with hydroxylamine hydrochloride, then tosylated using tosyl chloride in a pyridine/methanol mixture to give a tosyl-oxime. The tosyl-oxime is then converted to a diaziridine upon reaction with liquid ammonia, then finally to a diazirine via a variety of oxidants (*i.e*. Swern, Dess-Martin, MnO_2, Ag_2O) (Figure 17). The trifluoromethylketone can be installed on the aromatic ring via a synthetic handle, such as a halide, through a variety of methods including direct reaction of an aryl anion formed via lithium-halogen exchange chemistry,[154] Friedel-Crafts reactions, Fries rearrangements,[155] Stille couplings,[156] and magnesium-halogen exchange reactions.

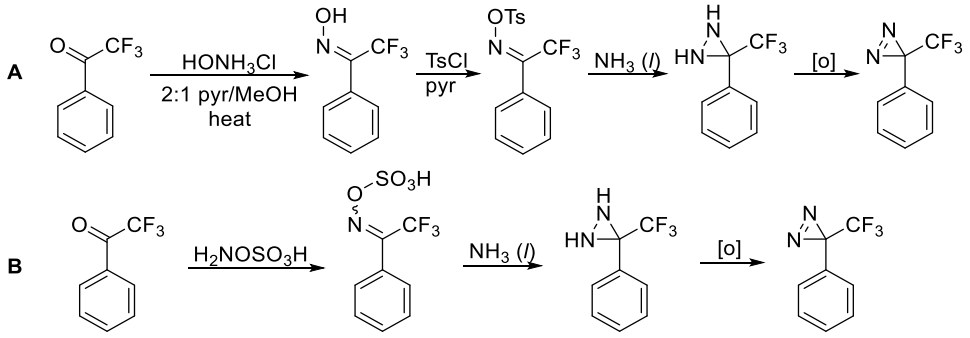

Figure 17 Common synthetic routes to obtaining diazirines from trifluoromethylketones

1.5. Diazirine containing ivacaftor PAL probe

After generating or using an established structure-activity-relationship (SAR) of the ivacaftor scaffold, putative sites can be identified for photo-label installation. Recently, our collaborators at the University of Toronto and Ryerson University used a similar approach to generate an azide containing PAL of the CFTR potentiator VX-532 following generation of a SAR for that compound.[157] Similarly, it can be hypothesized that a PAL based on an ivacaftor analogue containing a diazirine functional group (Figure 19) could be used to elucidate the binding site on mutant CFTR. Binding studies could be performed with purified mutant-CFTR, as well as studies in whole-cell constructs overexpressing ΔF508-CFTR to elucidate any secondary binding interactions for ivacaftor.

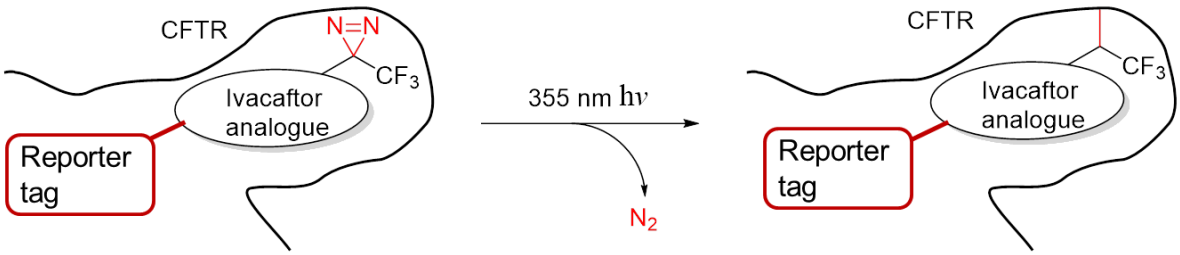

Figure 18 Schematic of a PAL ivacaftor probe binding to residues lining the binding site on CFTR.

Upon successful labelling of mutant CFTR with the ivacaftor PAL probe, limited proteolysis of the protein-label complex into the constituent domains will allow mass spectrometry studies to identify the domain to which ivacaftor is bound. Further proteolysis studies would identify the exact residue(s) that is labeled and then homology modelling can then be used to characterize the structural features of the putative binding site on CFTR (Figure 19).[40,154,158–162] As well, if successful, future probes containing a synthetic handle to allow for purification may be used to confirm that similar labelling takes place in cells and a second affinity element can be incorporated into the probe to allow crosslinking to closely associated proteins that may be complexed with the target (i.e., CFTR) in the cell.[137]

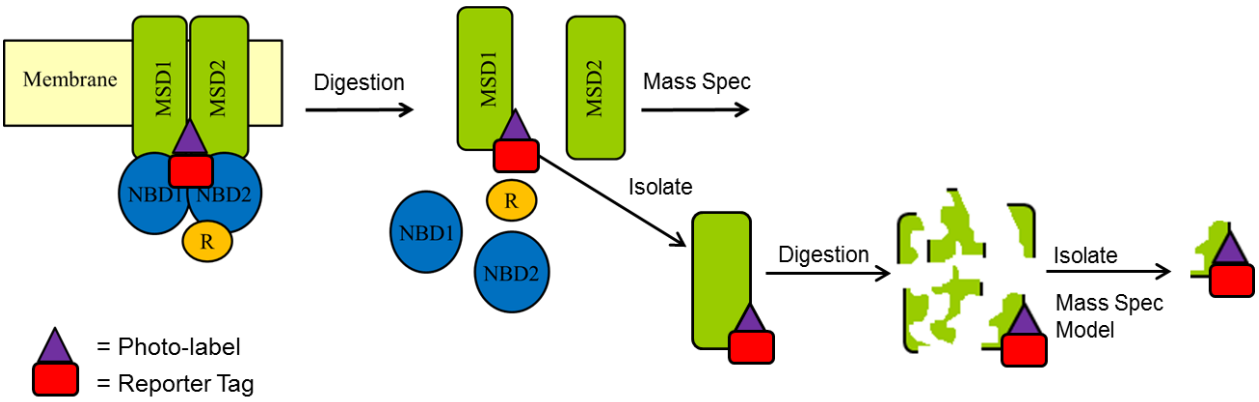

Figure 19 Schematic representing the process used to identify site of labelling by PAL probe on CFTR.

Schematic demonstrates the process by which one could analyze a photolabeled CFTR protein. While the schematic shows the photolabel attached to MSD1, this is just for illustrative purposes and is not meant to imply that the binding site is located on this domain. Following labelling of the CFTR protein with a PAL ivacaftor probe, the CFTR protein can be isolated and partially digested into its constituent domains. Through use of a reporter tag, the labelled domain can be isolated and further digested into peptide fragments. Then through use of mass spectrometry and computer modelling, the binding site can be identified and modelled.

Chapter 2.

Design and Retrosynthesis of PAL Ivacaftor Probe

Along with our collaborators (Dr. Christine E. Bear, University of Toronto; Dr. Russel Viirre, Ryerson University) a set of ivacaftor analogues were synthesized and tested in an adapted fluorescence assay measuring potentiation of ΔF508-CFTR (unpublished data).[64] The results from this assay showed that removal of either *t*-butyl group from the ivacaftor scaffold could be tolerated with retention of potentiating activity while at least one was critical for potent activity. These results indicated that substitution of either *t*-butyl group with a photo-labelling motif could be possible, leading to the design of the diazirine targets **2**, **3** (Figure 20).

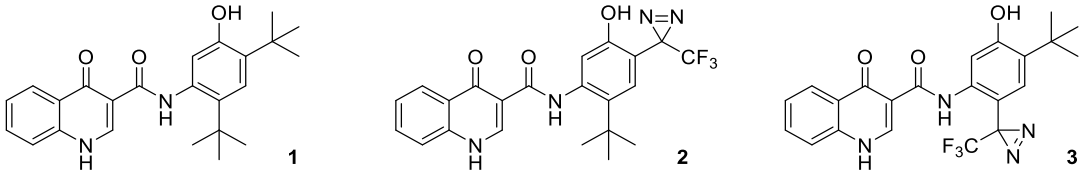

Figure 20 Ivacaftor and the target PAL diazirine analogues

After initiating a synthesis program towards these analogues, Hadida *et al.*[70] published the paper on the medicinal chemistry program which produced ivacaftor (§1.3.4). In this paper, it was found that while the phenol was critical for activity, alkyl substituents of varying size were tolerated at the positions both *ortho* and *para* to the phenol. While their results indicated that the *t*-butyl group ortho to the phenol increased potency, potentially making favourable contacts with residues in the binding site, there remained potential for substitution at this position. While a compound with a *t*-butyl group *para* to the phenol but lacking the *t*-butyl group *ortho* to the phenol was not reported, these combined results supported our original hypothesis that replacing either *t*-butyl group with a PAL motif could be tolerated without significantly altering the binding/activity of the compound.

2.1. Retrosynthetic analysis of desired PAL ivacaftor probes

Retrosynthetic analyses were performed for the two regio-isomers containing diazirines (**2**, **3**). For both compounds **2** and **3**, there are two important retrosynthetic steps (Figure 21): a functional-group interconversion from the diazirine to a synthetic handle allowing trifluoromethylketone installation on the phenol “right-hand side” (RHS) ring, and an amide disconnection to the 4-oxo-quinolne “left-hand side” (LHS) ring.

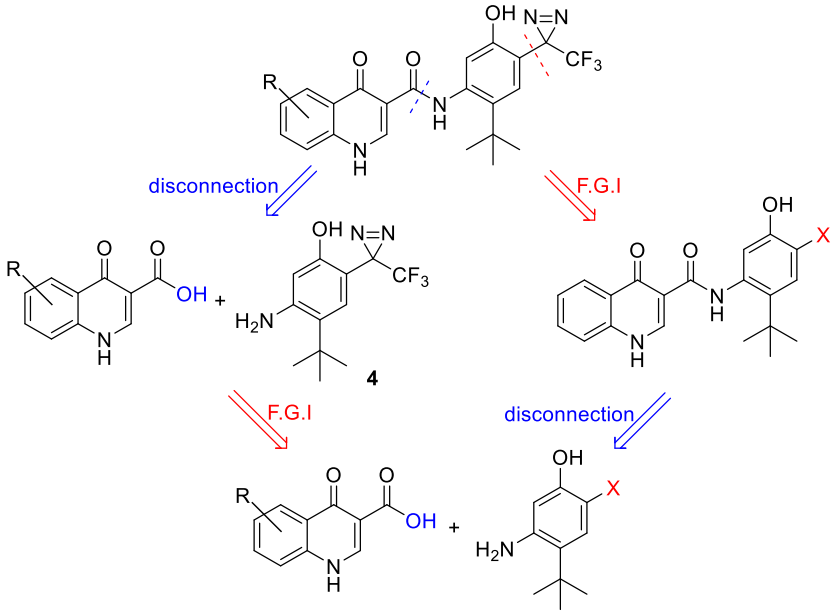

Figure 21 Retrosynthetic disconnection options

From a medicinal chemistry perspective, performing the amide bond formation after installing the diazirine (compound **4**), would allow for late-stage elaboration to LHS analogues containing various synthetic, purification, or analysis handles such as: acetylenes for “click-chem”, dansyl groups for FRET, or iodine to allow for installation of a tritium radio-label. However, this route requires use of protecting groups during the diazirine synthesis to mask the aniline functionality, which adds synthetic steps and possible complications in removal of the protecting groups.

Performing the amide bond formation prior to the diazirine synthesis would be a more linear synthetic approach; however, this would mean that for any LHS analogues, elaboration would happen at an early stage requiring synthetic optimization for each LHS-RHS analogue

combination. As such, initial synthetic efforts were focused on installing the diazirine prior to forming the amide bond.

Regardless of which synthetic approach is taken, for both compounds **2** and **3**, both retro-synthetic options lead back to a RHS aniline-phenol intermediate featuring a synthetic handle allowing installation of the trifluoromethylketone (§1.4.2), as well as the commercially available LHS 4-oxo-1,4-dihydroquinoline-3-carboxylic acid (**5**).

In considering the retrosynthesis of the aniline-diazirine-phenol **4** and the corresponding intermediate (compound **8**) for the synthesis of compound **3**, possible options involved installing the trifluoromethylketone required for the diazirine (compounds **6** and **9**) via lithium-halogen exchange reactions from a halide or Friedel-Crafts type reactions. In searching the literature, compounds **7** and **10** were identified as potential intermediates that would afford the trifluoromethylketones **6** and **9**. The syntheses for **7** and **10** were adapted from the Vertex patent literature (Figure 23).[163,164]

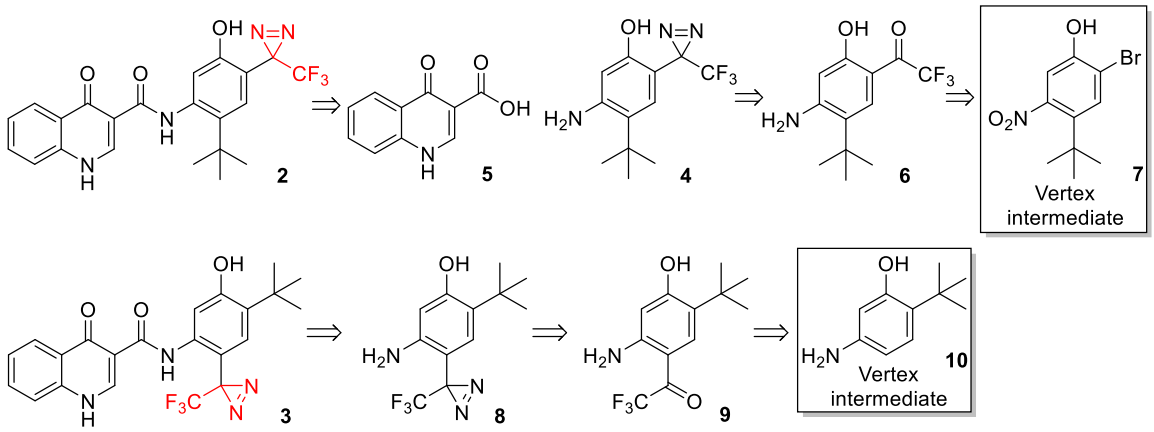

Figure 22 **Retrosynthetic analyses for the aniline-diazirine-phenols 4 and 8 to be used in the synthesis of the PAL ivacaftor probes.**

2.2. Adapted Vertex Chemistry

The RHS intermediate **7** required for the synthesis of **2** was prepared from commercially available phenol **11**, the synthesis of which was adapted from a Vertex Patent.[163] Namely, (Figure 23) bromination of 4-*tert*-butyl phenol **11** afforded bromo-phenol **12** in quantitative yield. Phenol **12** was then protected as a carbonate to give compound **13**, which during the

subsequent nitration produced a 9:1 mixture of the desired regioisomer nitro **14** and the corresponding 6-nitro isomer.[163,165] The mixture was subsequently treated with potassium hydroxide in methanol to remove the carbonate groups, and the nitro-phenol regioisomers were then separated via silica chromatography to provide crystalline solid bromo-nitro-phenol **7** in ~60% yield over 4 steps.

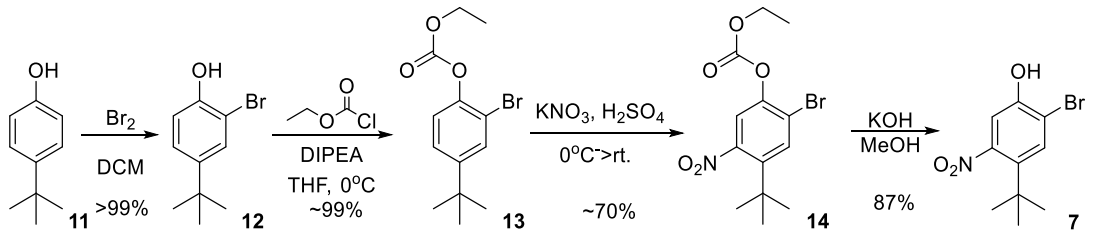

Figure 23 Synthesis of 2-bromo-4-(*tert*-butyl)-5-nitrophenol.

Compound **10** was prepared based on a procedure adapted from a Vertex Patent (Figure 24).[164] Aniline **15** was nitrated in a mixture of H_2SO_4 and solid KNO_3 to produce aniline-nitro **17** in 72% yield. The amino group of compound **16** was diazotized and subsequently hydrolyzed to produce phenol **17** in 66% yield as red/brown crystals. The nitro group of compound **17** was hydrogenated to produce aniline-phenol **10** in 84% yield as white crystalline solid.

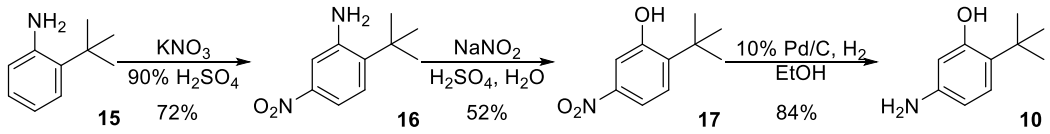

Figure 24 Synthesis of 5-amino-2-(*tert*-butyl)phenol.

Chapter 3.

Synthesis of 5-amino-4-(*tert*-butyl)-2-(3-(trifluoromethyl)-3*H*-diazirin-3-yl)phenol (4)

Having identified intermediate **4** as a desired intermediate in the synthesis of **2**, initial efforts focused on utilizing compound **7** as a starting point. In order to mask the phenol and aniline moieties of compound **4** during the installation of the diazirine, various protecting groups were utilized. The following chapter will discuss some of the various routes which were attempted, as well as the ultimately successful synthesis of the aniline-phenol-diazirine **4**.

3.1. Synthesis of the diazirine with the use of benzyl protecting groups on the aniline and phenol moieties

The first synthetic route attempted towards compound **4** began with protecting the phenol of compound **7** with a benzyl group to give compound **18**. As aryl-nitro groups are known to react with organolithium reagents,[166] conditions were established to selectively reduce the nitro group of compound **18** over the aryl-bromide bond with iron and ammonium chloride to give aniline **19**, which was then protected with benzyl groups to give compound **20**. The tri-benzylated species (Figure 25) was devised with the intent that following installation of the diazirine (giving compound **25**), it would be possible to selectively hydrogenate the benzyl protecting groups to afford the globally deprotected intermediate **4**.[167] Lithium-halogen exchange of bromide **20** with *n*-BuLi at -78^{o}C in THF followed by reaction with ethyl trifluoroacetate gave trifluoromethylketone **21**. Following methods similar to those described previously (§1.3.4), diazirine **25** was successfully prepared. While this route afforded the protected diazirine **25**, the global deprotection to give **4** was ultimately unsuccessful.

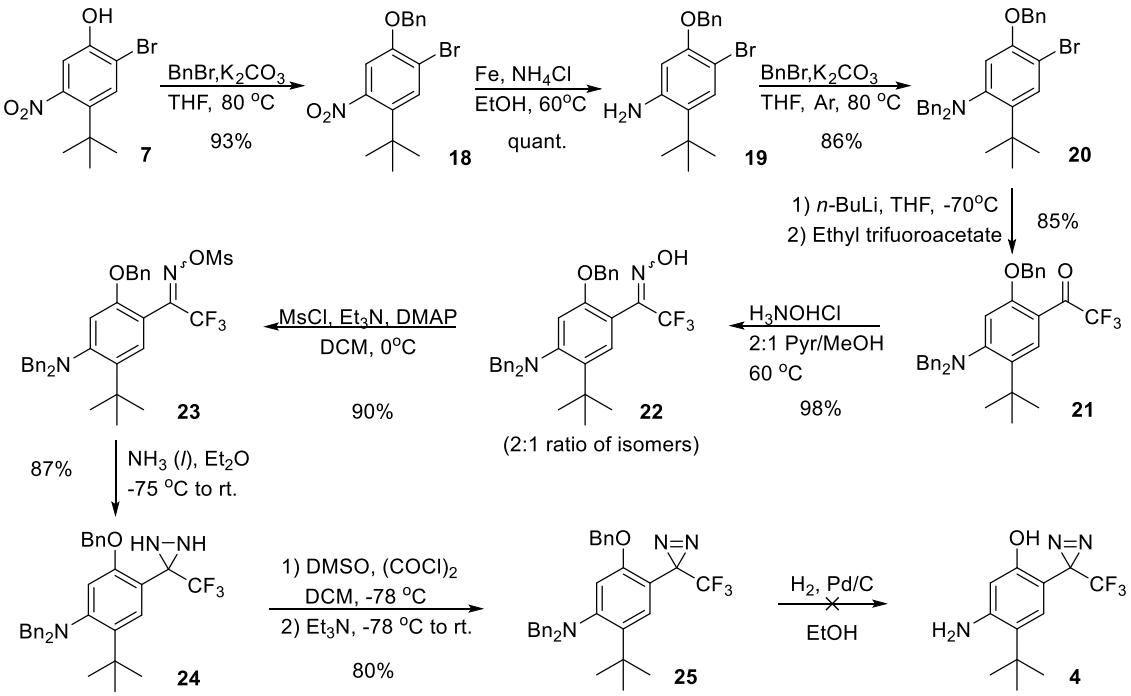

Figure 25 Installaion of the diaziring using benzyl protecting groups on the aniline and phenol moieties

While **4** was not observed by mass-spectrometry following hydrogenolysis, a species was isolated which had a mass consistent with decomposition of the diazirine as well as loss of the three benzyl groups. Although a variety of reduction conditions were attempted, conditions were not found which gave evidence of the desired compound **4**. Orthogonal approaches which aimed to remove the *O*- and *N*-benzyl groups were also attempted including, utilizing BBr_3 to remove the *O*-Bn protection; however, removal of the *N*-Bn_2 protecting groups was not successful.

3.2. Nitrating aromatic ring after diazirine installation

As an alternative to carrying a protected nitrogen species through the diazirine synthesis, the work by Brunner,[148] and Hatanaka *et al.*[168,169] suggested it could be possible to nitrate following the diazirine installation. It was hoped that the ethyl-carbonate group could be used in a similar manner as before to aid in directing the ultimate nitration to the position *meta* to the oxygen in the presence of the diazirine. However, as carbonate groups are base-labile and the diazirine synthesis involves multiple steps in basic conditions, the carbonate group

would have to be installed after synthesizing the diazirine and a base stable phenol protecting group would be required. In place of the *O*-Bn protecting group, the readily acid-labile ethoxymethyl ether (EOM, a MOM analogue) phenol protecting group was chosen.

After protection of phenol **12** with chloro-methyl ethyl ether to give compound **26**, lithium-halogen exchange with *n*-BuLi followed by quenching with ethyl trifluoroacetate gave trifluoromethylketone **27**. Diazirine **31** was synthesized in four steps from compound **27** following established methodology; proceeding through oxime **28**, to the mesyl-oxime **29**, followed by rearrangement to diaziridine **30**, and oxidization using a Swern reaction to give diazirine **31**. The EOM group of compound **31** was successfully removed using TFA in DCM to give phenol **32** which was protected using ethyl chloroformate to give carbonate **33**. However, unlike in the previous nitration reactions, conditions could not be established which directed the nitration to the position *meta* to the oxygen.[145,152] The loss of selectivity for directing the nitration may be because the *o,p*-directing character of bromide is stronger than that of the diazirine. A similar report in the literature using a phenyl-carbonate to direct the nitration to the *meta* position lost selectivity with the removal of a halide *ortho* to the oxygen, suggesting that the carbonate aids in directing the nitration by tuning the directing capability of the oxygen, and allowing the *o,p*-directing character of the halide to play a dominant role in the selectivity.[165]

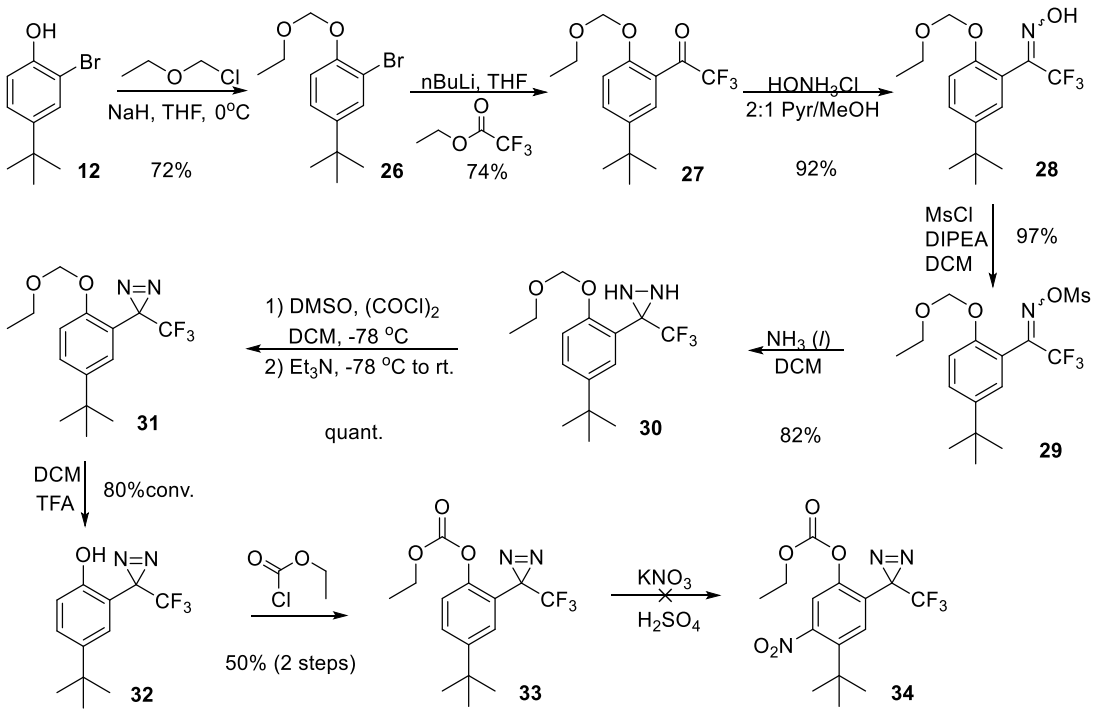

Figure 26 Synthesis of the diazirine prior to the installation of the aniline moiety

3.3. Installation of diazirine with acid-labile protecting groups on the aniline and phenol moieties

As efforts to install the nitrogen functionality onto the ring after installation of the diazirine were unsuccessful, synthetic routes to install the diazirine were again attempted with the nitrogen functionality on the ring already in place. Having found that the *O*-EOM protecting group was readily removed with acid in the previous series (compound **31** to **32**), two synthetic routes were devised which utilized acid-labile aniline protecting groups in order to enable a 1-step global deprotection (following installation of the diazirine group) to give compound **4**. It was hoped that following global deprotection compound **4** could be used in amide coupling reactions to give easy access to compound **2** as well as any other desired LHS analogues. Two aniline protecting groups, (which are both base-stable and acid-labile) that could be used are the pivaloyl (Piv) and *t*-butyl carbonyl (Boc) groups. Syntheses were performed for both *N*-Boc (Figure 27) and *N*-Piv (Figure 28) RHS analogues.

The synthesis using the *N*-Boc protecting group began with protection of phenol **7** with chloromethylethyl ether to give compound **35**. Reduction of the nitro group on compound **35**

with iron and ammonium chloride gave aniline **36**. Protection of aniline **36** was performed successfully with di-*tert*-butyl dicarbonate (Boc_2O) in THF to give compound **37**. To perform the lithium-halogen exchange of the bromide of compound **37** to give the trifluoromethylketone **38**, methyl lithium (MeLi), was added to deprotonate the carbamate; followed by addition of *n*-BuLi, and reaction with ethyl trifluoroacetate. Trifluoromethylketone **38** was reacted with hydroxylamine hydrochloride in a 2:1 pyridine/methanol mixture to give a mixture of isomers of oxime **39**. Tosylation (or mesylation, not shown) of **39** with tosyl chloride (or mesyl chloride) gave tosyl-oxime **40**. While the reaction of tosyl-oxime **40** (or the mesyl-oxime equivalent) with liquid ammonia successfully gave diaziridine **42**, a significant amount of material was converted to a byproduct which was later identified as amidine **41** (discussed later). While compounds **41** and **42** had similar retention times on silica chromatography, it was possible to obtain partial separation of the two compounds by recrystallization (amidine **41** crystallized slightly before diaziridine **42** from a DCM/Hexanes mixture), as well good separation on a small scale by high-pressure liquid chromatography (HPLC). While this process was useful for characterization, it was noted that the (at this point unidentified) amidine **41** was not affected by the oxidation conditions which successfully converted diaziridine **42** to diazirine **43**. Using this observation, when subsequent repeats of the synthesis were performed on larger scales, the oxidation to give diazirine **43** was performed on the mixture of compounds **41** and **42**. This enabled separation and isolation of the less polar diazirine **43** from amidine **41** via silica chromatography.

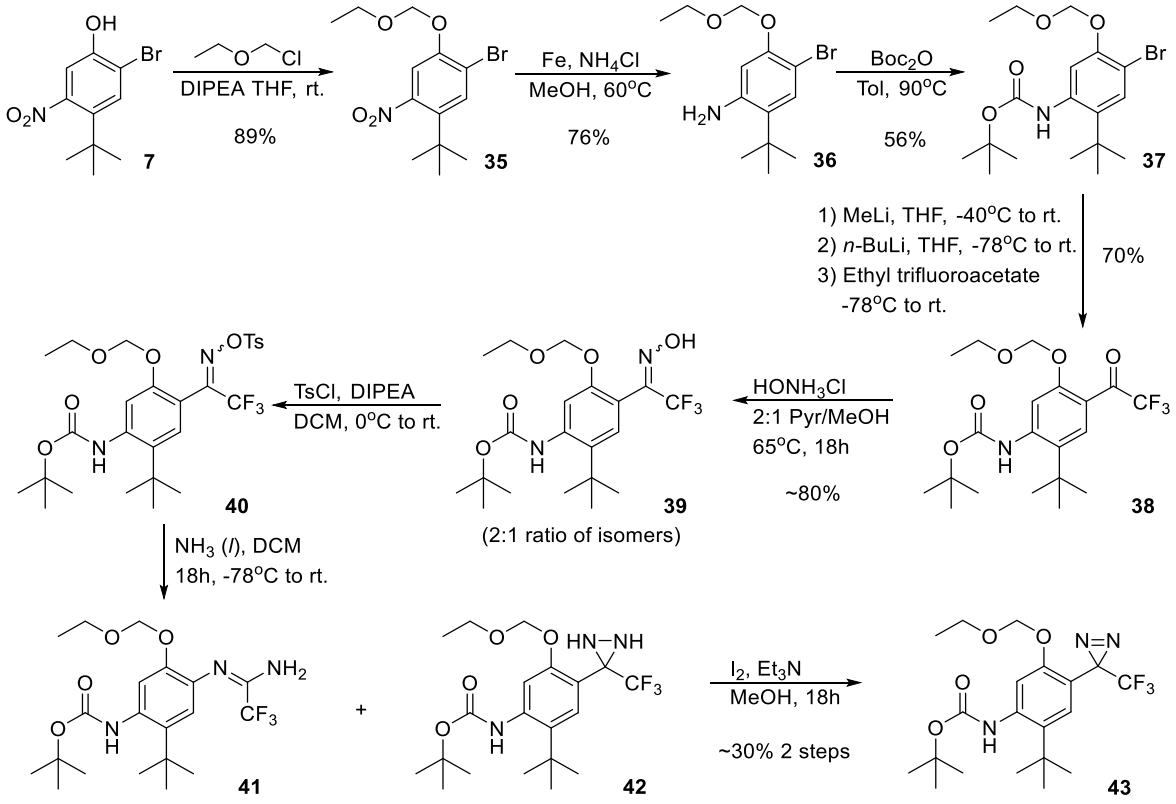

Figure 27 Synthetic scheme for diazirine installation utilizing an *N*-Boc protecting group.

Prior to and concurrent with the synthesis of compound **43**, a similar synthesis was performed utilizing an *N*-Piv protecting group (Figure 28). Reaction of aniline **39** with pivaloyl chloride (PivCl) in dichloromethane (DCM) in a microwave reactor gave compound **44**. Similar to the *N*-Boc metalation (Figure 27), in order to perform the lithium-halogen exchange on compound **44**, methyl lithium (MeLi), was added to deprotonate the pivalyl group; followed by addition of *n*-BuLi, and reaction with ethyl trifluoroacetate to provide compound **45**. The synthesis of diaziridine **49** proceeded in a similar manner as that of diaziridine **42** with significant conversion of mesyl-oxime **47** to byproduct amidine **48** and a lesser amount of compound **49**. The timeline for this synthesis arrived at diaziridine **49** around a similar time as for the *N*-Boc diazirine **43** and while evidence of the conversion of diaziridine **49** to diazirine **50** was observed by mass spectrometry in test reactions, this species was not isolated and the *N*-Piv route was halted while exploring the results of the *N*-Boc synthetic route (Figure 27).

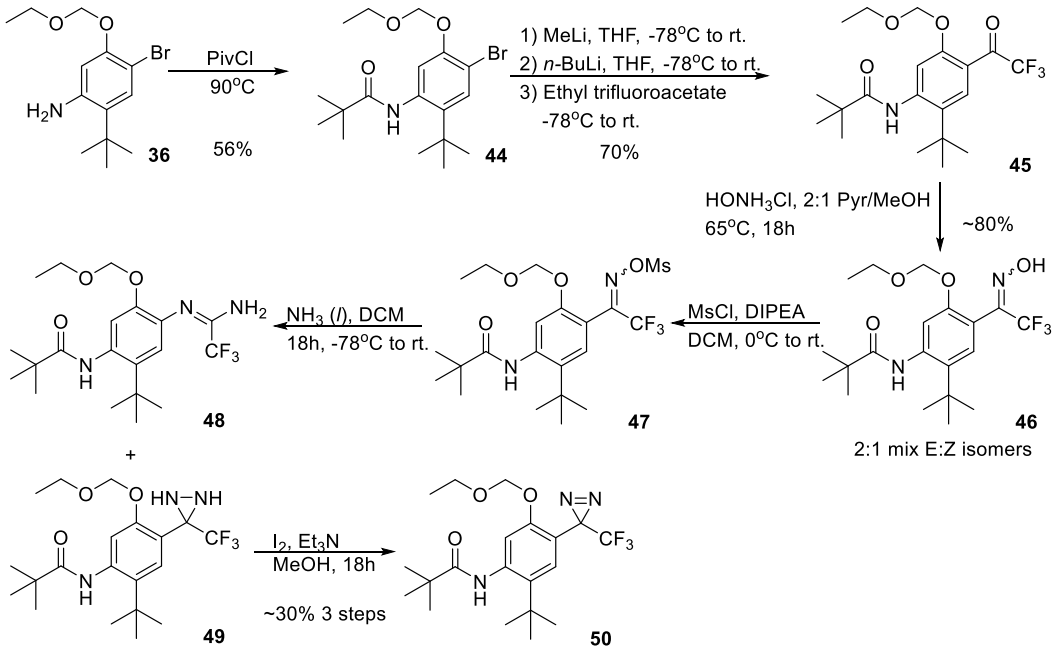

Figure 28 Synthetic scheme for diazirine installation utilizing an *N*-Piv protecting group.

3.3.1. Identification of the amidine byproduct obtained during diaziridine synthesis

During the synthesis of both compounds **42** and **49** a byproduct was observed with identical mass to their diaziridine counterparts but containing a broad 2H singlet in the ^{1}H NMR instead of the characteristic pair of 1H doublets expected for the diaziridine. Ultimately species **41** was confirmed to be an amidine through x-ray crystallography (Figure 29). These amidine byproducts were most likely the result of a Beckmann rearrangement, and were observed for both tosyl- and mesyl-oxime versions of compounds **39** and **47**. Although trifluoroacetamidines have previously been prepared in the past by reaction of nitriles and amines[170,171], the work presented here is the first report in the literature of a trifluoromethylamidine produced via a trifluoromethyl tosyl-oxime. As well, placing the double bond in conjugation with the phenyl ring is supported by data from the single crystal x-ray diffraction of **41** (Figure 29-B), which indicated that the bond between N1-C11 was shorter than the bond between N3-C11 (Table 1).

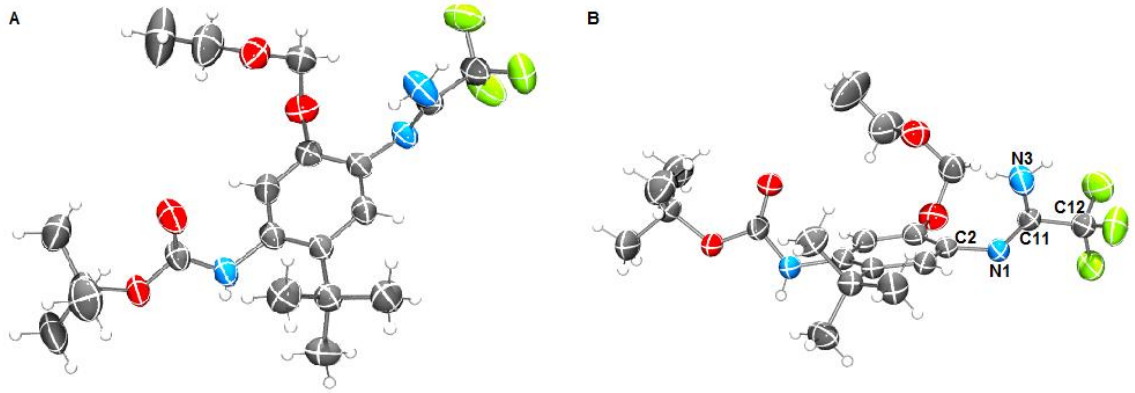

Figure 29 **Crystal structure of compound 41. A) View describing connectivity B) Confirming tautomeric form of amidine in the crystal structure, bond distances listed in Table 1**

Table 1. **Bond distances of residues in the amidine moeity**

Bond	Distance /Å
N1 - C11	1.270(3)
N3 - C11	1.327(3)
C11 - C12	1.519(4)
N1 - C2	1.426(3)

While Beckmann rearrangements are classically performed at high temperatures in harsh conditions,[172] a report by Takuwa *et al.*[173] showed that an oxime following subsequent treatment with trifluoromethanesulfonic anhydride and ammonia at low temperature can undergo Beckmann rearrangement to an amidine. Takuwa *et a.l*[173] propose a mechanism similar to that shown in Figure 30-A, in which a tosyl oxime undergoes a [1,2]-shift to form the imino-carbocation **51** which is subsequently attacked by ammonia to give the amidine; however, in the case of the trifluoromethyltoxyl-oximes **40** and **47** one would expect the alpha trifluoromethyl group would supress this reaction. An alternative mechanism (Figure 30-B) could involve a concerted rearrangement involving the formation of a three membered ring (structure **52**) followed by attack of ammonia to finish the rearrangement.[174]

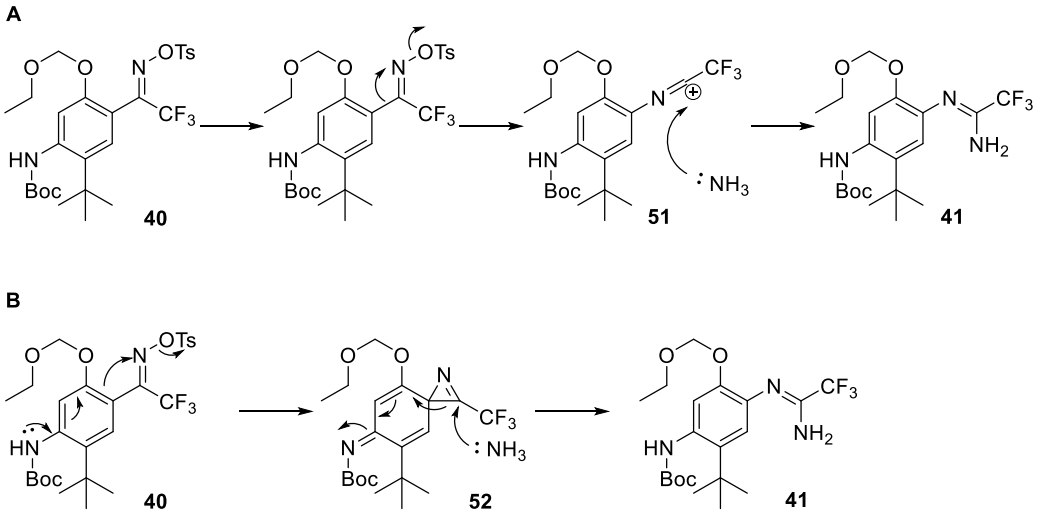

Figure 30 Proposed mechanisms for Beckmann rearrangement to amidine 41.

Presumably, as the Beckmann rearrangement was not observed in the conversion of the previous trifluoromethyl mesyl-oximes **25** and **32**, the *para*-NH may play a role in favouring this transformation, through electron donation into the aromatic ring. Interestingly, conversion to the amidine from the tosyl –oximes (or mesyl-oximes) was greater for the *N*-Boc analogue versus the *N*-Piv analogue, and both formed an amidine species in a greater ratio than for the 4-oxoquinoline analogue **65** (Figure 37, p.51). These observations suggest that the electronics of the *para*-nitrogen may play a role in enabling this transformation. Although circumstantial, this may explain the scarcity of published examples of diaziridines with a protic-*para*-nitrogen. In a series of phenyltrifluoromethyltosyl oximes featuring hydrazine groups, conversion to a diaziridine for a *para*hydrazine analogue gave a 7% yield compared to 77% for the *meta*-hydrazine analogue (Figure 31),[175] though the authors make note of the discrepancy in yields they do not ascribe a cause.

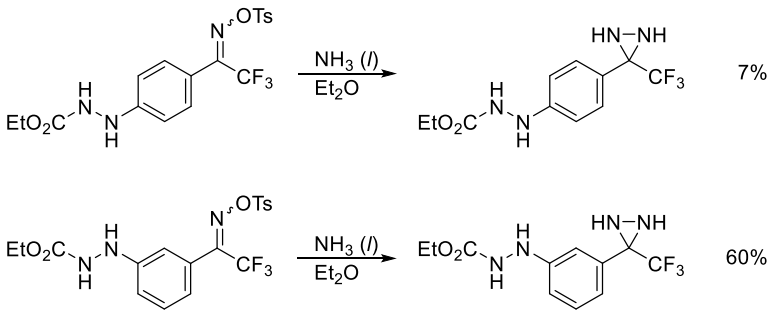

Figure 31 Literature yields for trifluoromethylphenyldiaziridines with a hydrazine in *para* and *meta* positions.[175]

3.3.2. Deprotection of diazirine 43 and attempted amide bond formation with compound 5

In order to confirm that the diazirine exhibited photolytic reactivity, a solution of diazirine **43** in methanol was exposed to UV light to generate the methanol photo-adduct **53** (Figure 32). This species was confirmed by mass spectrometry and NMR spectroscopy.

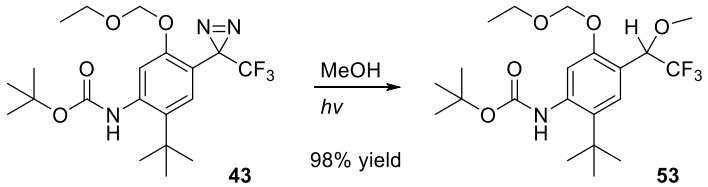

Figure 32 Photolysis of compound 43 in methanol

The deprotection of the diazirine **43** with methanolic hydrogen chloride was successful in giving the desired intermediate aniline **4**; however this intermediate proved too unstable to survive the subsequent amide bond formation with 4-oxo-1,4-dihydroquinoline-3-carboxylic acid (**5**). Indeed, this compound had degraded ~30% by ^{1}H and ^{19}F NMR within 10 minutes in an amber NMR tube and interior lighting turned off, giving what appeared to be the deuterated methanol photo-adduct by LC-MS, though this potentially implies a “dark” reaction, possibly via isomerization to the diazo and subsequent carbene formation, regardless, the compound readily degraded on a short time-scale. For the amide bond forming reactions, attempting to give compound **2**, the major species from these reactions contained a proton (and another group) apparently attached in place of the diazirine. Many conditions were evaluated to affect the amide coupling of aniline **4** with the LHS acid **5** but without success.

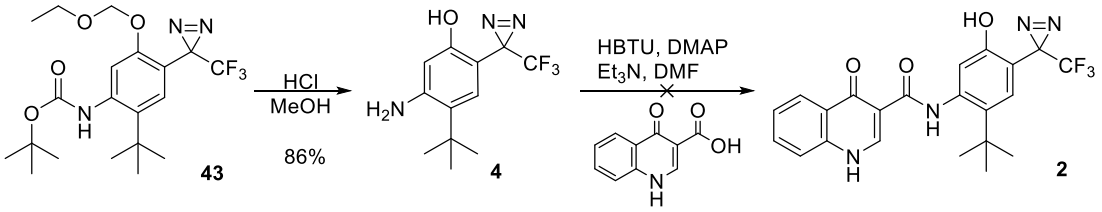

Figure 33 Global deprotection of compound 43 to give compound 4 and attempted amide coupling reactions

Other phenol-aniline-diazirines have been reported by Kosemura *et al.*[176] who were able to generate the phenol-aniline-diazirine **55** (Figure 34). Although the authors were able to quickly protect the *ortho*-phenol-aniline as carbamate **57**, they note that the intermediate **55** was highly susceptible to degradation, though the authors ascribe this to possible oxidation in air.[176]

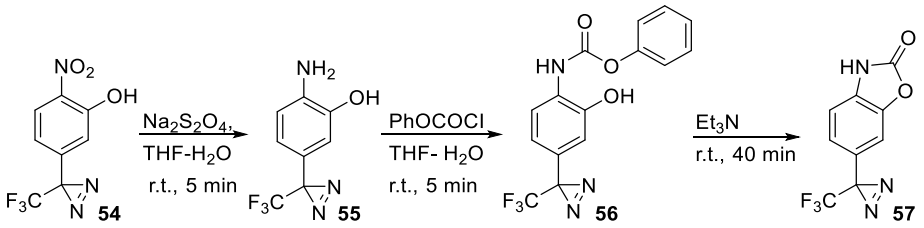

Figure 34 Synthesis by Kosemura *et al* of diazirine 57

Due to the instability of aniline **4** it was hoped that a fast amide bond forming reaction could be found to enable the synthesis of compound **2** before decomposition. The work by Hadida *et al*.[70] on the discovery of ivacaftor reported use of HATU in the amide bond formation, with an 18 hour reaction time with yields ranging from 50-80%. Indeed, experiments using the intermediate **58** (obtained through deprotection of compound **40** using methanolic hydrogen chloride similar the conditions used to produce aniline **4**) (Figure 35), indicated that the amide bond formation was slow and only partial conversion was observed after 18 hours at room temperature. A search through the patents filed by Vertex on the synthesis of their analogues indicated that many other amide bond forming conditions were tolerated, including the use of pentafluorophenyl esters, mixed anhydrides, T3P, acyl chlorides, and other agents similar to HATU.[163,164] Despite attempts with a variety of amide bond forming conditions, compound **2** could not obtained from aniline **4**.

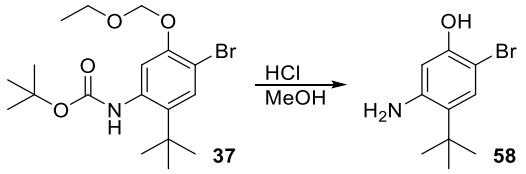

Figure 35 Modelling global deprotection conditions with methanolic HCl

However, synthesizing aniline **4** was an important milestone for exploring the possibility of route towards compound **2** that would afford late-stage elaboration to LHS analogues. Having found the aniline-diazirine-phenol **4** to be too sensitive to survive the amide bond formation in the attempted conditions, the possibility of an orthogonal deprotection was explored. One possible route was the selective removal of the *N*-Boc group resulting in an intermediate that could be stable enough to survive the amide bond formation. While conditions were found which selectively removed the Boc group from compounds bromo **37** and trifluoromethylketone **38** using TBAF in THF[177], similar reactions were unsuccessful for the deprotection of the diaziridine **42** or diazirine **43**.[178] These studies showed that the diazirine was stable as long as the *N*-H was in an amide bond and with this result, it was decided that forming the amide bond at an earlier stage in the synthesis of the diazirine might be a more successful option.

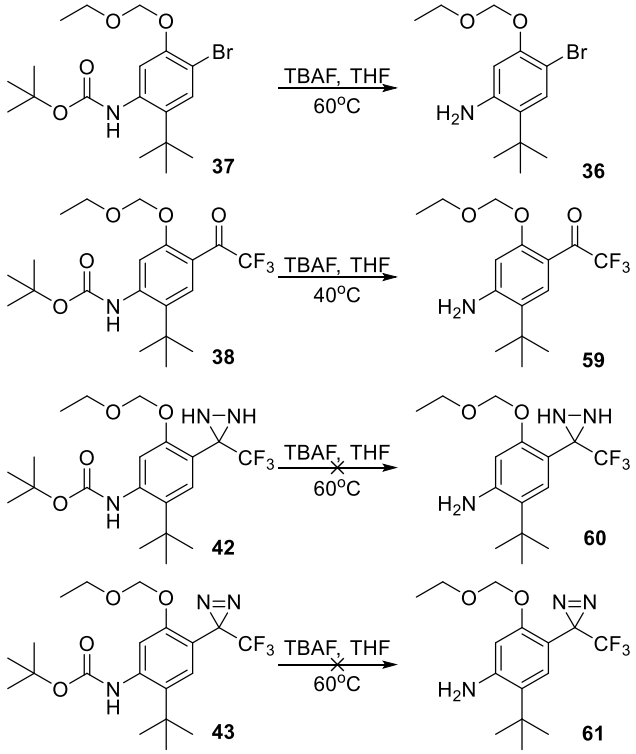

Figure 36 Methods attempted for the selective deprotection of the *N*-Boc group

Chapter 4.

Synthesis of *N*-(2-(*tert*-butyl)-5-hydroxy-4-(3-(trifluoromethyl)-3*H*-diazirin-3-yl)phenyl)-4-oxo-1,4-dihydroquinoline-3-carboxamide (2)

Having a significant quantity of compounds *N*-Boc-bromo **37** and *N*-Boc-trifluoromethylketone **38** on hand, as well as effective conditions for selective *N*-Boc cleavage to give anilines **36** and **59**, an attempt was made to pursue a synthetic approach towards target diazirine **2** which involved forming the amide bond prior to installing the diazirine. Formation of the amide bond was attempted with both anilines **36** and **59** in concurrent efforts. The amide bond formation with **36** using HATU, DMAP, HOBt, and DIPEA in DMF at 60^{o}C for 48 h gave bromo-amide **62** in good yield; however, conditions could not be established which produced trifluoromethylketone-amide **63** from aniline **59**.

Lithium-halogen exchange of bromo **62** was achieved with MeLi added first to deprotonate the 4-oxoquinoline and amide nitrogens (to prevent proton quenching of the carbanion during the lithium-halogen exchange), and then *n*-BuLi was added to generate the tri-anion, which upon reaction with ethyl trifluoroacetate produced trifluoromethylketone **63** as one of a mixture of products. Analysis of the product mixture by high pressure liquid chromatography (HPLC) and mass spectrometry (MS) identified five species including: the desired trifluoromethylketone **63**, its hydrate and ethanol hemi-acetal species, as well as unreacted starting material bromo **62**, and the proton-quenched product. Presumably the presence of bromo **62** and the proton quenched species indicated that the MeLi deprotonation did not go to completion. If the deprotonation did not proceed to completion, then on addition of *n*-BuLi, some of this reagent would be consumed generating butane; as well, some of the successfully lithium exchanged species would be quenched *in situ*. However, even significantly increasing the amount of MeLi failed to fully solve this issue. Regardless, in subsequent repetitions of this reaction, the crude material containing a mixture of trifluoromethylketone **63** and its related

species was carried forward without purification into the oxime **66** formation reactions. In these reactions all of the **63** related species were successfully converted to oxime **64** as a mixture of isomers, which were successfully isolated by precipitation from methanol/DCM/hexanes without need for further chromatography in 66% yield over the two steps.

In designing this synthetic route it was noted in the literature that it was possible to form a tosylate at the 4-oxoquinoline nitrogen,[179] although it was assumed that during the reaction with liquid ammonia this tosyl group would likely be removed. During the tosylation of **64** using 1 equivalent of *p*-TsCl, LC-MS data showed a mixture of species including starting material oxime **64**, and both a singly and doubly tosylated species, indicating tosylation of both the oxime moiety and the 4-oxoquinoline nitrogen. This crude reaction mixture was utilized in the diaziridine formation and, upon reaction with liquid ammonia, no tosylated species remained in the crude mixture, only the desired diaziridine **66**, amidine **65** (isolated, but only confirmed by characteristic ^{1}H NMR signals and by LC-MS), and unreacted oxime. In subsequent reactions with increasing equivalents of tosyl chloride, this profile improved to minimize remaining oxime, and confirming that tosylation of the 4-oxoquinoline nitrogen did not impact the formation of the desired diaziridine **66**. The diaziridine **66** was successfully isolated by preparative-scale HPLC (prep-HPLC) and oxidized with Dess-Martin periodinane to give diazirine **69**.

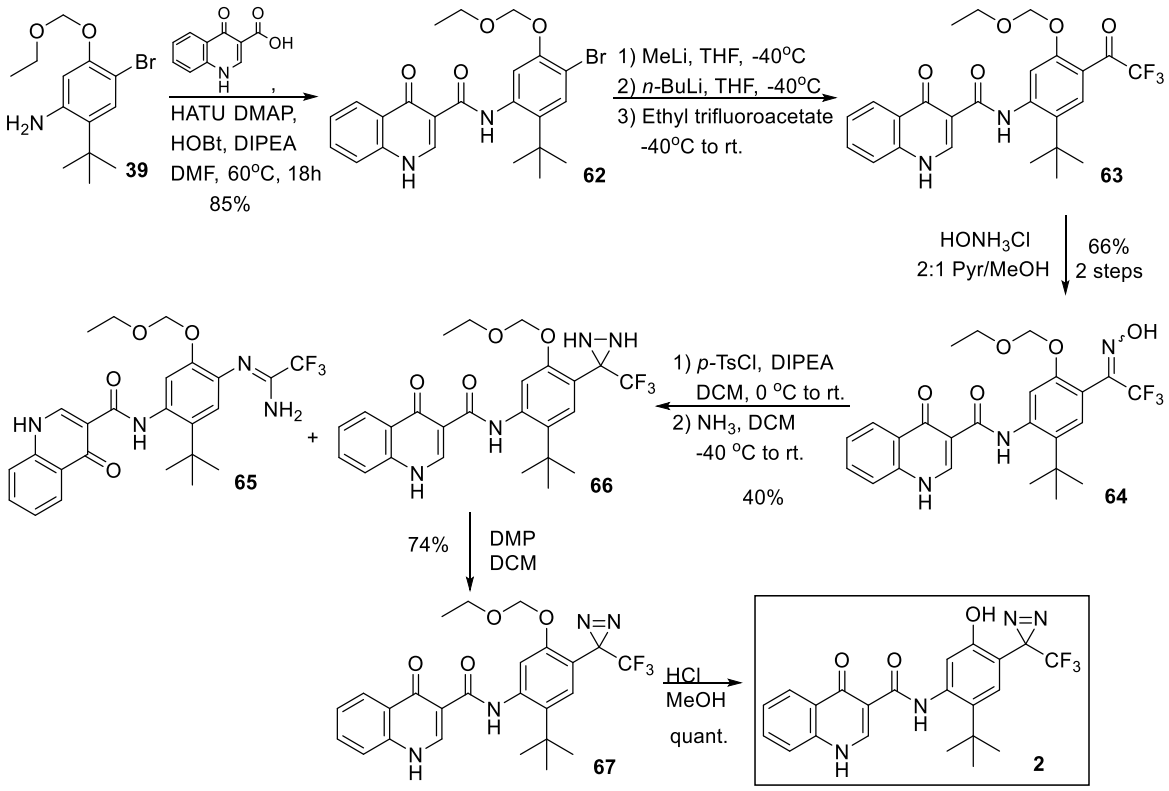

Figure 37 Successful synthesis of ivacaftor PAL probe 2

To model the deprotection of diazirine **67**, conditions were established for deprotection of bromo **62** to give phenol **68** using concentrated methanolic HCl (Figure 38). Using these conditions with diazirine **67** successfully gave the desired PAL probe **2** without need of further work-up or purification.

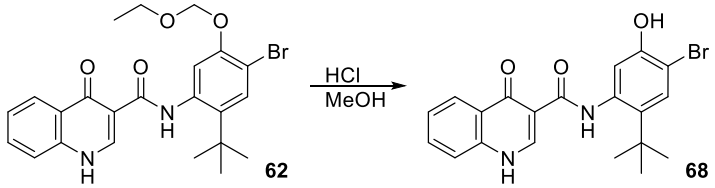

Figure 38 Modelling phenol deprotection conditions using compound 62

During initial attempts to characterize compound **2** in deuterated DMSO, it was found that diazirine **2** was quite unstable at room temperature in this solvent and formed multiple dimeric species apparently resulting from the photolysis of the diazirine. Subsequent attempts to characterize and analyze compound **2** using deuterated methanol were successful as compound **2** showed greater stability at room temperature in this solvent.

As part of the characterization process, the diazirine **2** was assessed in photolysis studies in methanol. Following the progress of the photo-decomposition of **2** in methanol by LC-MS under a mixture of UV and ambient light showed the methoxy photo-adduct product **69** was the major photolytic product; and importantly, species resulting from an intramolecular reaction of the carbene with the adjacent phenol were not observed.

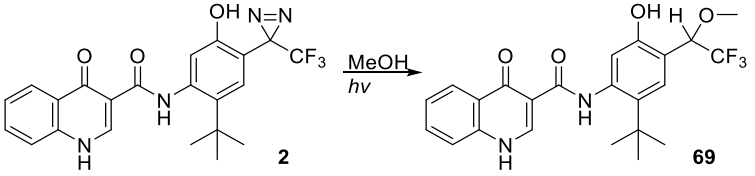

Figure 39 Photolysis of 2 in methanol to give the methoxy adduct 69

Chapter 5.

Conclusion and perspectives

Despite several challenges, a synthesis of the diazirine containing ivacaftor PAL probe **2** was achieved. Having confirmed that in methanol in the presence of light, diazirine **2** forms the methanol adduct **69**, future work will include determining the photolytic half-life of diazirine **2** in methanol and water (to generate an alcohol); as well as determining the confirming the activity and stability of compound **2** in a CFTR potentiation assay. Future synthetic efforts will also focus on completing the synthesis and characterization of compound **3**.

As ivacaftor is known to have significant interactions with plasma proteins (>97% plasma-protein bound),[180] model PAL experiments with **2** will be performed with the plasma proteins, human serum albumin (HSA), and α_1-acid glycoprotein (AGP). Both of these proteins are commercially available and small enough to be analyzed on the mass spectrometer in our lab. As both HSA and AGP are inexpensive and readily available (in stark contrast to CFTR), these proteins will be useful in developing an optimized protocol for the PAL studies with mutant CFTR.

HSA is the most prevalent plasma protein functioning as a transporter.[180] HSA has two major drug binding sites, as well as up to 7 fatty acid binding sites; however no difference was noted in the binding of ivacaftor to non-delipidated and delipidated HSA.[180] AGP is the principle extracellular lipocalin in the blood plasma and is responsible for the transport of a variety of compounds. Commercially available AGP preparations are a heterogeneous mixture of two major variants (A and F1*S); while this may complicate the analysis of PAL studies, many binding studies have utilized these preparations as they more closely resemble an *in vivo* setting. As well, as AGP is a glycosylated protein, it may require de-glycosylation prior to analysis by mass spectrometry.

The recent study by Schneider *et al*.[180] measured the binding affinities and inhibition constants (Ki's) of ivacaftor (and other drugs commonly used in the treatment of CF) to HSA and AGP proteins and showed that ivacaftor binds to AGP, with a K_i (a measure of drug affinity) of 0.13 ± 0.02 μM (indicating a strong affinity for AGP) and binding affinities for HSA of K_D = 15.3 μM[180]. As well, *in silico* modelling of the putative AGP binding of site of ivacaftor indicated that the *t*-butyl group on ivacaftor that is substituted for a diazirine on **2** may provide an interaction with the protein. While human serum albumin is more commonly used to test for drug-plasma protein interactions, the strong binding affinity of ivacaftor for AGP indicates it may be useful for modelling the conditions required for PAL with **2**

After confirming the potentiating activity of **2** and determining a protocol for the PAL studies with AGP and HSA. **2** will be utilized in PAL studies with both purified ΔF508-CFTR and whole cell constructs. Complicating the analysis of the PAL studies is the large size of CFTR (>170 kDa), which may require partial proteolytic digestion of the labelled protein into its constituent domains for analysis by mass spectrometry. In order to aid in the separation and isolation of labelled domains, future probes (currently in progress) will incorporate an acetylene moiety on the LHS which will enable "clicking" the labelled protein to either a biotin tag, or a fluorescence tag.

Appendix A.

Experimental Details

General Experimental:

THF was distilled from Na and benzophenone under N_2. *N,N'*-diisopropylethylamine (DIPEA) and triethylamine (Et_3N) were distilled from CaH_2 and stored under N_2. All other reagents and solvents were used as received from commercial suppliers unless otherwise stated. Analytical thin-layer chromatography (TLC) was performed on aluminum plates pre-coated with silica gel 60F-254 as the absorbent, and eluted with the solvent systems indicated, visualization of the plates was done with UV light (254 nm) and the indicated stains. Flash chromatography was performed with a Biotage Isolera One system using SiliCycle Silia*Sep*™ Cartridges of indicated size and solvent gradient. ^{1}H, ^{19}F and ^{13}C NMR spectra were recorded with either Bruker Avance II™ 600 MHz, Bruker Avance III™ 500 MHz or Bruker Avance III™ 400 MHz. ^{1}H and ^{13}C NMR spectra were referenced to the various solvent signals[181] and processing of the spectra was performed with MestRec™ software (Note: numbering of atoms for the purposes of signal assignment did not follow IUPAC numbering schemes). The high-resolution mass spectra were recorded in positive ion-mode with an ESI ion source on an Agilent™ Time-of-Flight LC/MS mass spectrometer Model 6210). All HPLC analyses were performed utilizing a Advanced Materials Technologies Halo™ C18 reverse-phase analytical 5µ column (4.6 × 50 mm). All HPLC purifications were carried out using a Phenomenex Kinetex 5µ C18 reverse-phase preparatory column (21.2 × 150 mm). UV-Vis spectra were collected in solution phase in a quartz cuvette on a Varian Cary 5000 UV-Vis-NIR Spectrophotometer. ATR spectra were collected with a Perkin Elmer Spectrum Two™ FT-IR spectrometer, and absorption bands were designated as weak (w), broad (br), medium (m), or strong (s). Photo-decomposition studies were performed (when indicated) in a light-box composed of two Dreamall 36W UV Acrylic Curing Light Lamps taped together each with 4 x 9W UV bulbs emitting at 365 nm.

Single-Crystal X-ray diffraction structure determinations for each compound single crystals were selected and mounted using Paratone oil on a 150 µm MiTeGen Dual-Thickness MicroMount. Data was collected at room temperature with a Bruker SMART APEX II Duo CCD diffractometer using a TRIUMPH graphite-monochromated Cu-Kα radiation (λ = 1.54184 Å).

Crystallographic information for **41** can be found in Table 2 in Appendix A. All diffraction data were processed with the Bruker Apex II software suite. Initial solutions were obtained by using the intrinsic phasing method[182] with subsequent refinements performed with SHELXL[183] on the SHELXle platform[184]. Diagrams were prepared by using ORTEP-3[185] and POV-RAY[186]

Experimental Procedures

1-(Benzyloxy)-2-bromo-4-(*tert*-butyl)-5-nitrobenzene (18)

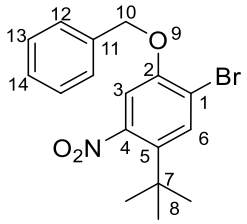

A mixture of 2-bromo-4-(*tert*-butyl)-5-nitrophenol (**7**) (2.82 g, 10.3 mmol), KI (170 mg, 1.0 mmol, 0.2 equiv.), and K_2CO_3 (3.55 g, 25.7 mmol, 2.5 equiv.) was dissolved in THF (10 mL) in a 10 mL microwave vial. Benzyl bromide (1.84 mL, 015.5 mmol, 1.5 equiv.) was added via syringe, and the reaction vessel was sealed then purged with Argon and the reaction mixture was heated at 80 °C for 2 hours in a microwave reactor. The progress of the reaction was monitored by TLC (5% EtOAc/Hexanes {Hex}, product rf. 0.3. The reaction mixture was cooled then quenched with water (5 mL) and sat. $NaHCO_3$ (*aq.*, 10 mL). The mixture was transferred to a separatory funnel and extracted into EtOAc (30 mL). The organic fractions were combined and washed with sat. aq. $NaHCO_3$ (30 mL), brine (30 mL) dried over Na_2SO_4, filtered and concentrated to dryness. The crude material was purified by automated flash chromatography on an 80 g silica cartridge, and eluted (0-10 % EtOAc/Hex gradient) to give compound **18** as a light yellow crystalline solid (3.5 g, 9.6 mmol, 93% yield).

^{1}H NMR (500 MHz, $CDCl_3$) δ 7.72 (s, 1H, C-6-*H*), 7.47 – 7.43 (m, 2H, C-12-*H*), 7.43 – 7.38 (m, 2H, C-13-*H*), 7.37 – 7.33 (m, 1H, C-14-*H*), 6.89 (s, 1H, C-3-*H*), 5.13 (s, 2H, C-10-*H*), 1.37 (s, 9H, C-8-*H*).

^{13}C NMR (126 MHz, CDCl3) δ 153.4 (*C*-2), 150.4 (*C*-4),135.5 (*C*-11), 135.1 (*C*-5), 133.5 (*C*-6), 128.9 (*C*-13), 128.5 (*C*-14), 127.3 (*C*-12), 115.1 (*C*-1), 109.0 (*C*-3), 71.5 (*C*-10), 35.3 (*C*-7), 30.8 (*C*-8).

HRMS: Did not observe ionization in positive or negative mode on ESI-MS.

m.p. = 77 - 78 °C

5-(Benzyloxy)-4-bromo-2-(*tert*-butyl)aniline (19)

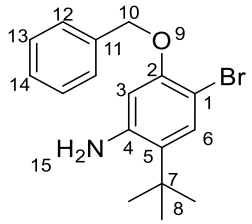

Compound **18** (447 mg, 1.23 mmol) was dissolved in MeOH (10 mL), then Fe powder (400 mg, 7.16 mmol, 5.8 equiv.) and AcOH (glacial, 1 mL) were added and the mixture was stirred at 80 °C for 1 hour. The reaction was monitored by TLC (20% EtOAc/Hex product rf. 0.35, visualized using a ninhydrin stain). Upon completion of the reaction, the mixture was cooled, filtered through a bed of celite, washing solids with MeOH, and then the filtrate was concentrated to dryness. The crude residue was purified by automated flash chromatography on a 25 g silica cartridge (5-50% EtOAc/Hex gradient) to give compound **19** (411 mg, 1.23 mmol, quantitative yield) as a yellow solid foam.

^{1}H NMR (400 MHz, $CDCl_3$) δ 7.50 – 7.45 (m, 2H), 7.42 – 7.36 (m, 2H), 7.35 (s, 1H), 7.35 – 7.29 (m, 1H), 6.26 (s, 1H), 5.08 (s, 2H), 3.83 (s, 2H), 1.38 (s, 9H).

^{13}C NMR (101 MHz, $CDCl_3$) δ 153.8, 145.0, 137.0, 131.3, 128.7, 128.3, 127.9, 127.0, 103.8, 100.4, 70.9, 33.9, 29.8.

HRMS: *m/z* calcd. for $C_{17}H_{20}BrNO$: 336.0781 (M+H); found 336.0801.

m.p. = 85 - 86 ^{o}C

***N,N*-Dibenzyl-5-(benzyloxy)-4-bromo-2-(*tert*-butyl)aniline (20)**

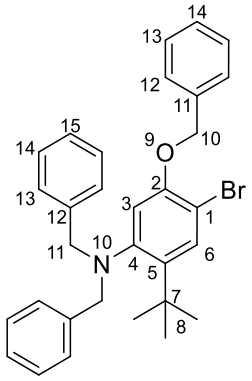

To a solution of aniline **19** (2.57 g, 7.7 mmol) dissolved in acetonitrile (ACN) (20 mL), K_2CO_3 (9.3 g, 76.8 mmol, 8.8 equiv.) was added. The reaction vessel was sealed, purged with argon then BnBr (6.4 mL, 53.9 mmol, 5.0 equiv.) was added via syringe. The reaction mixture was heated at 80 °C overnight and monitored by TLC (5% EtOAc/Hex, product rf. 0.6). Upon completion the reaction mixture was cooled and quenched with H_2O (20 mL), transferred to a separatory funnel and extracted into EtOAc (200 mL). The organic fractions were combined, washed with sat. $NaHCO_3$ (100 mL), brine (100 mL) and dried over Na_2SO_4 then concentrated to dryness. The crude residue was purified by automated flash chromatography on a 120 g silica cartridge (0-1% EtOAc/Hex gradient) to give compound **20** (3.41 g, 6.6 mmol, 86% yield) as a white crystalline solid.

^{1}H NMR (500 MHz, $CDCl_3$) δ 7.54 (s, 1H), 7.39 – 7.27 (m, 11H), 7.19 – 7.14 (m, 4H), 6.41 (s, 1H), 4.83 (s, 2H), 3.96 (bs, 2H), 3.91 (bs, 2H), 1.39 (s, 9H).

^{1}H NMR (400 MHz, $CDCl_3$) δ 7.44 (s, 1H), 7.32 – 7.26 (m, 2H), 7.25 – 7.13 (m, 8H), 7.13 – 7.04 (m, 5H), 6.32 (s, 1H), 4.73 (s, 2H), 3.84 (m, 4H), 1.29 (s, 9H).

^{13}C NMR (101 MHz, $CDCl_3$) δ 152.5, 151.0, 141.9, 137.4, 136.9, 132.0, 130.0, 128.7, 128.3, 128.2, 128.0, 127.3, 127.2, 115.3, 109.2, 77.2, 70.6, 58.3, 35.6, 31.5.

HRMS: *m/z* calcd. for $C_{31}H_{32}{}^{79}BrNO$: 514.1740 (M+H); found 514.1808

m.p. = 133 - 135 ^oC

1-(2-(Benzyloxy)-5-(*tert*-butyl)-4-(dibenzylamino)phenyl)-2,2,2-trifluoroethan-1-one (21)

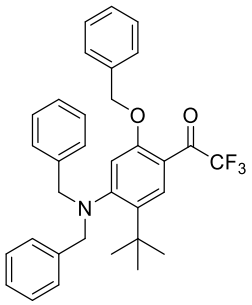

Compound **20** (1.0 g, 1.9 mmol) was dissolved in THF (20 mL) and cooled to -78 °C, then *n*-BuLi (1.5 M in Hex, 2.9 mL, 4.3 mmol, 2.2 equiv.) was added slowly and the reaction mixture was stirred for 15 min. Ethyl trifluoroacetate (2.0 mL, 21 mmol,11 equiv.) was added rapidly and the reaction mixture was warmed to room temperature. The reaction mixture was quenched with sat. NH_4Cl (20 mL), and transferred to a separatory funnel and extracted into EtOAc (50 mL). The organic fractions were washed with brine (60 mL) and dried over Na_2SO_4, and concentrated to dryness. The crude residue was purified by automated flash chromatography on a 50 g silica cartridge (1-20% EtOAc/Hex gradient) to give compound **21** (860 mg, 1.62 mmol, 78 % yield) as a white crystalline solid.

^{1}H NMR (500 MHz, $CDCl_3$) δ 7.82 (s, 1H), 7.42 – 7.27 (m, 11H), 7.21 – 7.09 (m, 4H), 6.40 (s, 1H), 4.80 (s, 2H), 3.97 (s, 4H), 1.47 (s, 9H).

^{19}F NMR (471 MHz, $CDCl_3$) δ -73.3.

HRMS: *m/z* calcd. for $C_{33}H_{32}F_3NO_2$: 532.2467 (M+H); found 532.2467

m.p. = 90 - 92 ^oC

1-(2-(Benzyloxy)-5-(*tert*-butyl)-4-(dibenzylamino)phenyl)-2,2,2-trifluoroethan-1-one oxime (22)

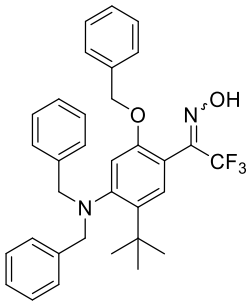

To a solution of trifluoromethylketone **21** (775 mg, 1.14 mmol) dissolved in a 2:1 pyridine/MeOH mixture (18 mL), hydroxylamine hydrochloride (118 mg, 1.71 mmol, 1.5 equiv.) was added and the reaction mixture was heated at 60 °C for 24 hours and monitored by TLC (15% EtOAc/Hex, product rf. 0.3). The reaction mixture was cooled and concentrated to dryness. The crude residue was purified by automated flash chromatography on a 50 g silica cartridge (2-30 % EtOAc/Hex gradient) to give compound **22** (592 mg, 1.08 mmol, 95 % yield) as a white crystalline solid as a 2:1 mixture of isomers.

^{1}H NMR (500 MHz, $CDCl_3$) δ 8.29 (s, 1H), 7.99 (s, 1H), 7.40 – 7.27 (m, 16H), 7.23 – 7.13 (m, 7H), 6.46 (s, 1H), 6.40 (s, 1H), 4.77 (s, 1H), 4.74 (s, 2H), 3.97 (s, 7H), 1.44 (s, 9H), 1.43 (s, 5H).

^{13}C NMR (151 MHz, $CDCl_3$) δ 155.0, 154.4, 154.3, 153.8, 148.3 (q, $^{2}J_{C\text{-}F}$ = 32 Hz), 147.2 (q, $^{2}J_{C\text{-}F}$ = 34 Hz), 140.0, 139.9, 137.3, 137.3, 137.0, 136.7, 130.1, 130.1, 129.9, 128.6, 128.6, 128.3, 128.3, 128.3, 128.0, 127.9, 120.7 (q, $^{1}J_{C\text{-}F}$ = 275 Hz), 118.2 (q, $^{1}J_{C\text{-}F}$ = 282 Hz), 117.0, 114.0, 113.8, 113.2, 70.3, 70.1, 58.1, 58.0, 35.6, 35.6, 31.6.

^{19}F NMR (471 MHz, $CDCl_3$) δ -64.9, -67.4.

HRMS: *m/z* calcd. for $C_{33}H_{33}F_3N_2O_2$: 547.2566 (M+H); found 547.2565

m.p. = 80-89 ^{o}C

***N,N*-Dibenzyl-5-(benzyloxy)-2-(*tert*-butyl)-4-(3-(trifluoromethyl)diaziridin-3-yl)aniline (24)**

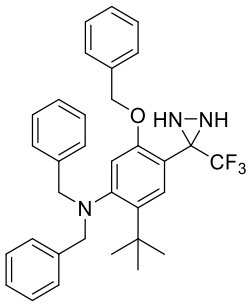

To a solution of oxime **22** (577 mg, 1.06 mmol) dissolved in DCM (15 mL), DIPEA (220 µL, 1.27 mmol, 1.2 equiv.) was added with stirring for 5 minutes at 0 °C. MsCl (95 µL, 1.21 mmol, 1.15 equiv.) was added slowly via syringe, and the solution was stirred for 30 minutes while warming to room temperature. The reaction mixture was washed with sat. aq. $NaHCO_3$ (20 mL), brine (20 mL), dried over Na_2SO_4 and concentrated to dryness to give crude mesyl-oxime **23** (489 mg) as a yellow oily foam. The crude mesyl-oxime **23** (46 mg, ~0.07 mmol) was dissolved in Et_2O (100 µL), transferred to a sealable reaction vessel and cooled to -78 °C. NH_3 was condensed (~ 200 µL) into the reaction vessel which was sealed and let warm to room temperature and stirred overnight. The reaction vessel was again cooled to -78 ^oC for 15 minutes and then opened carefully. The reaction mixture was allowed to warm to room temperature with stirring and the reaction mixture was washed with sat. aq. $NaHCO_3$ (1 mL), dried over Na_2SO_4 and concentrated to dryness. The crude residue was purified by automated flash chromatography on a 4 g silica cartridge (14% EtOAc/Hex isocratic elution) to give compound **24** (34 mg, 0.062 mmol, 84% yield) as an off-white crystalline solid.

^1H NMR (500 MHz, $CDCl_3$) δ 7.51 (s, 1H), 7.41 – 7.27 (m, 11H), 7.19 (d, *J* = 6.9 Hz, 4H), 6.40 (s, 1H), 4.78 (s, 2H), 3.96 (s, 4H), 2.71 (d, *J* = 8.92 Hz, 1H), 2.56 (d, *J* = 8.8 Hz, 1H), 1.45 (s, 9H).

^{13}C NMR (151 MHz, $CDCl_3$) δ 155.0, 139.9, 137.2, 136.9, 130.1, 129.0, 128.8, 128.4, 128.0, 127.4, 127.0, 126.5, 123.8 (q, *J* = 279 Hz), 117.1, 113.8, 69.9, 58.1, 56.3 (q, *J* = 37 Hz), 35.6, 31.6.

^{19}F NMR (471 MHz, $CDCl_3$) δ -76.9.

HRMS: *m/z* calcd. for $C_{33}H_{34}F_3N_3O$: 546.2700 (M+H); found 546.2700

m.p. = 119 - 121 ^{o}C

***N,N*-Dibenzyl-5-(benzyloxy)-2-(*tert*-butyl)-4-(3-(trifluoromethyl)-3H-diazirin-3-yl)aniline (25)**

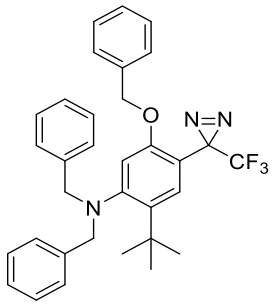

A solution of DMSO (12 µL, 0.17 mmol, 2.2 equiv.) in DCM (500 µL), was cooled to -78 °C, then $(COCl)_2$ (13 µL, 0.16 mmol, 2.0 equiv.) was added dropwise and stirred for 15 minutes. A solution of diaziridine **24** (43 mg, 0.079 mmol, 1 equiv.) in DCM was added and stirred for 15 minutes. Et_3N (55 µL, 0.40 mmol, 5 equiv.) was added, and the solution was allowed to warm to room temperature. The reaction mixture was concentrated to dryness and the crude material was separated via silica chromatography on a 12 g silica cartridge (12% EtOAc/Hex isocratic elution) to give diazirine **25** (34 mg, 0.063 mmol, 80% yield) as a pale yellow oil.

^{1}H NMR (500 MHz, $CDCl_3$) δ 7.47 (s, 1H), 7.42 – 7.27 (m, 10H), 7.18 – 7.11 (m, 5H), 6.38 (s, 1H), 4.82 (s, 2H), 3.95 (s, 4H), 1.41 (s, 9H).

^{13}C NMR (151 MHz, $CDCl_3$) δ 156.4, 140.5, 137.0, 136.9, 130.1, 130.0, 128.7, 128.4, 128.1, 127.4, 127.1, 122.4 (q, *J* = 275 Hz), 114.1, 113.9, 70.0, 58.1, 35.6, 31.6, 26.7 (q, *J* = 42 Hz).

^{19}F NMR (471 MHz, $CDCl_3$) δ -68.7.

FT-IR (cm^{-1}): 2955.4 s, 2922.9 s, 2854.2 s, 1602.0 w, 1566.7 w, 1502.3 s, 1454.4 s, 1259.6 m, 1219.4 m, 1166.4 s, 1027.8 w, 995.7 w, 735.5 s, 697.3 s.

HRMS: *m/z* calcd. for $C_{33}H_{32}F_3N_3O$: 544.2566 (M+H); found 544.2744

2-Bromo-4-(*tert*-butyl)-1-(ethoxymethoxy)benzene (26)

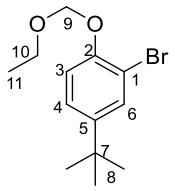

In a round bottom flask, under nitrogen, NaH (60% dispersion in mineral oil, 7.05 g, 176.4 mmol, 2.0 equiv.) was washed with hexanes (50 mL) and suspended in THF (90 mL) and cooled to 0 °C. A solution of 2-bromo-4-(*tert*-butyl)phenol **12** (20.2 g, 88.2 mmol) dissolved in THF (10 mL) was added dropwise over a span of 30 minutes. The reaction mixture was warmed to room temperature and stirred for 45 minutes then cooled to 0 °C. Chloromethylethyl ether (9.0 mL, 97 mmol, 1.1 equiv.) was added dropwise via syringe, and the reaction mixture was warmed to room temperature and stirred for 2 hours. The reaction mixture was quenched with 2*N* aq. NaOH (50 mL) and extracted into Et_2O (400 mL). The organic fractions were combined, and washed with H_2O (200 mL), brine (200 mL), dried over $MgSO_4$ and concentrated to dryness to give compound **26** (19.0 g, 68.3 mmol, 77% yield) as a pale yellow oil.

^{1}H NMR (400 MHz, $CDCl_3$) δ 7.53 (d, *J* = 2.4 Hz, 1H, C-6-*H*), 7.25 (dd, *J*=2.4, 8.5 1H, C-4-*H*), 7.10 (d, *J* = 8.6 Hz, 1H, C-3-*H*), 5.26 (s, 2H, C-9-*H*), 3.78 (q, *J* = 7.1 Hz, 2H, C-10-*H*), 1.29 (s, 9H, C-8-*H*), 1.24 (t, *J* = 7.1 Hz, 3H, C-11-*H*).

^{13}C NMR (101 MHz, $CDCl_3$) δ 151.7 (*C*-2), 146.5 (*C*-5), 130.5 (*C*-6), 125.5 (*C*-4), 116.1 (*C*-3), 112.6 (*C*-1), 94.1 (*C*-9), 64.7 (*C*-10), 34.4 (*C*-7), 31.5 (*C*-8), 15.2 (*C*-11).

HRMS: *m/z* calcd. for $C_{13}H_{19}{}^{79}BrO_2$: 241.0223 (M-C_2H_6O fragment); found 241.0191

1-(5-(*tert*-Butyl)-2-(ethoxymethoxy)phenyl)-2,2,2-trifluoroethan-1-one (27)

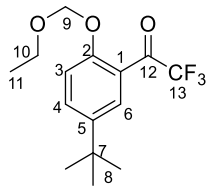

A solution of compound **26** (3.27 g, 11.7 mmol) dissolved in THF (11 mL) under nitrogen, was cooled to -78 °C. *n*-BuLi (1.5 M in Hex, 9.42 mL, 14.0 mmol, 1.2 equiv.) was added dropwise via syringe and stirred for 5 minutes resulting in a cloudy colourless solution. Ethyl trifluoroacetate (3.2 mL, 33.6 mmol, 2.9 equiv.) was added rapidly via syringe, and the reaction mixture was warmed to room temperature. The reaction mixture was quenched with sat. aq. NH_4Cl (10 mL), and extracted into EtOAc (50 mL). The organic fractions were combined and washed with 1M aq. NaOH (20 mL), sat. aq. $NaHCO_3$ (20 mL), brine (60 mL), dried over Na_2SO_4 and concentrated to dryness to give a pale yellow oil. The crude material was recrystalized from an MTBE/Hex mixture to give compound **27** (2.63 g, 8.64 mmol, 74% yield) as a white crystalline solid.

^{1}H NMR (500 MHz, $CDCl_3$) δ 7.64 (d, *J* = 2.1 Hz, 1H, C-6-*H*), 7.59 (dd, *J* = 2.4, 8.8 Hz, 1H, C-4-*H*), 7.23 (d, *J* = 8.8 Hz, 1H, C-3-*H*), 5.27 (s, 2H, C-9-*H*), 3.75 (q, *J* = 7.1 Hz, 2H, C-10-*H*), 1.32 (s, 9H, C-8-*H*), 1.23 (t, *J* = 7.1 Hz, 3H, C-11-*H*).

^{13}C NMR (126 MHz, $CDCl_3$) δ 183.9 (q, $^{2}J_{C\text{-}F}$ = 37 Hz, *C*-12), 155.5 (*C*-2), 144.8 (*C*-5), 133.1 (*C*-4), 127.9 (*C*-6), 122.2 (*C*-1), 116.4 (q, $^{1}J_{C\text{-}F}$ = 291 Hz, *C*-13), 115.1 (*C*-3), 93.7 (*C*-9), 64.9 (*C*-10), 34.5 (*C*-7), 31.4 (*C*-8), 15.1 (*C*-11).

^{19}F NMR (471 MHz, $CDCl_3$) δ -74.3.

HRMS: *m/z* calcd. for $C_{15}H_{19}F_3O_3$: 343.0923 (M+K); found 343.0907.

m.p. = 27-29 ^{o}C

1-(5-(*tert*-butyl)-2-(ethoxymethoxy)phenyl)-2,2,2-trifluoroethan-1-one oxime (28)

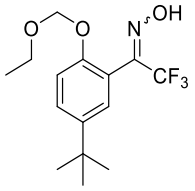

To a solution of trifluoromethylketone **27** (200 mg, 0.657 mmol) dissolved in a 2:1 pyridine/MeOH mixture (9 mL), hydroxylamine hydrochloride (68 mg, 0.99 mmol, 1.5 equiv.) was added and the solution was heated at 60 °C for 24 hours. The progress of the reaction was monitored by TLC (15% EtOAc/Hex, product rf. 0.33). The reaction mixture was cooled to room temperature and concentrated to dryness. The crude material was purified by automated flash chromatography on a 12 g silica cartridge (3-30 % EtOAc/Hex gradient) to give compound **28** (178 mg, 0.58 mmol, 85 % yield) as a clear colourless oil in a 2:1 mixture of isomers.

^{1}H NMR (400 MHz, $CDCl_3$) δ 8.63 (s, 2H), 8.31 (s, 1H), 7.43 (dd, *J* = 2.5, 8.8 Hz, 1H), 7.42 (dd, *J* = 2.5, 8.7 Hz, 2H), 7.25 (d, *J* = 2.5 Hz, 2H), 7.19 (d, *J* = 8.9 Hz, 2H), 7.17 (d, *J* = 2.6 Hz, 1H), 7.15 (d, *J* = 8.7 Hz, 2H), 5.21 (s, 4H), 5.21 (s, 2H), 3.72 (q, *J* = 7.1 Hz, 4H), 3.71 (q, *J* = 7.1 Hz, 2H), 1.30 (s, 27H), 1.22 (t, *J* = 7.1 Hz, 6H), 1.21 (t, *J* = 7.1 Hz, 3H).

^{13}C NMR (151 MHz, $CDCl_3$) δ 153.6, 152.1, 147.9 (q, *J* = 32.5 Hz), 147.0 (q, *J* = 33.5 Hz), 144.0, 144.0, 128.4, 128.3, 127.1, 125.5, 120.0 (obs. d, *J* = 274.5 Hz), 119.2, 117.4 (q, *J* = 282.2 Hz) 115.4, 113.7, 113.4, 92.9, 92.8, 63.9, 63.8, 33.7, 30.9, 30.9, 14.5.

^{19}F NMR (471 MHz, CDCl3) δ -65.2, -67.7.

HRMS: *m/z* calcd. for $C_{15}H_{20}F_3NO_3$: 318.1323 (M-H); found 318.1400.

1-(5-(*tert*-butyl)-2-(ethoxymethoxy)phenyl)-2,2,2-trifluoroethan-1-one *O*-methylsulfonyl oxime (29)

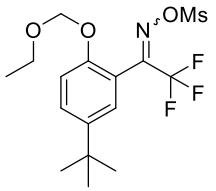

To a solution of oxime **28** (1.07 g, 3.36 mmol) dissolved in DCM (30 mL), DIPEA (0.70 mL, 4.03 mmol, 1.2 equiv.) was added with stirring, and the solution was cooled to 0 °C for 5 minutes. MsCl (300 µL, 3.86 mmol, 1.15 equiv.) was added slowly via syringe, and the reaction mixture was stirred for 30 minutes and allowed to warm to room temperature. The reaction mixture was washed with sat. aq. $NaHCO_3$ (20 mL), brine (20 mL), and dried over Na_2SO_4 and concentrated to dryness to give compound **29** (1.30 g, 3.27 mmol, ~97% yield) as a yellow oil as a 2:1 mix of isomers.

^{1}H NMR (500 MHz, $CDCl_3$) δ 7.51 (dd, *J* = 2.5, 8.8 Hz, 3H), 7.47 (dd, *J* = 2.4, 8.9 Hz, 1H), 7.27 (d, *J* = 2.5 Hz, 3H), 7.21 (d, *J* = 9.0 Hz, 1H), 7.19 (d, *J* = 8.8 Hz, 3H), 7.16 (d, *J* = 2.4 Hz, 1H), 5.23 (s, 5H), 5.22 (s, 3H), 3.71 (q, *J* = 7.1 Hz, 5H), 3.71 (q, *J* = 7.1 Hz, 3H), 3.24 (s, 8H), 3.24 (s, 4H), 1.32 (s, 22H), 1.30 (s, 11H), 1.22 (t, *J* = 7.1 Hz, 8H), 1.22 (t, *J* = 7.1 Hz, 4H).

^{13}C NMR (151 MHz, $CDCl_3$) δ 156.5 (q, *J* = 34.6 Hz), 154.4, 154.2 (q, *J* = 34.6 Hz), 152.6, 144.9, 144.7, 130.6, 130.2, 127.5, 125.1, 119.7 (d, *J* = 277.3 Hz), 117.1 (q, *J* = 283.0 Hz), 114.5, 114.2, 114.1, 93.6, 93.5, 64.8, 64.7, 37.0, 36.9, 34.5, 34.4, 31.5, 31.5, 15.2, 15.1.

^{19}F NMR (471 MHz, $CDCl_3$) δ -64.4, -67.8.

HRMS: *m/z* calcd. for $C_{16}H_{22}F_3NO_5S$: 415.1509 (M+(NH_4^+); found 415.1490

3-(5-(*tert*-butyl)-2-(ethoxymethoxy)phenyl)-3-(trifluoromethyl)diaziridine (30)

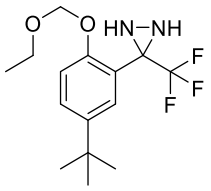

A solution of mesyl-oxime **29** (1.15 g, 2.90 mmol) dissolved in DCM (2 mL) was transferred to a sealable reaction vessel and cooled to -78 °C. NH_3 was condensed (~ 2 mL) into the reaction vessel and the vessel was sealed and let warm to room temperature and stirred overnight. The reaction vessel was again cooled to -78 ^{o}C for 15 minutes then opened and allowed to warm to room temperature with stirring. The reaction mixture was transferred to a separatory vessel and washed with sat. aq. $NaHCO_3$ (1 mL), dried over Na_2SO_4 and concentrated to dryness. The crude residue was purified by automated flash chromatography on a 4 g silica cartridge (14% EtOAc/Hex isocratic) to give compound **30** (902 mg, 2.83 mmol, 97 % yield) as an off-white crystalline solid.

^{1}H NMR (600 MHz, $CDCl_3$) δ 7.48 (d, *J* = 2.5 Hz, 1H), 7.40 (dd, *J* = 2.6, 8.8 Hz, 1H), 7.14 (d, *J* = 8.8 Hz, 1H), 5.29 – 5.21 (m, 2H), 3.73 (q, *J* = 7.1 Hz, 2H), 2.72 – 2.68 (m, 1H), 2.55 – 2.49 (m, 1H), 1.31 (s, 9H), 1.22 (t, *J* = 7.1 Hz, 3H).

^{13}C NMR (151 MHz, $CDCl_3$) δ 154.3, 144.4, 128.5, 127.9, 123.7 (q, *J* = 278.7 Hz), 119.9, 114.0, 93.3, 64.6, 56.5 (q, *J* = 37.1 Hz), 34.3, 31.5, 15.2.

^{19}F NMR (471 MHz, $CDCl_3$) δ -77.05.

HRMS: *m/z* calcd. for $C_{15}H_{21}F_3N_2O_2$: 319.1628 (M+H); found 319.1617

m.p. = 36 - 37 ^{o}C

3-(5-(*tert*-Butyl)-2-(ethoxymethoxy)phenyl)-3-(trifluoromethyl)-3H-diazirine (31)

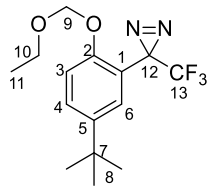

To a solution of DMSO (90 µL, 1.3 mmol, 3 equiv.) in DCM (5 mL), at -78 °C under nitrogen, $(COCl)_2$ (55 µL, 0.64 mmol, 1.5 equiv.) was added via syringe, and the solution was stirred for 15 minutes. A solution of diaziridine **30** (135 mg, 0.424 mmol, 1 equiv.) in DCM (3 mL) was added slowly via syringe and stirred for 60 minutes. Then Et_3N (295 µL, 2.12 mmol, 5 equiv.) was added via syringe, and the solution was allowed to warm to room temperature. The reaction mixture was quenched with sat. aq. NH_4Cl (10 mL), transferred to a separatory funnel, washed with brine (10 mL), dried over Na_2SO_4 and concentrated to dryness to give compound **31** (135 mg, 0.042 mmol, quantitative yield) as an orange oil.

^{1}H NMR (500 MHz, $CDCl_3$) δ 7.43 (d, *J* = 2.23 Hz, 1H), 7.37 (dd, *J* = 2.4, 8.8 Hz, 1H), 7.11 (d, *J* = 8.8 Hz, 1H), 5.31 (s, 2H), 3.78 (q, *J* = 7.07 Hz, 2H), 1.29 (s, 9H), 1.24 (t, *J* = 7.09 Hz, 3H).

^{13}C NMR (151 MHz, $CDCl_3$) δ 155.5 (*C*-2) , 145.1 (*C*-5), 129.1 (*C*-4), 127.6 (*C*-6), 122.3 (q, $^1J_{C\text{-}F}$ = 274.8 Hz, *C*-13), 116.6 (*C*-1), 114.5 (*C*-3), 93.2 (*C*-9), 64.6 (*C*-10), 34.4 (*C*-7), 31.5 (*C*-8), 26.9 (q, $^2J_{C\text{-}F}$ = 42.4 Hz, *C*-12), 15.2 (*C*-11).

^{19}F NMR (471 MHz, $CDCl_3$) δ -69.03.

HRMS: did not observe positive or negative ionization by ESI-MS.

4-(*tert*-Butyl)-2-(3-(trifluoromethyl)-3H-diazirin-3-yl)phenol (32)

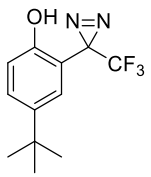

To a solution of compound **31** (601 mg, 1.90 mmol) dissolved in DCM (5 mL), TFA (10 mL) was added and the solution was stirred for 1 hour. The reaction was monitored via TLC and HPLC

and upon completion, the reaction mixture was concentrated to dryness to give **32** (0.48 g, 1.8 mmol) which was used immediately (appeared to decompose/oxidise rapidly as a crude residue) in the next step.

^{1}H NMR (400 MHz, $CDCl_3$) δ 7.44 (d, *J* = 2.4 Hz, 1H), 7.32 (dd, *J* = 2.4, 8.6 Hz, 1H), 6.78 (d, *J* = 8.6 Hz, 1H), 5.12 (s, 1H), 1.28 (s, 9H).

^{19}F NMR (471 MHz, $CDCl_3$) δ -68.52.

HRMS: *m/z* calcd. for $C_{12}H_{13}F_3N_2O$: 257.0907 (M-H); found 257.0908

4-(*tert*-Butyl)-2-(3-(trifluoromethyl)-3H-diazirin-3-yl)phenyl ethyl carbonate (33)

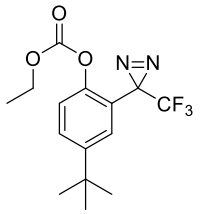

To a solution of compound **32** (0.48 g, 1.8 mmol) dissolved in THF (30 mL), DIPEA (490 µL, 2.8 mmol, 1.5 equiv.) was added, and the solution was cooled to 0 °C. Ethyl chloroformate (195 µL, 2.0 mmol, 1.1 equiv.) was added via syringe and the solution was stirred and let warm to room temperature overnight. The reaction was not complete by TLC (10% EtOAc/Hex, product rf. 0.8). The solution was cooled to 0 °C, then DIPEA (980 µL, 5.6 mmol, 3 equiv.) and ethyl chloroformate (200 µL, 4 mmol, 2.2 equiv.) were added and the solution was stirred for 6 hours, and warmed to rt. Upon consumption of the starting material by TLC, the reaction mixture was quenched with 0.1 M HCl aq. (50 mL), transferred to a separatory funnel and extracted into Et_2O (200 mL). The organic fractions were combined, washed with brine (100 mL) dried over Na_2SO_4 and concentrated to dryness to give crude compound **33** (640 mg). An aliquot of the crude material of compound **33** (130 mg) was purified by automated flash chromatography on a 12 g silica cartridge (0-40% Toluene/Hex gradient) to give compound **33** (66 mg, 0.2 mmol, 55% recovery) as a yellow oil.

^{1}H NMR (500 MHz, $CDCl_3$) δ 7.54 (d, *J* = 2.4 Hz, 1H), 7.49 (dd, *J* = 2.4, 8.7 Hz, 1H), 7.17 (d, *J* = 8.7 Hz, 1H), 4.39 (q, *J* = 7.1 Hz, 2H), 1.43 (t, *J* = 7.1 Hz, 3H), 1.32 (s, 9H).

^{13}C NMR (151 MHz, $CDCl_3$) δ 153.4, 150.4, 149.0, 129.4, 127.6, 122.9, 122.0 (q, *J* = 274.9 Hz), 119.9, 65.5, 34.8, 31.3, 26.3 (q, *J* = 42.6 Hz), 14.3.

^{19}F NMR (471 MHz, $CDCl_3$) δ -68.43.

HRMS: *m/z* calcd. for $C_{15}H_{17}F_3N_2O_3$: 331.1264 (M+H); found 331.1279

1-Bromo-5-(*tert*-butyl)-2-(ethoxymethoxy)-4-nitrobenzene (35)

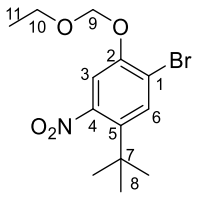

To a solution of compound **7** (9.9 g, 36 mmol) in THF (60 mL) at room temperature under N_2, DIPEA (19 mL, 109 mmol) was added followed by chloromethylethyl ether (5.3 mL, 58 mmol) and stirred overnight. The reaction mixture was quenched with sat. aq. NH_4Cl (100 mL) extracted with Et_2O (50 mL, 3x). The organic layers were combined, washed with brine (100 mL) dried over Na_2SO_4, filtered, and concentrated to dryness to give compound **35** (10.7 g, 32 mmol, 89%) as a yellow crystalline solid.

^{1}H NMR (600 MHz, CDCl3) δ: 7.69 (s, 1H, *C*-6-H), 7.17 (s, 1H, *C*-3-H), 5.28 (s, 2H, *C*-9-H), 3.76 (q, *J* = 7.07 Hz, 2H, *C*-10-H), 1.37 (s, 9H, *C*-8-H), 1.23 (t, *J* = 7.07 Hz, 3H, *C*-11-H).

^{13}C NMR (151 MHz, $CDCl_3$) δ: 152.4 (*C*-2), 150.5 (*C*-4), 135.8 (*C*-5), 133.3 (*C*-6), 115.3 (*C*-1), 111.4 (*C*-3), 94.3 (*C*-9), 65.2 (*C*-10), 35.3 (*C*-7), 30.8 (*C*-8), 15.1 (*C*-11).

HRMS: Did not observe positive or negative ionization by ESI-MS.

m.p. = 62 - 63 ^{o}C.

4-Bromo-2-(*tert*-butyl)-5-(ethoxymethoxy)aniline (36)

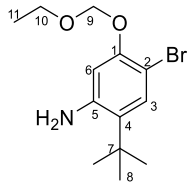

Method A: To a solution of 1-bromo-5-(*tert*-butyl)-2-(ethoxymethoxy)-4-nitrobenzene (**35**) (502 mg, 1.51 mmol) dissolved in MeOH (15 mL), Fe powder (2 g, 36 mmol, 24 equiv.), and NH_4Cl (1.5 g, 28 mmol, 18 equiv.) were added and the reaction was heated at 60 ^oC for 4 hours. The progress of the reaction was monitored by TLC. The crude mixture was allowed to cool and was filtered through a bed of celite, washed with MeOH, and the filtrate was concentrated to dryness. The crude residue was purified by automated flash chromatography on a 25 g silica cartridge (20% EtOAc/Hex isocratic ellution) to give compound **36** (345 mg, 1.14 mmol, 76% yield) as a yellow oil.

Method B: To a solution of *tert*-butyl (4-bromo-2-(*tert*-butyl)-5-(ethoxymethoxy)phenyl) carbamate (**37**) (500 mg, 1.24 mmol) in THF, TBAF (1M in THF, 1.86 mL, 1.86 mmol, 1.5 equiv.) was added and the reaction mixture was heated at 60^oC for 2 hours, and the progress of the reaction was monitored by TLC (20% EtOAc/Hex). The reaction mixture was cooled to room temperature and diluted with DCM (20 mL). The solution was transferred to a separatory funnel and washed with H_2O (25 mL), and brine (25 mL). The organic layer was dried over Na_2SO_4 concentrated to dryness to give **36** as yellow oil (384 mg, quantitative yield).

^{1}H NMR (400 MHz, $CDCl_3$) δ 7.33 (s, 1H, C-3-*H*), 6.54 (s, 1H, C-6-*H*), 5.25 (s, 2H, C-9-*H*), 3.87 (s, 2H, N-12-*H*), 3.80 (q, *J* = 7.1 Hz, 2H, C-10-*H*), 1.40 (s, 9H, C-8-*H*), 1.26 (t, *J* = 7.1 Hz, 3H, C-11-*H*).

^{13}C NMR (101 MHz, $CDCl_3$) δ 152.7 (*C*-5), 145.1 (*C*-1), 131.1 (*C*-3), 129.3 (*C*-2), 105.7 (*C*-6), 100.7 (*C*-4), 94.1 (*C*-9), 64.7 (*C*-10), 34. (*C*-7), 29.8 (*C*-8), 15.2 (*C*-11).

HRMS: *m/z* calcd. for $C_{13}H_{20}BrNO_2$: 302.0750 (M+H); found 302.0781.

***tert*-Butyl (4-bromo-2-(*tert*-butyl)-5-(ethoxymethoxy)phenyl)carbamate (37)**

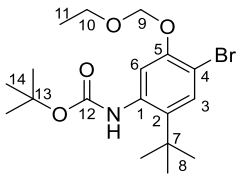

A solution of aniline **36** (2.6 g, 8.6 mmol) dissolved in toluene (5 mL) was placed in a microwave vial, sealed and then degassed under argon. Under a bed of Argon, Boc_2O (7.5 g, 34.4 mmol, 4 equiv.) was added, the microwave vial was sealed and the reaction mixture was heated in the microwave reactor for 18 h at 105 ^oC. The reaction mixture was cooled to room temperature and the vial was vented by puncturing the septa with a large bore needle. The crude mixture was concentrated to dryness, and the crude residue was purified by column chromatography on an 80 g silica cartridge (2-20 % EtOAc/Hex gradient) to give **37** (2.49 g, 6.2 mmol, 72 %) as a white crystalline solid. Remaining S.M. (369 mg, 1.2 mmol, 14%) was recovered and recycled.

^1H NMR (500 MHz, $CDCl_3$) δ 7.48 (s, 1H), 7.46 (s, 1H), 6.35 (s, 1H), 5.28 (s, 2H), 3.79 (q, *J* = 7.1 Hz, 2H), 1.50 (s, 9H), 1.37 (s, 9H), 1.24 (t, *J* = 7.1 Hz, 3H).

^{13}C NMR (126 MHz, $CDCl_3$) δ 153.2, 152.2, 136.2, 130.9, 114.0, 108.3, 94.0, 80.8, 77.2, 64.9, 34.2, 30.8, 28.5, 15.2.

HRMS: *m/z* calcd. for $C_{18}H_{28}BrNO_4$: 402.1274 (M+H); found 402.1271.

m.p. = 94 - 95 ^oC.

***tert*-Butyl (2-(*tert*-butyl)-5-(ethoxymethoxy)-4-(2,2,2-trifluoroacetyl)phenyl)carbamate (38)**

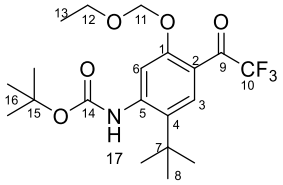

A solution of bromo **37** (526 mg, 1.31 mmol) in distilled THF under N_2 was cooled to -40^oC. MeLi (1.75 mL, 2.6 mmol, 2 equiv.) was added via syringe and the reaction mixture was warmed to 0 ^oC for 2 minutes. The reaction mixture was cooled to -78^oC and *n*-BuLi (1.30 mL, 1.96 mmol, 1.5

equiv.) was added dropwise via syringe and the reaction mixture was stirred for 1 hour. Ethyl trifluoroacetate (2.0 mL, 17 mmol, 13 equiv) was added quickly via syringe and the reaction mixture was warmed to room temperature and quenched with sat. aq. NH_4Cl (10 mL), transferred to a separatory funnel and extracted with EtOAc (50 mL). The organic fractions were combined and washed with Brine (30 mL) dried over Na_2SO_4, filtered and concentrated to dryness. The crude residue was purified via automated flash chromatography on a 12 g silica cartridge, to afford compound **41** (520 mg, 1.24 mmol, 95 % yield) as a white crystalline solid.

^{1}H NMR (400 MHz, $CDCl_3$) δ 7.97 (s, 1H, C-6-*H*), 7.72 (s, 1H, C-3-*H*), 6.88 (s, 1H, N-17-*H*), 5.32 (s, 2H, C-14-*H*), 3.77 (q, *J* = 7.1 Hz, 2H, C-12-*H*), 1.54 (s, 9H, C-16-*H*), 1.42 (s, 9H, C-8-*H*), 1.24 (t, *J* = 7.1 Hz, 3H, C-13-*H*).

^{13}C NMR (101 MHz, $CDCl_3$) δ 181.3 (q, $^2J_{C\text{-}F}$ = 36.1 Hz, *C*-9), 157.4 (*C*-1), 152.1 (*C*-14), 144.0 (*C*-5), 131.1 (*C*-4), 130.2 (*C*-3), 116.7 (q, $^1J_{C\text{-}F}$ = 290.8 Hz, *C*-10), 116.4 (*C*-2), 107.9 (*C*-6), 93.6 (*C*-11), 81.8 (*C*-15), 65.1 (*C*-12), 33.9 (*C*-7), 30.7 (*C*-16), 28.5 (*C*-8), 15.1 (*C*-13).

^{19}F NMR (376 MHz, $CDCl_3$) δ -73.68.

HRMS: *m/z* calcd. for $C_{20}H_{28}F_3NO_5$: 420.1992 (M+H); found 420.2003.

m.p. = 89.5 – 90.5 ^{o}C.

tert-butyl (2-(_tert_-butyl)-5-(ethoxymethoxy)-4-(2,2,2-trifluoro-1-(hydroxyimino)ethyl)phenyl)carbamate (39)

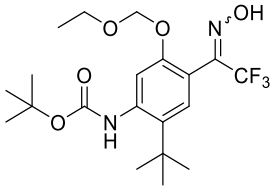

A solution of compound **38** (110 mg, 0.262 mmol) and hydroxylamine hydrochloride (22 mg, 0.315 mmol) in a 2:1 mixture of pyridine/MeOH (7.5 mL) was stirred at 60^{o}C overnight. The reaction mixture was cooled to room temperature and concentrated to dryness. The crude residue was purified via automated flash chromatography (12 g silica cartridge, 4-40 %

EtOAc/Hex gradient) to afford compound **39** (90 mg, 207 mmol, 79 % yield) as a white crystalline solid.

^{1}H NMR (400 MHz, $CDCl_3$) δ 8.08 (s, 1H), 7.72 (s, 1H), 7.69 (s, 1H), 7.63 (s, 2H), 7.18 (s, 2H), 7.11 (s, 1H), 6.56 (s, 2H), 5.24 (s, 4H), 5.23 (s, 2H), 3.72 (q, *J* = 7.1, 6H), 3.71 (q, *J* = 7.2 Hz, 6H),1.52 (s, 11H), 1.52 (s, 16H), 1.39 (s, 11H), 1.39 (s, 16H), 1.22 (td, *J* = 7.1, 2.1 Hz, 9H).

^{13}C NMR (151 MHz, $CDCl_3$) δ 154.8, 153.6, 147.6 (q, *J* = 32.0 Hz), 146.6 (q, *J* = 33.6 Hz), 139.1, 128.7, 127.1, 120.7 (q, *J* = 274.4 Hz), 118.2 (q, *J* = 282.3 Hz), 116.3, 112.3, 111.3, 93.5, 93.4, 81.3, 64.7, 64.6, 34.1, 34.0, 30.8, 30.7, 28.5, 15.1.

HRMS: *m/z* calcd. for $C_{20}H_{29}F_3N_2O_5$: 433.1956 (M-H); found 433.2044.

m.p. = 149 - 157 °C

tert-butyl (2-(_tert_-butyl)-5-(ethoxymethoxy)-4-(2,2,2-trifluoro-1-((tosyloxy)imino)ethyl)phenyl)carbamate (40)

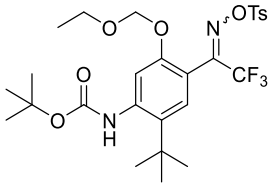

Method A: To a solution of oxime **39** (353 mg, 0.81 mmol) in DCM (10 mL) at 0^{o}C, Et_3N (170 µL, 1.22 mmol, 1.5 equiv.) was added via syringe and stirred for 5 minutes. *p*-TsCl (170 mg, 0.89 mmol, 1.1 equiv.) was added and the reaction mixture was stirred for 15 minutes while warming to room temperature. The reaction mixture was quenched with sat. aq. $NaHCO_3$ (10 mL), the organic layer was washed with brine (10 mL), dried over Na_2SO_4, filtered and concentrated to dryness to give compound **40** (495 mg) as a yellow foam which can be utilized as a crude product. Alternatively, the crude residue of compound **40** can be recrystallized from a 8:2 DCM/Hex mixture to give compound **40** as a white crystalline solid.

Method B: To a solution of oxime **39** (87 mg, 0.20 mmol) in DCM (3 mL) at 0^{o}C, Et_3N (42 µL, 0.30 mmol, 1.5 equiv.), DMAP (3 mg, 0.02 mmol, 0.1 equiv.) and *p*-TsCl (42 mg, 0.22 mmol, 1.1 equiv.) were added. The reaction mixture was stirred for 15 minutes while warming to room

temperature then used immediately as a crude solution during the reaction with ammonia to give diaziridine **42**.

^{1}H NMR (400 MHz, $CDCl_3$) δ 7.9-7.85 (m, 7H), 7.76 (s, 1H), 7.69 (s, 2H), 7.38-7.35 (m, 7H), 7.02 (s, 1H), 6.90 (s, 2H), 6.61 (s, 1H), 6.60 (s, 2H), 5.15 (s, 4H), 5.13 (s, 2H), 3.63 (q, J=7.1 Hz, 4H), 3.62 (q, J=7.0 Hz, 2H), 2.48 (s, 3H), 2.46 (s, 6H), 1.53 (s, 9H), 1.51 (s, 18H), 1.38 (s, 9H), 1.34 (s, 18H), 1.19 (t, *J* = 7.1, 3H), 1.18 (t, *J* = 7.1, 6H).

^{19}F NMR (376 MHz, $CDCl_3$) δ -64.5, -67.6.

***tert*-butyl (2-(*tert*-butyl)-5-(ethoxymethoxy)-4-(3-(trifluoromethyl)diaziridin-3-yl)phenyl)carbamate (42)** and ***tert*-butyl (*Z*)-(4-((1-amino-2,2,2-trifluoroethylidene)amino)-2-(*tert*-butyl)-5-(ethoxymethoxy)phenyl)carbamate (41)**

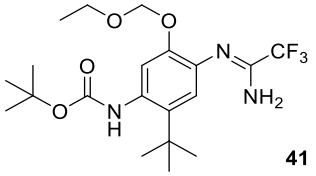

41

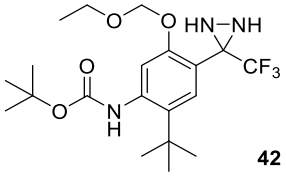

42

Method A: Ammonia was condensed (~1.5 mL) at -78^{o}C into a sealable reaction vessel, the reaction mixture of tosyl-oxime **40** (theoretical mass of 118 mg, 0.2 mmol) in DCM (3 mL) was transferred via pipette into the liquid ammonia. The reaction vessel was sealed and the reaction mixture was warmed to room temperature in a water bath and stirred overnight. The reaction vessel was cooled at -78 ^{o}C for 15 minutes then carefully opened and the reaction mixture was warmed at room temperature for 30 minutes. The reaction mixture was concentrated to dryness and the residue was purified by column chromatography to afford a mixture of diaziridine **42** and amidine **41** in ratios varying from 1:1.6 to 1:2.5 by ^{1}H NMR. Recrystallization of the mixture from an 8:2 Et_2O/Hex mixture gave amidine **41** as a crystalline product used to confirm structure by X-ray crystallography (performed by Michael Hamilton with instruction and assistance from John Thompson, Ph.D.).

Alternatively, the mixture of **42** and **41** can be utilized in the next step (oxidation to the diazirine) and separation of the diazirine **43** and amidine **41** post-oxidation can be performed by automated flash chromatography.

Conversely, an 80 mg mixture of **42** and **41** was separated by semi-preparative HPLC to give 45 as a white crystalline solid (16 mg).

Characterization data for 41

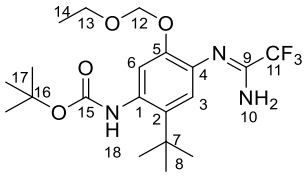

^{1}H NMR (400 MHz, $CDCl_3$) δ 7.29 (s, 1H, C-6-*H*), 6.89 (s, 1H, C-3-*H*), 6.28 (s, 1H, C-18-*H*), 5.10 (s, 2H, C-12-*H*), 5.07 (s, 2H, N-10-*H*), 3.67 (q, *J* = 7.1 Hz, 2H, C-13-*H*), 1.48 (s, 9H, C-17-*H*), 1.34 (s, 9H, C-8-*H*), 1.18 (t, *J* = 7.1 Hz, 3H, C-14-*H*).

^{13}C NMR (101 MHz, $CDCl_3$) δ 153.9 (*C*-15), 145.3 (*C*-5), 145.3 (q, $^{2}J_{C\text{-}F}$ = 35.2 Hz, *C*-9), 137.7 (*C*-2), 133.0 (*C*-4), 132.7 (*C*-1), 121.3 (*C*-3), 118.3 (q, $^{1}J_{C\text{-}F}$ = 277.9 Hz, *C*-11), 116.6 (*C*-6), 94.5 (*C*-12), 80.4 (*C*-16), 64.6 (*C*-13), 34.3 (*C*-7), 30.8 (*C*-8), 28.5 (*C*-17), 15.0 (*C*-14).

^{19}F NMR (376 MHz, $CDCl_3$) δ -72.80.

HRMS: *m/z* calcd. for $C_{20}H_{30}F_3N_3O_4$: 434.2261 (M+H); found 434.2249

m.p. = 124 - 126 °C

IR (cm^{-1}) 3427 (w), 3288 (w), 3186 (w), 2981-2896 (m), 1700 (s), 1682 (s), 1625 (w), 1483 (s),1139 (s).

Table 2 Single-Crystal X-ray Diffraction of compound 41

Compound reference	CMH-04-045amidine
Chemical formula	$C_{20}H_{29}F_3N_3O_4$
Formula Mass	432.46
Crystal system	Triclinic
a/Å	9.6508(3)
b/Å	10.7941(4)
c/Å	11.6332(3)
α/°	68.832(2)
β/°	87.760(2)
γ/°	87.527(3)
Unit cell volume/Å^3	1128.67(6)
Temperature/K	296(2)
Space group	$P\bar{1}$
No. of formula units per unit cell, *Z*	2
Radiation type	CuKα
Absorption coefficient, μ/mm^{-1}	0.894
No. of reflections measured	10993
No. of independent reflections	3923
R_{int}	0.0719
Final R_1 values ($I > 2\sigma(I)$)	0.0566
Final $wR(F^2)$ values ($I > 2\sigma(I)$)	0.1479
Final R_1 values (all data)	0.0913
Final $wR(F^2)$ values (all data)	0.1721
Goodness of fit on F^2	1.048

Characterization data for 42

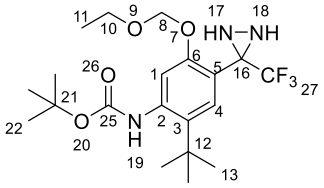

^{1}H NMR (500 MHz, $CDCl_3$) δ 7.59 (s, 1H, C-1-*H*), 7.41 (s, 1H, C-4-*H*), 6.53 (s, 1H, N-19-*H*), 5.35 – 5.18 (m, 2H, C-8-*H*), 3.78 – 3.70 (m, 2H, C-10-*H*), 2.65 (d, *J* = 9.0 Hz, 1H, N-17-*H*), 2.49 (d, *J* = 8.7 Hz, 1H, N-18-*H*), 1.51 (s, 9H, C-13-*H*), 1.39 (s, 9H, C-22-*H*), 1.24 (t, *J* = 7.1 Hz, 3H, C-11-*H*).

^{13}C NMR (126 MHz, $CDCl_3$) δ 154.9(*C*-6), 153.0(*C*-25), 138.9(*C*-2), 133.3(*C*-3), 128.9(*C*-4), 123.7 (q, $^{1}J_{C\text{-}F}$ = 278.8 Hz, *C*-27), 115.8(*C*-5), 110.7(*C*-1), 93.3(*C*-8), 81.0(*C*-6), 64.8(*C*-10), 56.2 (q, $^{2}J_{C\text{-}F}$ = 37.1 Hz, *C*-16), 34.0 (*C*-12), 30.8 (*C*-13-15), 28.5 (*C*-22-24), 15.2 (*C*-11).

^{19}F NMR (471 MHz, $CDCl_3$) δ -77.0.

HRMS: *m/z* calcd. for $C_{20}H_{30}F_3N_3O_4$: 472.1825 (M+K); found 472.1837

m.p. = 127-128 ^{o}C.

***tert*-Butyl (2-(*tert*-butyl)-5-(ethoxymethoxy)-4-(3-(trifluoromethyl)-3*H*-diazirin-3-yl)phenyl)carbamate (43)**

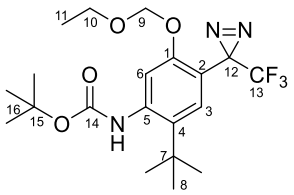

The residue containing amidine **41** and diaziridine **42** (222 mg, 1:1.6 ratio of diaziridine/amidine, approx. 0.2 mmol diaziridine **42**, total 0.5 mmol of combined **42** and **41** species) was dissolved in MeOH (3 mL), then Et_3N (180 µl, 1.28 mmol, 2.5 equiv.) was added and the reaction mixture was stirred for 5 minutes. I_2 (71 mg, 0.56 mmol, 1.1 equiv) was added and the reaction mixture was stirred overnight and monitored by TLC. The reaction mixture was quenched with $Na_2S_3O_4$ (*aq.*) and extracted into EtOAc (10 mL). The organic fractions were combined and washed with

sat. aq. $NaHCO_3$ (10 mL), brine (10 mL), and dried over Na_2SO_4 and concentrated to dryness. The crude residue was purified by automated flash chromatography on a 12 g silica cartridge (4-40% EtOAc/Hex gradient) to give compound **43** (63 mg, 0.15 mmol, 18% yield over 3 steps) as a white crystalline solid.

^{1}H NMR (400 MHz, MeOD) δ 7.46 (s, 1H), 7.16 (s, 1H), 5.34 (s, 2H), 3.78 (q, *J* = 7.1 Hz, 2H), 3.31 (s, 5H), 1.50 (s, 9H), 1.37 (s, 9H), 1.22 (t, *J* = 7.1 Hz, 3H).

^{13}C NMR (151 MHz, MeOD) δ 157.3 (*C*-1), 156.6 (*C*-14), 140.9 (*C*-4), 140.7 (*C*-2), 129.7 (*C*-3), 123.6 (q, $^1J_{C\text{-}F}$ = 273.9 Hz, *C*-13), 117.8 (*C*-6), 115.6 (*C*-5), 94.4 (*C*-9), 81.5 (*C*-15), 65.7 (*C*-10), 35.5 (*C*-7), 31.1 (*C*-8), 28.7 (*C*-16), 27.6 (q, $^2J_{C\text{-}F}$ = 42.4 Hz, *C*-12), 15.4 (*C*-11).

^{19}F NMR (376 MHz, MeOD) δ -70.7.

HRMS: *m/z* calcd. for $C_{20}H_{28}F_3N_3O_4$: 449.2370 ($M+NH_4^+$); found 449.2365.

***N*-(4-bromo-6-(*tert*-butyl)-3-(ethoxymethoxy)cyclohexa-1,3-dien-1-yl)pivalamide (44)**

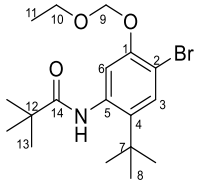

To a solution of aniline **36** (2.06 g, 6.82 mmol) in DCM (20 mL) under argon, DIPEA (5.9 mL, 34 mmol, 5 equiv.) and PivCl (2.5 mL, 21 mmol, 3 equiv.) were added and the reaction mixture was heated at 40 °C overnight. The reaction mixture was allowed to cool and was quenched with sat. aq. NH_4Cl (10 mL) and extracted with DCM (50 mL). The organic layers were combined and washed with brine (50 mL), dried over Na_2SO_4 and concentrated to dryness. The crude material was recrystallized in batches, the crystalline material was combined and purified by automated flash chromatography on a 25 g silica column (0-50% EtOAc/Hex gradient) to give **44** (1.19 g, 3.08 mmol, 45 % combined yield) as white crystalline solid. The mother liquor from the crystallization contained significant amounts of **36** which was recovered and recycled.

^{1}H NMR (400 MHz, $CDCl_3$) δ 7.69 (s, 1H), 7.49 (s, 1H), 7.45 (s, 1H), 5.28 (s, 2H), 3.79 (q, *J* = 7.1 Hz, 2H), 1.39 (s, 9H), 1.34 (s, 9H), 1.24 (t, *J* = 7.1 Hz, 3H).

^{13}C NMR (101 MHz, $CDCl_3$) δ 176.0 (*C*14), 152.0 (*C*1), 136.0 (*C*4), 135.9 (*C*5), 130.9 (*C*3), 114.1 (*C*6), 108.8 (*C*2), 93.9 (*C*9), 64.8 (*C*10), 39.7 (*C*12), 34.0 (*C*7), 30.6 (*C*8), 27.7 (*C*13), 15.0 (*C*11).

HRMS: *m/z* calcd. for $C_{18}H_{28}BrNO_3$: 386.1325 (M+H); found 386.1373

m.p. = 111 - 113 ^{o}C

_N_-(6-(_tert_-butyl)-3-(ethoxymethoxy)-4-(2,2,2-trifluoroacetyl)cyclohexa-1,3-dien-1-yl)pivalamide (45)

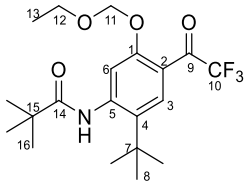

A solution of compound **44** (76 mg, 0.20 mmol) dissolved in THF (2.5 mL) under nitrogen was cooled to -45 °C. MeLi (1.5 M in Et_2O, 250 µL, 0.38 mmol, 1.9 equiv.) was added via syringe and the reaction mixture was warmed to ~0 °C and stirred for 2 minutes. The reaction mixture was cooled to -78 °C, then *n*-BuLi (1.5 M in hexanes, 215 µL, 0.33 mmol, 1.7 equiv.) was added via syringe, and let stir for 2 hours giving a cloudy white reaction mixture. Ethyl trifluoroacetate (700 µL, 7.3 mmol, 36 equiv.) was added rapidly via syringe and the reaction mixture was quickly warmed to room temperature. The reaction mixture was quenched with sat. aq. NH_4Cl (2 mL) and extracted into Et_2O (20 mL). The organic fractions were combined and washed with brine (15 mL) dried over Na_2SO_4 and concentrated to dryness to give **45** (74 mg, no remaining starting material by ^{1}H NMR) as a crude mixture which was used immediately in next step.

^{1}H NMR (500 MHz, $CDCl_3$) δ 8.26 (s, 1H), 7.84 (s, 1H), 7.74 (s, 1H), 5.32 (s, 2H), 3.77 (q, *J* = 7.1 Hz, 2H), 1.45 (s, 9H), 1.36 (s, 9H), 1.27 – 1.22 (m, 3H).

^{13}C NMR (151 MHz, $CDCl_3$) δ 181.7 (q, *J* = 36.3 Hz, C9), 176.3 (C19), 157.1 (C1), 143.5 (C2), 131.7 (C4), 130.0 (C3), 117.3 (C5), 116.7 (q, *J* = 290.7 Hz, C10), 109.5 (C6), 93.6 (C11), 65.3 (C12), 40.4 (C15), 33.9 (C7), 30.7 (C8), 27.8 (C16), 15.1 (C13).

HRMS: *m/z* calcd. for $C_{20}H_{28}F_3NO_4$: 404.2043 (M+H); found 404.2049

m.p. = 118 - 119 ^{o}C

***N*-(2-(*tert*-butyl)-5-(ethoxymethoxy)-4-(2,2,2-trifluoro-1-(hydroxyimino)ethyl)phenyl)pivalamide (46)**

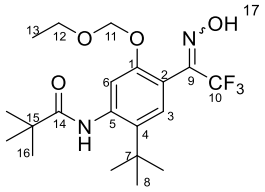

The crude trifluoromethylketone **45** (70 mg, 0.17 mmol) residue was dissolved in a 2:1 pyridine/MeOH mixture (3 mL), hydroxylamine hydrochloride (18 mg, 0.26 mmol, 1.5 equiv.) was added and the reaction mixture was heated at 60 °C for 2 hours and monitored by TLC (30% EtOAc/Hex product rf. 0.25). The reaction mixture was allowed to cool and concentrated to dryness. The crude residue was purified by automated flash chromatography on a 12 g silica cartridge (6-60 % EtOAc/Hex gradient) to give compound **46** (60 mg, 0.14 mmol, 84 % yield) as a clear colourless oil as a 2:1 ratio of isomers.

^{1}H NMR (600 MHz, $CDCl_3$) δ 9.00 (s, 1H), δ 8.27 (s, 1H), 7.88 (s, 1H), 7.73 (s, 1H), 7.61 (s, 1H), 7.58 (s, 1H), 7.14 (s, 1H),7.14 (s, 1H), 5.22 (s, 4H),5.22 (s, 2H), 3.70 (m {overlapping q}, *J* = 7.1, Hz, 3H), 1.41 (s, 9H), 1.40 (s, 9H), 1.36 (s, 9H), 1.35 (s, 22H), 1.23 – 1.19 (m {overlapping t}, 4H), 1.23 – 1.19 (m, 11H).

^{13}C NMR (151 MHz, $CDCl_3$) δ 176.5, 176.3, 154.7, 153.5, 147.5 (q, $^{2}J_{C\text{-}F}$ = 32.0 Hz), 146.9(obs. d, $^{2}J_{C\text{-}F}$ = 33.58 Hz), 139.0, 138.7, 133.8, 133.3, 128.8, 127.2, 120.7(obs. d, $^{1}J_{C\text{-}F}$=274.56 Hz), 118.1(q, $^{1}J_{C\text{-}F}$ = 282.27 Hz) 117.1, 112.7, 111.7, 111.6, 93.4, 93.3, 77.2, 64.8, 64.7, 39.9, 34.0, 30.8, 29.9, 27.8, 27.8, 15.1.

HRMS: *m/z* calcd. for $C_{20}H_{29}F_3N_2O_4$: 417.2007 (M-H); found 417.1963.

m.p. = 162 - 168 ^{o}C

***N*-(2-(*tert*-butyl)-5-(ethoxymethoxy)-4-(3-(trifluoromethyl)diaziridin-3-yl)phenyl)pivalamide (49)**

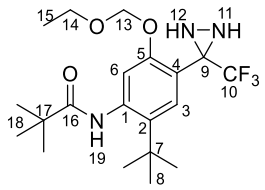

To a solution of oxime **46** (28 mg, 0.067 mmol) dissolved in DCM (2.8 mL), DIPEA (15 µL, 0.086 mmol, 1.3 equiv.) was added and the solution was cooled at 5 °C for 5 minutes. MsCl (6.5 µL, 0.081 mmol, 1.2 equiv.) was added via syringe, and the reaction mixture was stirred for 30 minutes and allowed to warm to room temperature. The reaction mixture was washed with sat. aq. NH_4Cl (5 mL), brine (5 mL), dried over Na_2SO_4 and concentrated to dryness to give crude intermediate **47** (38 mg) as a yellow oil. The crude mesyl-oxime **47** (46 mg, ~0.07 mmol) was dissolved in DCM (1 mL), transferred to a sealable reaction vessel and cooled to -78 °C. Then NH_3 was condensed (1 mL) into reaction vessel which was sealed and let warm to room temperature and stirred overnight. The reaction mixture was cooled at -78 ^oC for 15 minutes and opened, and allowed to warm to room temperature. The reaction mixture was filtered and concentrated to dryness. The crude material was purified by automated flash chromatography on a 4 g silica cartridge (7-70% EtOAc/Hex gradient) to give a mixture of **49** (34 mg, 0.062 mmol, 84% yield) and amidine byproduct **48**. The mixture of compounds **48** and **49** were recrystallized from an 8:2 Et_2O/Hex mixture to give a mixture of two crystalline species which were manually separated to give diaziridine **49** (8 mg, 0.019 mmol, 29% yield) as cubic yellow crystals and amidine **48** (11mg, 0.026 40% yield) as whilte spindles.

^{1}H NMR (500 MHz, $CDCl_3$) δ 7.82 (s, 1H), 7.59 (s, 1H), 7.46 (s, 1H), 5.33 – 5.24 (m, 2H), 3.74 (qd, *J* = 1.6, 7.1 Hz, 2H), 2.64 (d, *J* = 9.1 Hz, 1H), 2.50 (dd, *J* = 1.7, 8.9 Hz, 1H), 1.42 (s, 9H), 1.35 (s, 9H), 1.23 (t, *J* = 7.1 Hz, 3H).

^{13}C NMR (151 MHz, $CDCl_3$) δ 176.2, 154.8, 138.7, 133.3, 129.0, 124.9 (observed d, *J* = 626.7 Hz), 116.5, 111.2, 93.3, 77.2, 64.9, 40.0, 34.0, 30.8, 27.8, 15.2.

^{19}F NMR (471 MHz, $CDCl_3$) δ -77.0.

HRMS: *m/z* calcd. for $C_{20}H_{30}F_3N_3O_3$: 418.2312 (M+H); found 418.2322

m.p. = 113-116 °C

***tert*-Butyl (2-(*tert*-butyl)-5-(ethoxymethoxy)-4-(2,2,2-trifluoro-1-methoxyethyl)phenyl)carbamate (53)**

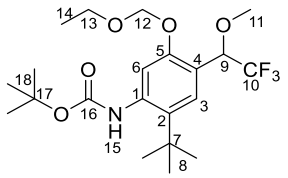

A solution of diazirine **43** (3 mg, 7 µmol) dissolved in MeOH (300 µL) was placed in an NMR tube, which was suspended in a UV light box and irradiated for 48h. The reaction mixture was concentrated to dryness. The crude residue was dissolved in MeOD (500 µL) and concentrated to dryness (repeated this process 3 times to remove residual MeOH) to give **53** as a clear colourless oil (3 mg, 6.9 µmol, 98% yield).

^{1}H NMR (600 MHz, MeOD) δ 7.50 (s, 1H, C-3-*H*), 7.10 (s, 1H, C-6-*H*), 5.29 – 5.23 (m, 2H, C-12-*H*), 5.14 (q, *J* = 6.7 Hz, 1H, C-9-*H*), 3.72 (q, *J* = 7.1 Hz, 2H, C-13-*H*), 3.35 (s, 3H, C-11-*H*), 1.51 (s, 9H, C-18-*H*), 1.38 (s, 9H, C-8-*H*), 1.21 (t, *J* = 7.1 Hz, 3H, C-14-*H*).

^{13}C NMR (151 MHz, MeOD) δ 157.0 (*C*-20), 155.7 (*C*-5), 140.8 (*C*-2), 138.8 (*C*-1), 127.5 (*C*-3), 125.6 (obs. d, $^{1}J_{C\text{-}F}$ = 281.3 Hz, *C*-10), 120.4 (*C*-4), 117.6 (*C*-6), 94.5 (*C*-12), 81.2 (*C*-17), 75.3 (q, $^{2}J_{C\text{-}F}$ = 31.2 Hz (*C*-9)), 65.5 (*C*-13), 58.3 (*C*-11), 35.6 (*C*-7), 31.3 (*C*-8), 28.8 (*C*-18), 15.4 (*C*-14).

^{19}F NMR (376 MHz, MeOD) δ -78.2.

MS: *m/z* calcd. for $C_{21}H_{32}F_3NO_5$: 453.2571 $[M+NH_4]^+$; found 453.2577.

m.p. = 71 – 73 °C

5-Amino-4-(*tert*-butyl)-2-(3-(trifluoromethyl)-3H-diazirin-3-yl)phenol (4)

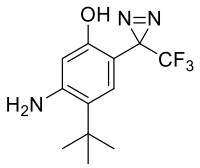

To a solution of compound **46** (62 mg, 0.144 mmol) dissolved in MeOH (1 mL), sat. methanolic HCl (1 mL, prepared by bubbling HCl (*g*) through methanol) was added and the reaction mixture was stirred for 1 hour, monitored by TLC and LC-MS. The reaction mixture was blown dry under a stream of nitrogen (*g*), concentrated *in vacuo* to give compound **4** (34 mg, 0.124 mmol, 86 % yield) as an HCl salt as a crystalline solid which was used immediately in subsequent reactions.

^{1}H NMR (500 MHz, MeOD) δ 7.29 (s, 1H), 6.44 (s, 1H), 1.38 (s, 9H).

^{19}F NMR (471 MHz, MeOD) δ -70.68.

HRMS: *m/z* calc'd. for $C_{12}H_{14}F_3N_3O$: 274.1162 (M+H); found 274.1142.

5-Amino-2-bromo-4-(*tert*-butyl)phenol (58)

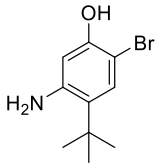

To a solution of compound **37** (30 mg, 0.075 mmol) dissolved in MeOH (1 mL), sat. methanolic HCl (1 mL, prepared by bubbling HCl (*g*) through methanol) was added and the reaction mixture was stirred for 1 hour. The reaction mixture was blown dry under a stream of nitrogen (*g*) to give compound **58** as the HCl salt as a crystalline solid, which was used immediately in subsequent reactions.

^{1}H NMR (400 MHz, $CDCl_3$) δ 7.22 (s, 1H), 6.33 (s, 1H), 5.22 (s, 1H), 3.82 (s, 2H), 1.37 (s, 9H).

^{13}C NMR (101 MHz, $CDCl_3$) δ 150.9 (C1), 145.8 (C5), 129.7 (C3), 128.6 (C4), 104.6 (C6), 98.5(C2), 34.0 (C7), 29.9 (C8).

HRMS: *m/z* calc'd. for $C_{10}H_{14}BrNO$: 244.0332 (M+H); found 244.0327.

1-(4-Amino-5-(*tert*-butyl)-2-(ethoxymethoxy)phenyl)-2,2,2-trifluoroethan-1-one (59)

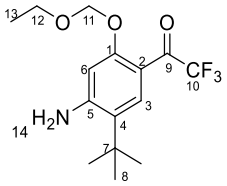

To a solution of compound **38** (50 mg, 0.119 mmol) in THF (1mL), TBAF (1 M in THF, 125 µL, 0.125 µL, 1.05 equiv.) was added and the reaction mixture was heated at 40°C for 5 hours, and monitored by TLC (20% EtOAc/Hex). The reaction mixture was cooled to room temperature and extracted into DCM (4 mL). The organic fractions were combined and washed with H_2O (6 mL), brine (3 mL), dried over Na_2SO_4 and concentred to dryness to give compound **59** (36 mg, 0.113 mmol, 95% yield) as an orange solid.

^{1}H NMR (500 MHz, $CDCl_3$) δ 7.72 (s, 1H), 6.42 (s, 1H), 5.24 (s, 2H), 4.56 (s, 2H), 3.75 (q, *J* = 7.1 Hz, 2H), 1.39 (s, 9H), 1.23 (t, *J* = 7.1 Hz, 3H).

^{13}C NMR (151 MHz, $CDCl_3$) δ 179.3, 179.1, 178.9, 178.6, 158.9, 152.8, 131.9, 126.7, 120.1, 118.2, 116.3, 114.4, 111.4, 102.1, 93.5, 77.2, 64.9, 33.9, 29.7, 15.1.

^{19}F NMR (471 MHz, $CDCl_3$) δ -72.7.

HRMS: *m/z* calcd. for $C_{15}H_{20}F_3NO_3$: 318.1323 (M-H); found 318.1369

_N_-(4-bromo-2-(_tert_-butyl)-5-(ethoxymethoxy)phenyl)-4-oxo-1,4-dihydroquinoline-3-carboxamide (62)

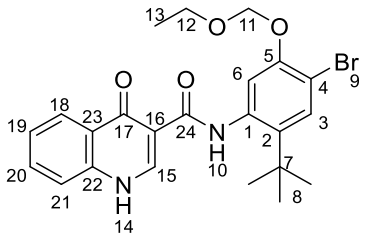

A mixture of aniline **36** (2.00 g, 6.62 mmol), HATU (5.03 g, 6.62 mmol, 2 equiv.), 1,4-dihydro-4-oxoquinoline-3-carboxylic acid (commercially obtained, 1.88 g, 9.93 mmol, 1.5 equiv.), DMAP (81 mg, 0.66 mmol, 0.1 equiv.), and HOBt (895 mg, 6.62 mmol, 1 equiv.) were dissolved in DMF (20 mL). DIPEA (3.5 mL, 19.9 mmol, 3 equiv.) was added and the reaction mixture was stirred overnight at 60 ^{o}C. The reaction mixture was cooled to room temperature and concentrated to remove DMF. The crude residue was diluted with EtOAc (200 mL) and washed with sat. aq. $NaHCO_3$ (100 mL), and brine (50 mL) dried over Na_2SO_4 and concentrated to dryness. The crude residue was purified by automated flash chromatography on an 80 g silica cartridge (75-100% EtOAc/Hex) to give **62** as a white crystalline solid (2.6 g, 5.5 mmol, 83 % yield).

^{1}H NMR (400 MHz, MeOD) δ 8.89 (s, 1H), 8.43 (ddd, *J* = 8.2, 1.4, 0.5 Hz, 1H), 7.82 (ddd, *J* = 8.4, 7.0, 1.5 Hz, 1H), 7.68 (d, *J* = 8.3 Hz, 1H), 7.60 (s, 1H), 7.56 (ddd, *J* = 8.2, 7.0, 1.1 Hz, 1H), 7.47 (s, 1H), 5.29 (s, 2H), 3.77 (q, *J* = 7.1 Hz, 2H), 1.45 (s, 9H), 1.22 (t, *J* = 7.1 Hz, 3H).

^{1}H NMR (500 MHz, $CDCl_3$) δ 12.60 (s, 1H, N-10-*H*), 12.52 (d, *J* = 6.4 Hz, 1H, N-14-*H*), 9.08 (d, *J* = 6.8 Hz, 1H, C-15-*H*), 8.43 (dd, *J* = 1.8, 7.8 Hz, 1H, C-18-*H*), 7.77 (s, 1H, C-3-*H*), 7.46 (dq, *J* = 7.2, 1.2 Hz, 1H, C-20-*H*), 7.43 (dq, *J* = 7.0, 1.3 Hz, 1H, C-19-*H*), 7.34 (s, 1H, C-6-*H*), 6.02 (dd, *J* = 1.2, 7.4 Hz, 1H, C-21-*H*), 5.08 (s, 2H, C-11-*H*), 3.48 (q, *J* = 7.1 Hz, 2H, C-12-*H*), 1.45 (s, 9H, C-8-*H*), 0.97 (t, *J* = 7.1 Hz, 3H, C-13-*H*).

^{13}C NMR (126 MHz, $CDCl_3$) δ 177.9 (*C*-17), 165.8 (*C*-24), 152.5 (*C*-5), 144.4 (*C*-15), 141.4 (*C*-2), 139.2 (*C*-22), 135.5 (*C*-1), 133.1 (*C*-20), 131.7 (*C*-3), 126.6 (*C*-23), 126.1 (*C*-18), 125.6 (*C*-19), 118.6 (*C*-21), 117.9 (*C*-6), 111.1 (*C*-4), 110.3 (*C*-16), 93.8 (*C*-11), 64.8 (*C*-12), 34.8 (*C*-7), 30.8 (*C*-8), 14.9 (*C*-13).

HRMS: *m/z* calcd. for $C_{23}H_{25}BrN_2O_4$: 473.1071 (M+H); found 473.1051.

m.p. = 205 - 206.5 ^{o}C.

***N*-(2-(*tert*-butyl)-5-(ethoxymethoxy)-4-(2,2,2-trifluoroacetyl)phenyl)-4-oxo-1,4-dihydroquinoline-3-carboxamide (63)**

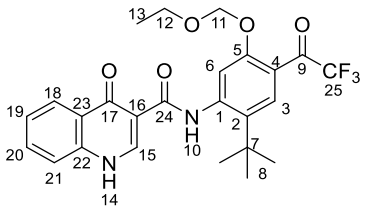

To a solution of compound **62** (20 mg, 0.042 mmol) in THF (1 mL) under N_2, cooled at -40 ^{o}C, MeLi (1.5 M, 70 µL, 2.5 equiv.) was added via syringe, and the reaction mixture was warmed to 0^{o}C and stirred for 2 minutes. The reaction mixture was cooled to -78 ^{o}C then *n*-BuLi (1.5 M, 42 µL, 1.5 equiv.) was added slowly via syringe. The reaction mixture was warmed to 0^{o}C, then cooled to -78 ^{o}C, and stirred for 15 minutes. Ethyl trifluoroacetate (300 µL, 60 equiv.) was added quickly via syringe and the reaction mixture was warmed to 0^{o}C then quenched with sat. aq. NH_4Cl (1 mL). The reaction mixture was extracted into EtOAc (5 mL) and the organic fractions were combined and washed with brine (2 mL) dried over Na_2SO_4 and concentrated to dryness. The crude residue was purified by HPLC then lyophilized to give **63** (11 mg, 0.022 mmol, 53 % yield) as a white crystalline solid.

To a solution of compound **62** (230 mg, 0.486 mmol) in THF (10 mL) under N_2, cooled at -40 ^{o}C, MeLi (1.6 M, 700 µL, 1.12 mmol, 2.3 equiv.) was added via syringe, the reaction mixture was stirred for 2 minutes. At -40 ^{o}C, *n*-BuLi (1.58 M, 370 µL, 0.583 mmol, 1.5 equiv.) was added slowly via syringe and the reaction mixture was stirred for 15 minutes. Ethyl trifluoroacetate (1.7 mL, 15 mmol, 30 equiv.) was added quickly via syringe and the reaction mixture was warmed to 0^{o}C then quenched with sat. aq. NH_4Cl (1 mL). The reaction mixture was extracted into EtOAc (5 mL) and the organic fractions were combined and washed with brine (2 mL) dried over Na_2SO_4 and concentrated to dryness to give crude compound **63** as a mixture of species as a yellow oil (270 mg, prep-HPLC analysis at 254 nm showed conversion of approximately 65 %, based on this value the theoretical yield ≈ 0.32 mmol). This crude material was utilized without purification in the subsequent oxime formation reaction (Compound **64**, Methods B and C).

^{1}H NMR (600 MHz, $CDCl_3$) δ 12.66 (s, 1H, C-10-*H*), 11.63 (s, 1H, C-14-*H*), 9.01 (s, 1H, C-15-*H*), 8.49 – 8.42 (m, 1H, C-20,21-*H*), 7.91 (s, 1H, C-3-*H*), 7.78 (s, 1H, C-10-*H*), 7.44 (m, 2H), 6.65 (d, *J* = 7.4 Hz, 1H), 5.19 (s, 2H), 3.59 (q, *J* = 7.1 Hz, 2H), 1.52 (s, 9H), 1.08 (t, *J* = 7.1 Hz, 3H).

^{13}C NMR (151 MHz, $CDCl_3$) δ 182.4 (q, $^{2}J_{C\text{-}F}$ = 36.0 Hz, *C*-9), 177.7 (*C*-17), 165.2 (*C*-24), 156.2 (*C*-5), 144.4 (*C*-15), 142.8 (*C*-1), 139.0 (*C*-22), 137.9 (*C*-2), 133.2 (*C*-20), 130.4 (*C*-3), 126.7 (*C*-23), 126.6 (*C*-18), 125.9 (*C*-19), 119.4 (*C*-4), 118.2 (*C*-21), 116.5 (q, $^{1}J_{C\text{-}F}$ = 290.7 Hz, *C*-25), 114.8 (*C*-6), 110.7 (*C*-16), 93.4 (*C*-11), 65.2 (*C*-12), 34.8 (*C*-7), 30.5 (*C*-8), 15.0 (*C*-13).

HRMS: *m/z* calcd. for $C_{25}H_{26}F_3N_2O_5$: 491.1788 (M+H); found 491.1741 *m/z*.

m.p. = 107 – 109 °C.

_N_-(2-(*tert*-butyl)-5-(ethoxymethoxy)-4-(2,2,2-trifluoro-1-(hydroxyimino)ethyl)phenyl)-4-oxo-1,4-dihydroquinoline-3-carboxamide (64)

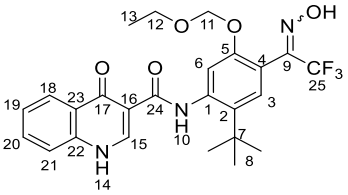

Method A: To a solution of trifluoromethylketone **63** (37 mg, 0.075 mmol) in a 2:1 mixture of pyridine/MeOH (6 mL), hydroxylamine hydrochloride (6 mg, 0.083 mmol, 1.1 equiv) was added and the reaction mixture was heated at 60^{o}C for 24 hours concentrated to dryness, purified by semi-prep HPLC (75% ACN/H_2O, 5mM NH_4AcOH) to give compound **64** as a white residue (rt. 2.7 min).

Method B: To the crude residue of compound **63** (52 mg, 0.106 mmol of ketone) dissolved in 2:1 pyridine/MeOH mixture, hydroxylamine hydrochloride (9 mg, 0.132 mmol, 1.1 eqiuv.) was added. The reaction mixture was heated at 60 ^{o}C overnight. Progress of the reaction was monitored by HPLC. Another aliquot of hydroxylamine hydrochloride (2 mg, 0.03 mmol, 0.3 equiv.) was added and the reaction mixture was heated at 60 ^{o}C for 72 hours. The reaction mixture was cooled to room temperature and concentrated to dryness. The crude residue was purified by semi-preparative HPLC (70% isocratic eluent ACN/H_2O, 5 mM NH_4OAc, rt 2.7 min.) to give compound **64** as a white fluffy powder, (35 mg, 0.069 mmol, 65 % yield over 2 steps).

Method C: To the crude residue of compound **63** (270 mg, ~0.32 mmol), in a 2:1 mixture of pyridine/MeOH, hydroxylamine hydrochloride (42 mg, 0.61 mmol, ~1.9 equiv.) was added and the reaction mixture was heated overnight at 60 ^{o}C. The progress of the reaction was monitored by HPLC. The crude reaction mixture was cooled to room temperature concentrate to dryness, and the crude residue was purified by automated flash chromatography on a 12 g silica column (30-100% EtOAc/Hex gradient). The recovered material was then, recrystallized from a 1:10:2 MeOH/DCM/Hexanes mixture to give compound **64** (285 mg, 0.56 mmol, 53% yield over two steps) as a white solid >90% pure by HPLC.

^{1}H NMR (600 MHz, $CDCl_3$) δ 12.46 (d, *J* = 9.8 Hz, 1H), 11.75 (s, 1H), 9.02 (t, *J* = 2.7 Hz, 1H), 8.41 (dt, *J* = 8.2, 2.0 Hz, 1H), 7.57 (s, 0H), 7.49 – 7.45 (m, 2H), 7.37 – 7.33 (m, 2H), 7.33 (s, 0H), 6.64 (dd, *J* = 8.0, 3.8 Hz, 1H), 5.13 (s, 1H), 5.10 (s, 1H), 3.56 (q, *J* = 7.0 Hz, 2H), 3.54 (d, *J* = 12.8 Hz, 0H), 1.43 (s, 3H), 1.34 (s, 6H), 1.06 (t, *J* = 7.1 Hz, 2H), 1.05 (t, *J* = 7.0 Hz, 1H).

^{13}C NMR (151 MHz, $CDCl_3$) δ 198.4, 177.8, 177.7, 154.7, 154.5, 153.2, 144.3, 139.1, 139.0, 138.4, 138.3, 133.3, 129.4, 127.7, 126.6, 126.4, 125.6, 118.6, 118.5, 115.2, 114.4, 93.3, 93.2, 77.2, 64.8, 64.6, 34.6, 30.7, 30.7, 15.0, 15.0.

HRMS: *m/z* calcd. for $C_{25}H_{26}F_3N_3O_5$: 506.1897 (M+H); found 506.1920.

m.p. = 207 - 210 ^{o}C.

***N*-(2-(*tert*-butyl)-5-(ethoxymethoxy)-4-(3-(trifluoromethyl)diaziridin-3-yl)phenyl)-4-oxo-1,4-dihydroquinoline-3-carboxamide (66)**

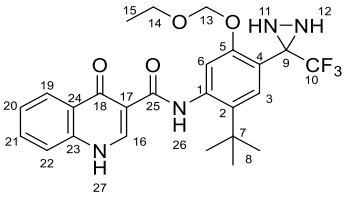

To a solution of oxime **64** (126 mg, 0.250 mmol) in DCM, DIPEA (133 µL, 0.75 mmol, 3 equiv.) was added and stirred until all solids dissolved, then the reaction mixture was cooled to 0°C and *p*-TsCl (62 mg, 1.3 equiv.) was added. The reaction mixture was stirred for 15 minutes, then warmed to room temperature and stirred for 15 minutes. The progress of the reaction was monitored by LC-MS. The crude reaction mixture was added directly to a sealable vessel containing NH_3 (*l*) at -40 °C. The reaction mixture was sealed in the vessel and stirred overnight at room temperature. The reaction mixture was cooled to -60 °C and stirred for 15 minutes, then the reaction vessel was opened, and the reaction mixture was allowed to warm to room temperature and stirred for 15 minutes. The reaction mixture was purified by preparatory scale HPLC, (55% ACN/H_2O, 5mM NH_4OAc isocratic elution) and lyophilized to give diaziridine **66** (44 mg, 0.087 mmol, 35% over 2 steps) as a white amorphous solid.

^{1}H NMR (601 MHz, $CDCl_3$) δ 12.51 (s, 1H, C-26-*H*), 11.97 (s, 1H, C-27-*H*), 9.05 (d, *J* = 4.5 Hz, 1H, C-16-*H*), 8.45 (dd, *J* = 1.5, 8.1 Hz, 1H, C-19-*H*), 7.70 (s, 1H, C-3-*H*), 7.51 – 7.45 (m, 2H, C-6-*H*, C-21-*H*), 7.44 – 7.39 (m, 1H, C-20-*H*), 6.35 (d, *J* = 8.2 Hz, 1H, C-22-*H*), 5.11 (s, 2H, C-13-*H*), 3.59 – 3.45 (m, 2H, C-14-*H*), 2.72 (d, *J* = 9.0 Hz, 1H, C-11-*H*), 2.32 (d, *J* = 9.0 Hz, 1H, C-12-*H*), 1.50 (s, 8H, C-8-*H*), 1.04 (t, *J* = 7.1 Hz, 3H, C-15-*H*).

^{13}C NMR (151 MHz, $CDCl_3$) δ 177.7 (*C*-18), 165.4 (*C*-25), 154.6 (*C*-5), 144.4 (*C*-16), 139.1 (*C*-23), 138.5 (*C*-2), 138.1 (*C*-1), 132.9 (*C*-21), 129.7 (*C*-3), 126.7 (*C*-24), 126.5 (*C*-19), 125.6 (*C*-20), 123.6 (q, $^1J_{C\text{-}F}$ = 279.1 Hz, *C*-10), 118.3 (*C*-4), 118.3 (*C*-22), 115.1 (*C*-6), 110.7 (*C*-17), 93.1 (*C*-13), 64.8 (*C*-14), 56.3 (observed d, $^2J_{C\text{-}F}$ = 37.0 Hz, *C*-9), 34.7 (*C*-7), 30.8 (*C*-8), 15.0 (*C*-15).

^{19}F NMR (471 MHz, $CDCl_3$) δ -76.86.

HRMS: *m/z* calcd. for $C_{25}H_{27}F_3N_4O_4$: 505.2057 (M+H); found 505.2085

m.p. = 145 - 147 ^{o}C

IR (cm^{-1}): 3235 (w), 2959 (w), 1644 (m), 1568 (m), 1520 (s), 1476 (s), 1148 (s).

_N_-(2-(_tert_-butyl)-5-(ethoxymethoxy)-4-(3-(trifluoromethyl)-3_H_-diazirin-3-yl)phenyl)-4-oxo-1,4-dihydroquinoline-3-carboxamide (67)

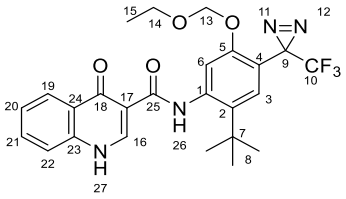

To a solution of diaziridine **66** (15 mg, 0.030 mmol) in DCM (300 µL) in an amber vial wrapped in foil, DMP (38 mg, 0.090 mmol, 3.0 equiv.) was added and the reaction mixture was stirred for 1 hour. The progress of the reaction was monitored by TLC (EtOAc) and HPLC. The reaction mixture was quenched with 1M aq. NaOH (2 mL), and the organic layer was washed with H_2O (2 mL), brine (1 mL), and dried over Na_2SO_4 filtered and blown dry under a stream of N_2 then placed under vacuum to give **67** (11 mg, 0.022 mmol, 74% yield) as a white powder >95% pure by ^{1}H NMR and LC-MS.

^{1}H NMR (600 MHz, $CDCl_3$) δ 12.57 (s, 1H, C-26-*H*), 12.08 (s, 1H, C-27-*H*), 9.04 (d, *J* = 4.9 Hz, 1H, C-16-*H*), 8.44 (dd, *J* = 1.5, 8.1 Hz, 1H, C-19-*H*), 7.64 (s, 1H, C-3-*H*), 7.48 (s, 1H, C-6-*H*), 7.42 (ddd, *J* = 1.1, 7.0, 8.1 Hz, 1H, C-20-*H*), 7.30 – 7.25 (m, 1H, C-21-*H*), 6.30 (d, *J* = 8.3 Hz, 1H, C-22-*H*), 5.15 (s, 2H, C-13-*H*), 3.56 (q, *J* = 7.1 Hz, 2H, C-14-*H*), 1.48 (s, 9H, C-8-*H*), 1.03 (t, *J* = 7.1 Hz, 3H, C-15-*H*).

^{13}C NMR (151 MHz, $CDCl_3$) δ 177.7 (*C*-18), 165.5 (*C*-25), 155.9 (*C*-5), 144.3 (*C*-16), 139.2 (*C*-2), 139.1 (*C*-23), 138.8 (*C*-1), 133.0 (*C*-21), 129.2 (*C*-3), 126.6 (*C*-17), 126.4 (*C*-19), 125.6 (*C*-20), 122.2 (q, $^{1}J_{C\text{-}F}$ = 274.9 Hz, *C*-10), 118.1 (*C*-22), 115.6 (*C*-6), 115.0 (*C*-4), 110.5 (*C*-17), 93.0 (*C*-13), 64.8 (*C*-14), 34.7 (*C*-7), 30.7 (*C*-8), 26.6 (q, $^{2}J_{C\text{-}F}$ = 42.6 Hz, *C*-13), 15.0 (*C*-15).

HRMS: *m/z* calcd. for $C_{25}H_{25}F_3N_4O_4$: 503.1901 (M+H); found 503.1914

***N*-(4-bromo-2-(*tert*-butyl)-5-hydroxyphenyl)-4-oxo-1,4-dihydroquinoline-3-carboxamide (68)**

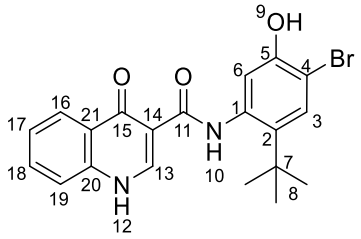

To a solution of compound **62** (3 mg, 6.3 µmol) dissolved in MeOH (0.5 mL), sat. methanolic HCl (0.5 mL, prepared by bubbling HCl (*g*) through methanol) was added and the reaction mixture was stirred for 1 hour. The reaction mixture was blown dry under a stream of nitrogen (*g*) to give compound **68** (2.5 mg, 6.0 µmol, 95 % yield) as a crystalline solid.

^{1}H NMR (600 MHz, MeOD) δ 8.88 (s, 1H), 8.42 (ddd, *J* = 0.7, 1.4, 8.2 Hz, 1H), 7.81 (ddd, *J* = 1.4, 7.1, 8.4 Hz, 1H), 7.67 (dt, *J* = 0.9, 8.3 Hz, 1H), 7.55 (ddd, *J* = 1.1, 7.1, 8.2 Hz, 1H), 7.50 (s, 1H), 7.17 (s, 1H), 1.43 (s, 8H).

^{13}C NMR (151 MHz, MeOD) δ 178.8 (*C*-15), 165.9 (*C*-11), 153.3 (*C*-5), 145.5 (*C*-13), 140.7 (*C*-20), 138.2 (*C*-2), 136.1 (*C*-1), 134.4 (*C*-18), 131.8 (*C*-3), 127.7 (*C*-21), 126.9 (*C*-16), 126.8 (*C*-17), 119.9 (*C*-19), 117.7 (*C*-6), 112.0 (*C*-14), 108.0 (*C*-4), 35.1 (*C*-7), 31.1 (*C*-8).

HRMS: *m/z* calcd. for $C_{20}H_{19}BrN_2O_3$: 415.0632 (M+H); found 415.0602.

***N*-(2-(*tert*-butyl)-5-hydroxy-4-(3-(trifluoromethyl)-3*H*-diazirin-3-yl)phenyl)-4-oxo-1,4-dihydroquinoline-3-carboxamide (2)**

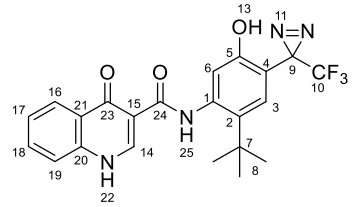

To a solution of diazirine **67** (11 mg, 0.022 mmol) in MeOH (400 µL), in an amber vial wrapped in foil, sat. methanolic HCl (250 µL) was added and the reaction mixture was stirred at room temperature for 2 hours. The progress of the reaction was monitored by LC-MS and TLC

(EtOAc). The reaction mixture was blown dry under a stream of N_2 (*g*) and then concentrated *in vacuo* to give phenol **2** (10 mg, 0.022 mmol, quantitative yield) as a white solid residue.

^{1}H NMR (601 MHz, DMSO) δ 12.95 (s, 1H, N-25-*H*), 12.15 (s, 1H, N-22-*H*), 10.27 (s, 1H, O-13-*H*), 8.87 (s, 1H, C-14-*H*), 8.31 (dd, *J* = 1.4, 8.1 Hz, 1H, C-16-*H*), 7.79 (t, *J* = 7.6 Hz, 1H, C-18-H), 7.74 (d, J = 8.2 Hz, 1H, C-19-H), 7.52 (s, 1H, C-3-H), 7.50 (t, J = 7.5 Hz, 1H, C-17-H), 7.31 (s, 1H, C-6-H), 1.40 (s, 9H, C-8-H).

^{1}H NMR (600 MHz, MeOD) δ 8.88 (s, 1H, C-*H*-14), 8.41 (d, J = 8.0 Hz, 1H, C-*H*-16), 7.82 (t, J = 7.5 Hz, 1H, C-*H*-18), 7.68 (d, J = 8.1 Hz, 1H, C-*H*-19), 7.56 (t, J = 7.4 Hz, 1H, C-*H*-17), 7.44 (s, 1H, C-*H*-3), 7.23 (s, 1H, C-*H*-6), 1.45 (s, 9H, C-*H*-8).

^{13}C NMR (151 MHz, MeOD) δ 178.7 (*C*-23), 165.8 (*C*-24), 157.7 (*C*-5), 145.6 (*C*-14), 140.7 (*C*-20), 139.4 (*C*-1), 136.5 (*C*-2), 134.5 (*C*-18), 129.4 (*C*-3), 127.6 (*C*-21), 126.9 (*C*-16), 126.8 (*C*-17), 123.8 (q, J = 273.9 Hz, *C*-10), 120.0 (*C*-19), 117.1 (*C*-6), 112.5 (*C*-4), 111.8 (*C*-16), 35.1 (*C*-7), 30.9 (*C*-8), 27.6 (q, J = 42.5 Hz, *C*-9).

^{19}F NMR (376 MHz, MeOD) δ -70.54.

HRMS: *m/z* calcd. for $C_{22}H_{19}F_3N_4O_3$: 445.1487 (M+H); found 445.1474

UV (MeOH) λmax 311 nm.

Appendix B.

Initial progress and experimental of synthetic efforts towards alternative ivacaftor PAL probe 3

Syntheses of the PAL probe compound **3** via diazirine **8** were attempted beginning with the use of aniline **10**. Although diazirine **8** was not synthesized prior to writing this manuscript, the route which progressed towards this species the furthest involved a Friedel-Crafts reaction of aniline **10** with trifluoroacetic anhydride and $AlCl_3$ which successfully installed the trifluoromethyl ketone moiety to give compound **70**. Protection of phenol **70** with an EOM group gave compound **71**. Concurrent to this synthesis, the stability issues experienced in the synthesis of compound **4** were experienced and therefore efforts towards aniline-diazirine **8** were paused for re-evaluation of the synthetic path.

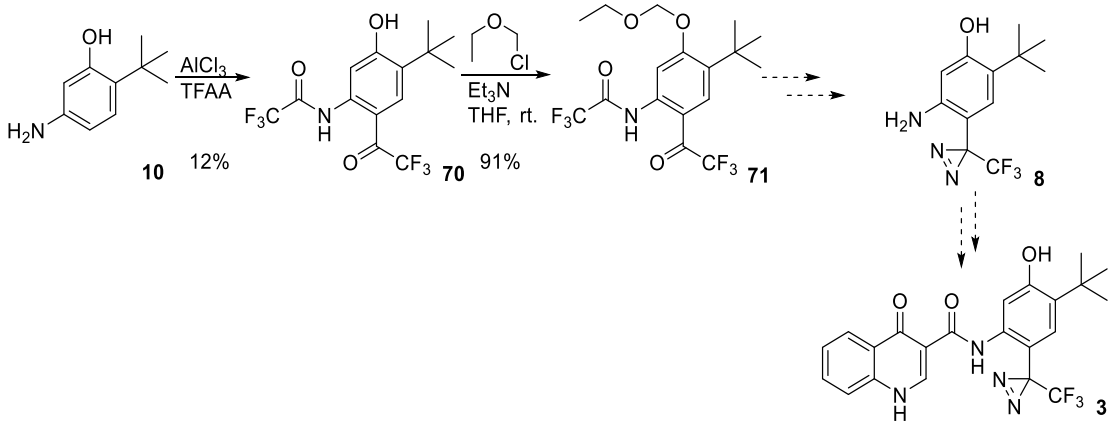

Figure 40 Synthetic progress towards intermediate 8

Following the successful tri-anion chemistry and diazirine synthesis towards **2** (see Chapter 4)**,** two possible routes to towards synthesizing compound **3** have been designed and will be attempted (Figure 41). Among the intermediates synthesized during synthetic efforts towards aniline-diazirine **8** was iodo **72**. Protection of the phenol moiety of compound **72** would lead to aniline **73**. This species could potentially be utilized in a similar manner as the bromo-aniline **39** in subsequent amide bond reactions with LHS acid **5** to give iodo **74** affording the ability to perform lithium-halogen exchange reactions to give trifluoromethylketone **76**. As well, rather than installing the diazirine prior to deprotection (which would yield **8**), the trifluoroacetamide could be removed from trifluoromethylketone **71**, giving aniline **75**. This

species could be used give generate amide **76** following amide bond formations with LHS acid **5**. In future efforts these options will be explored.

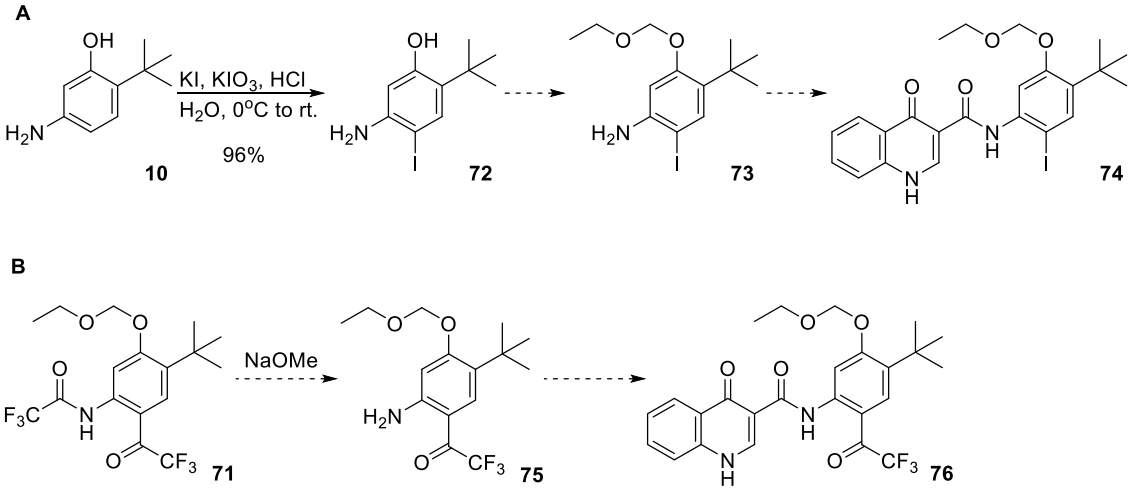

Figure 41 Possible synthetic routes to 3 via iodo 72 and via trifluoroacetamide 71

Experimental Procedures

N-(4-(*tert*-butyl)-5-hydroxy-2-(2,2,2-trifluoroacetyl)phenyl)-2,2,2-trifluoroacetamide (70)

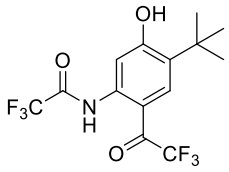

Aniline **10** (500 mg, 3.03 mmol) was placed in a vial, and TFAA (10 mL) was added slowly with stirring. $AlCl_3$ (403.5 mg, 3.03 mmol, 1.0 equiv.) was added and the reaction mixture was left to stir for 2 weeks. The reaction mixture was quenched into a mixture of ice and 1M HCl (20 mL) and stirred for 15 minutes. The mixture was extracted into DCM (50 mL), and the organic fractions were combined and washed with brine (50 mL), dried over Na_2SO_4 concentrated to dryness. The crude residue was diluted with MeOH (5 mL), stirred for 5 minutes, and concentrated to dryness. The crude residue was purified by automated flash chromatography on a 40 g silica cartridge (2-30 % EtOAc/Hex) to give compound **70** (128 mg, 0.358 mmol, 12 % yield) as a white crystalline solid.

^{1}H NMR (500 MHz, $CDCl_3$) δ 12.63 (s, 1H), 8.63 (s, 1H), 8.48 (s, 1H), 8.02 (d, *J* = 2.0 Hz, 1H), 1.43 (s, 9H).

^{13}C NMR (151 MHz, $CDCl_3$) δ 181.5 (q, *J* = 34.4 Hz), 163.5, 156.5 (q, *J* = 38.4 Hz), 140.0, 134.1, 131.8 (q, *J* = 4.1 Hz), 128.2, 118.4, 116.3 (q, *J* = 290.7 Hz), 115.0 (q, *J* = 287.9 Hz), 114.4, 108.7, 34.4, 28.5.

^{19}F NMR (471 MHz, $CDCl_3$) δ -69.10, -76.04.

HRMS: *m/z* calcd. for $C_{14}H_{13}F_6NO_3$: 358.0872 (M+H); found 358.0870

m.p. = 163-164 °C

_N_-(4-(_tert_-butyl)-5-(ethoxymethoxy)-2-(2,2,2-trifluoroacetyl)phenyl)-2,2,2-trifluoroacetamide (71)

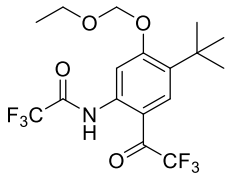

To a solution of phenol **70** (51 mg, 0.143 mmol) in THF (1 mL) at room temperature under N_2, DIPEA (55 µL, 0.315 mmol, 2.2 equiv.) was added via syringe, followed by chloromethylethyl ether (16 µL, 0.172 mmol, 1.2 equiv.) via syringe and the reaction mixture was stirred overnight. The reaction mixture was quenched with sat. aq. NH_4Cl (100 mL) extracted into Et_2O (50 mL, 3x). The organic layers were combined, washed with brine (100 mL) dried over Na_2SO_4, filtered, and concentrated to dryness to give compound **71** (54 mg, 0.13 mmol, 91%) as a yellow solid.

^{1}H NMR (601 MHz, $CDCl_3$) δ 12.19 (s, 1H), 8.55 (s, 1H), 7.99 (t, *J* = 2.0 Hz, 1H), 5.45 (s, 2H), 3.78 (q, *J* = 7.1 Hz, 2H), 1.40 (s, 9H), 1.27 (t, *J* = 7.1 Hz, 3H).

^{13}C NMR (151 MHz, $CDCl_3$) δ 182.1 (q, *J* = 34.4 Hz), 163.8, 155.9 (q, *J* = 38.1 Hz), 141.8, 135.7, 131.2 (d, *J* = 4.5 Hz), 125.7, 116.9 (q, *J* = 290.9 Hz), 115.6 (q, *J* = 288.6 Hz), 109.9, 106.7, 93.3, 65.7, 35.2, 29.4, 15.1.

^{19}F NMR (376 MHz, $CDCl_3$) δ -69.34, -76.32.

HRMS: *m/z* calcd. for $C_{17}H_{19}F_6NO_4$: 416.1291 (M+H); found 416.1290

m.p. = 29 - 31 °C

5-amino-2-(*tert*-butyl)-4-iodophenol (72)

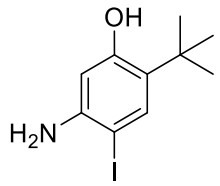

To a solution of aniline **10** (1.084 g, 6.56 mmol) suspended in H_2O (25 mL), HCl (conc., 550 µL, 6.56 mmol, 1 equiv.) was added and the reaction mixture was stirred at room temperature for 10 minutes until compound **10** dissolved. The reaction mixture was cooled to 0 °C then a solution of KI (719 mg, 4.33 mmol, 0.66 equiv.) and KIO_3 (463 mg, 2.16 mmol, 0.33 equiv.) in H_2O (2 mL), was added dropwise forming a brown precipitate The reaction mixture was stirred for 1 hour at room temperature and filtered to give compound **72** (1.84 g, 6.3 mmol, 96 % yield) as a brown solid.

^{1}H NMR (400 MHz, $CDCl_3$) δ 7.41 (s, 1H), 6.16 (s, 1H), 1.34 (s, 9H).

^{13}C NMR (101 MHz, $CDCl_3$) δ 155.5, 145.7, 137.0, 129.5, 103.4, 73.8, 34.0, 29.9.

HRMS: *m/z* calcd. for $C_{10}H_{14}INO$: 292.0193 (M+H); found 292.0174

m.p. = 136-139 °C

Appendix C

Supplemental Data File

Description:

The accompanying PDF file contains relevant characterization data for the final series of novel compounds (that were described in Chapter 4) that were generated in the synthesis of compound **2**, as well as for other select compounds in the thesis.

Filename:

Appendix C Supplemental data file.pdf

References

(1) Cant, N.; Pollock, N.; Ford, R. C. *Int. J. Biochem. Cell Biol.* **2014**, *52*, 15–25.

(2) Stephenson, A.; Beauchamp, N. *The Canadian Cystic Fibrosis Registry: 2013 Annual Report*; 2013.

(3) Andersen, D. H. *Am. J. Dis. Child.* **1938**, *56* (2), 344.

(4) Rommens, J.; Iannuzzi, M.; Kerem, B.; Drumm, M.; Melmer, G.; Dean, M.; Rozmahel, R.; Cole, J.; Kennedy, D.; Hidaka, N.; Et, A. *Science (80-.).* **1989**, *245* (4922), 1059–1065.

(5) Rowe, S. M.; Miller, S.; Sorscher, E. J. *N. Engl. J. Med.* **2005**, *352* (19), 1992–2001.

(6) Riordan; Rommens, J.; Kerem, B.; Alon, N.; Rozmahel, R.; Grzelczak, Z.; Zielenski, J.; Lok, S.; Plavsic, N.; Chou, J.; Et, A. *Science (80-.).* **1989**, *245* (4922), 1066–1073.

(7) *Worldwide survey of the delta F508 mutation;* Report from the cystic fibrosis genetic analysis consortium; American Journal of Human Genetics, **1990**, *47* (2), 354-359.

(8) *The molecular genetic epidemiology of cystic fibrosis*; Report of a joint meeting of WHO/ECFTN/ICF(M)A/ECFS; World Health Organization: Genoa, Italy, June 2004.

(9) Ratjen, F.; Döring, G. *Lancet* **2003**, *361* (9358), 681–689.

(10) Smith, S. S.; Steinle, E. D.; Meyerhoff, M. E.; Dawson, D. C. *J. Gen. Physiol.* **1999**, *114* (4), 799–818.

(11) Flume, P. A.; Van Devanter, D. R. *BMC Med.* **2012**, *10* (1), 88.

(12) Griesenbach, U.; Alton, E. W. F. W. *F1000Prime Rep.* **2015**, *7*, 64.

(13) Sloane, P. A.; Shastry, S.; Wilhelm, A.; Courville, C.; Tang, L. P.; Backer, K.; Levin, E.; Raju, S. V.; Li, Y.; Mazur, M.; Byan-Parker, S.; Grizzle, W.; Sorscher, E. J.; Dransfield, M. T.; Rowe, S. M. *PLoS One* **2012**, *7* (6), e39809.

(14) Solomon, G. M.; Hathorne, H.; Liu, B.; Raju, S. V.; Reeves, G.; Acosta, E. P.; Dransfield, M. T.; Rowe, S. M. *Lancet Respir. Med.* **2016**, *4* (6), e32–e33.

(15) Corvol, H.; Blackman, S. M.; Boëlle, P.-Y.; Gallins, P. J.; Pace, R. G.; Stonebraker, J. R.; Accurso, F. J.; Clement, A.; Collaco, J. M.; Dang, H.; Dang, A. T.; Franca, A.; Gong, J.; Guillot, L.; Keenan, K.; Li, W.; Lin, F.; Patrone, M. V; Raraigh, K. S.; Sun, L.; Zhou, Y.-H.; O'Neal, W. K.; Sontag, M. K.; Levy, H.; Durie, P. R.; Rommens, J. M.; Drumm, M. L.; Wright, F. A.; Strug, L. J.; Cutting, G. R.; Knowles, M. R. *Nat. Commun.* **2015**, *6*, 8382.

(16) Cutting, G. R. *Nat. Rev. Genet.* **2014**, *16* (1), 45–56.

(17) De Boeck, K.; Zolin, A. *J. Cyst. Fibros.* **2016**, 1–7.

(18) Michl, R. K.; Tabori, H.; Hentschel, J.; Beck, J. F.; Mainz, J. G. *Expert Rev. Respir. Med.* **2016**, *10* (11), 1177–1186.

(19) Withrock, I. C.; Anderson, S. J.; Jefferson, M. A.; McCormack, G. R.; Mlynarczyk, G. S. A.; Nakama, A.; Lange, J. K.; Berg, C. A.; Acharya, S.; Stock, M. L.; Lind, M. S.; Luna, K. C.; Kondru, N. C.; Manne, S.; Patel, B. B.; de la Rosa, B. M.; Huang, K.-P.; Sharma, S.; Hu, H. Z.; Kanuri, S. H.; Carlson, S. A. *Genes Dis.* **2015**, *2* (3), 247–254.

(20) Mak, D. Y. F.; Sykes, J.; Stephenson, A. L.; Lands, L. C. *J. Cyst. Fibros.* **2016**, *15* (3), 302–308.

(21) Ellemunter, H.; Eder, J.; Fuchs, S.; Gappa, M.; Steinkamp, G. *J. Cyst. Fibros.* **2016**, *15* (1), 123–126.

(22) Clancy, J. P.; Jain, M. *Am. J. Respir. Crit. Care Med.* **2012**, *186* (7), 593–597.

(23) Odolczyk, N.; Zielenkiewicz, P. *Int. J. Biochem. Cell Biol.* **2014**, *52*, 39–46.

(24) Boucher, R. C. *Annu. Rev. Med.* **2007**, *58* (1), 157–170.

(25) Pezzulo, A. A.; Tang, X. X.; Hoegger, M. J.; Abou Alaiwa, M. H.; Ramachandran, S.; Moninger, T. O.; Karp, P. H.; Wohlford-Lenane, C. L.; Haagsman, H. P.; van Eijk, M.; Bánfi, B.; Horswill, A. R.; Stoltz, D. A.; McCray, P. B.; Welsh, M. J.; Zabner, J. *Nature* **2012**, *487*, 109–113.

(26) Moran, A.; Becker, D.; Casella, S. J.; Gottlieb, P. A.; Kirkman, M. S.; Marshall, B. C.; Slovis, B. *Diabetes Care* **2010**, *33* (12), 2677–2683.

(27) Moran, A.; Becker, D.; Casella, S. J.; Gottlieb, P. A.; Kirkman, M. S.; Marshall, B. C.; Slovis, B.; Alexander, P.; Beall, R. J.; Brunzell, C.; Campbell, P. W.; Chin, M.; Cohen, R. C.; Brooks, J. F.; George, C.; Hazle, L.; Katz, M.; McKeon, C.; Onady, G.; Robinson, K. A.; Rodgers, T.; Sabadosa, K. A.; Schindler, T.; Stecenko, A.; Wood, M. E.; Young, D. *Diabetes Care* **2010**, *33* (12), 2677–2683.

(28) Koch, C.; Rainisio, M.; Madessani, U.; Harms, H. K.; Hodson, M. E.; Mastella, G.; McKenzie, S. G.; Navarro, J.; Strandvik, B. *Pediatr. Pulmonol.* **2001**, *32* (5), 343–350.

(29) Quinton, P. M. *Physiology* **2007**, *22* (3), 212–225.

(30) Sokol, R. Z. *Curr. Opin. Pulm. Med.* **2001**, *7* (6), 421–426.

(31) Ahmad, A.; Ahmed, A.; Patrizio, P. *Curr. Opin. Obstet. Gynecol.* **2013**, *25* (3), 167–172.

(32) Jones, G. H.; Walshaw, M. J. *Paediatr. Respir. Rev.* **2015**, *16*, 25–27.

(33) Vasiliou, V.; Vasiliou, K.; Nebert, D. W. *Hum. Genomics* **2009**, *3* (3), 281–290.

(34) Hwang, T.-C.; Sheppard, D. N. *J. Physiol.* **2009**, *587*, 2151–2161.

(35) Wilkens, S. *F1000Prime Rep.* **2015**, *7* (4), 426–431.

(36) Moran, O. *Int. J. Biochem. Cell Biol.* **2014**, *52*, 7–14.

(37) Pranke, I. M.; Sermet-Gaudelus, I. *Int. J. Biochem. Cell Biol.* **2014**, *52* (0), 26–38.

(38) Wilkinson, D. J.; Strong, T. V; Mansoura, M. K.; Wood, D. L.; Smith, S. S.; Collins, F. S.; Dawson, D. C. *Am. J. Physiol.* **1997**, *273* (1), L127-33.

(39) Pyle, L. C.; Ehrhardt, A.; Mitchell, L. H.; Fan, L.; Ren, A.; Naren, A. P.; Li, Y.; Clancy, J. P.; Bolger, G. B.; Sorscher, E. J.; Rowe, S. M. *AJP Lung Cell. Mol. Physiol.* **2011**, *301* (4), L587–L597.

(40) Chiaw, P.; Eckford, P. D. W.; Bear, C. E. *Essays Biochem.* **2011**, *50*, 233–248.

(41) Lewis, H. A.; Wang, C.; Zhao, X.; Hamuro, Y.; Conners, K.; Kearins, M. C.; Lu, F.; Sauder, J. M.; Molnar, K. S.; Coales, S. J.; Maloney, P. C.; Guggino, W. B.; Wetmore, D. R.; Weber, P. C.; Hunt, J. F. *J. Mol. Biol.* **2010**, *396* (2), 406–430.

(42) Lewis, H. a; Buchanan, S. G.; Burley, S. K.; Conners, K.; Dickey, M.; Dorwart, M.; Fowler, R.; Gao, X.; Guggino, W. B.; Hendrickson, W. a; Hunt, J. F.; Kearins, M. C.; Lorimer, D.; Maloney, P. C.; Post, K. W.; Rajashankar, K. R.; Rutter, M. E.; Sauder, J. M.; Shriver, S.; Thibodeau, P. H.; Thomas, P. J.; Zhang, M.; Zhao, X.; Emtage, S. *EMBO J.* **2004**, *23* (2), 282–293.

(43) Huang, S.-Y.; Bolser, D.; Liu, H.-Y.; Hwang, T.-C.; Zou, X. *J. Mol. Graph. Model.* **2009**, *27* (7), 822–828.

(44) Rosenberg, M. F.; Kamis, A. B.; Aleksandrov, L. a; Ford, R. C.; Riordan, J. R. *J. Biol. Chem.* **2004**, *279* (37), 39051–39057.

(45) Rosenberg, M. F.; O'Ryan, L. P.; Hughes, G.; Zhao, Z.; Aleksandrov, L. A.; Riordan, J. R.; Ford, R. C. *J. Biol. Chem.* **2011**, *286* (49), 42647–42654.

(46) Mornon, J. P.; Lehn, P.; Callebaut, I. *Cell. Mol. Life Sci.* **2009**, *66* (21), 3469–3486.

(47) Mornon, J.-P.; Hoffmann, B.; Jonic, S.; Lehn, P.; Callebaut, I. *Cell. Mol. Life Sci.* **2015**, *72* (7), 1377–1403.

(48) Corradi, V.; Vergani, P.; Tieleman, D. P. *J. Biol. Chem.* **2015**.

(49) Collaco, J. M.; Blackman, S. M.; Raraigh, K. S.; Morrow, C. B.; Cutting, G. R.; Paranjape, S. M. *BMC Pulm. Med.* **2014**, *14* (1), 159.

(50) Hunt, J. F.; Wang, C.; Ford, R. C. *Cold Spring Harb. Perspect. Med.* **2013**, *3* (2), a009514–a009514.

(51) Rahman, K. S.; Cui, G.; Harvey, S. C.; McCarty, N. a. *PLoS One* **2013**, *8* (9), e74574.

(52) Molinski, S. V. Functional Analysis of an α-helical region in the human multidrug and organic anion transporter MRP1, Ph.D. Thesis, Queen's University, 2010.

(53) Dawson, R. J. P.; Locher, K. P. *Nature* **2006**, *443* (7108), 180–185.

(54) Odolczyk, N.; Fritsch, J.; Norez, C.; Servel, N.; Da Cunha, M. F.; Bitam, S.; Kupniewska, A.; Wiszniewski, L.; Colas, J.; Tarnowski, K.; Tondelier, D.; Roldan, A.; Saussereau, E. L.; Melin-Heschel, P.; Wieczorek, G.; Lukacs, G. L.; Dadlez, M.; Faure, G.; Herrmann, H.; Ollero, M.; Becq, F.; Zielenkiewicz, P.; Edelman, A. *EMBO Mol. Med.* **2013**, *5* (10), 1484–

1501.

(55) Kalid, O.; Mense, M.; Fischman, S.; Shitrit, A.; Bihler, H.; Ben-Zeev, E.; Schutz, N.; Pedemonte, N.; Thomas, P. J.; Bridges, R. J.; Wetmore, D. R.; Marantz, Y.; Senderowitz, H. *J. Comput. Aided. Mol. Des.* **2010**, *24* (12), 971–991.

(56) Zheng, X.; Gan, L.; Wang, E.; Wang, J. *AAPS J.* **2013**, *15* (1), 228–241.

(57) Lahti, J. L.; Tang, G. W.; Capriotti, E.; Liu, T.; Altman, R. B. *J. R. Soc. Interface* **2012**, *9* (72), 1409–1437.

(58) Wang, Y.; Wrennall, J. A.; Cai, Z.; Li, H.; Sheppard, D. N. *Int. J. Biochem. Cell Biol.* **2014**, *52*, 47–57.

(59) Linsdell, P. *Biochim. Biophys. Acta - Biomembr.* **2016**, *1858* (4), 740–747.

(60) Furukawa-Hagiya, T.; Furuta, T.; Chiba, S.; Sohma, Y.; Sakurai, M. *J. Phys. Chem. B* **2013**, *117* (1), 83–93.

(61) Carlson, M. L.; Bao, H.; Duong, F. *J. Biol. Chem.* **2016**, *291* (23), 12119–12125.

(62) Higgins, C. F.; Linton, K. J. *Nat. Struct. Mol. Biol.* **2004**, *11* (10), 918–926.

(63) Jih, K.-Y.; Hwang, T.-C. *Physiology* **2012**, *27* (6), 351–361.

(64) Verkman, A. S.; Jayaraman, S. In *Cystic Fibrosis Methods and Protocols*; Methods in Molecular Medicine; Humana Press: New Jersey, 2002; Vol. 70, pp 187–196.

(65) Jih, K.-Y.; Hwang, T.-C. *Proc. Natl. Acad. Sci. U. S. A.* **2013**, *110* (11), 4404–4409.

(66) Mihályi, C.; Töröcsik, B.; Csanády, L. *Elife* **2016**, *5*, 1–12.

(67) Molinski, S.; Eckford, P. D. W.; Pasyk, S.; Ahmadi, S.; Chin, S.; Bear, C. E. *Front. Pharmacol.* **2012**, *3*, 160.

(68) Rogan, M. P.; Stoltz, D. A.; Hornick, D. B. *Chest* **2011**, *139* (6), 1480–1490.

(69) Kopito, R. R. *Physiol. Rev.* **1999**, *79* (1), S167-173.

(70) Hadida, S.; Van Goor, F.; Zhou, J.; Arumugam, V.; McCartney, J.; Hazlewood, A.; Decker, C.; Negulescu, P.; Grootenhuis, P. D. J. *J. Med. Chem.* **2014**, *57* (23), 9776–9795.

(71) Van Goor, F.; Hadida, S.; Grootenhuis, P. D. J.; Burton, B.; Stack, J. H.; Straley, K. S.; Decker, C. J.; Miller, M.; McCartney, J.; Olson, E. R.; Wine, J. J.; Frizzell, R. a; Ashlock, M.; Negulescu, P. a. *Proc. Natl. Acad. Sci. U. S. A.* **2011**, *108* (46), 18843–18848.

(72) Pranke, I. M.; Sermet-Gaudelus, I. *Int. J. Biochem. Cell Biol.* **2014**, *52* (0), 26–38.

(73) Clinical and functional translation of CFTR: List of CFTR2 mutations http://www.cftr2.org/files/CFTR2_13August2015.pdf (accessed Nov 1, 2016).

(74) Sosnay, P. R.; Siklosi, K. R.; Van Goor, F.; Kaniecki, K.; Yu, H.; Sharma, N.; Ramalho, A. S.; Amaral, M. D.; Dorfman, R.; Zielenski, J.; Masica, D. L.; Karchin, R.; Millen, L.; Thomas, P. J.; Patrinos, G. P.; Corey, M.; Lewis, M. H.; Rommens, J. M.; Castellani, C.;

Penland, C. M.; Cutting, G. R. *Nat. Genet.* **2013**, *45* (10), 1160–1167.

(75) Fanen, P.; Wohlhuter-Haddad, A.; Hinzpeter, A. *Int. J. Biochem. Cell Biol.* **2014**, *52*, 94–102.

(76) Fanen, P.; Wohlhuter-Haddad, A.; Hinzpeter, A. *Int. J. Biochem. Cell Biol.* **2014**, *52*, 94–102.

(77) Bobadilla, J. L.; Macek, M.; Fine, J. P.; Farrell, P. M. *Hum. Mutat.* **2002**, *19* (6), 575–606.

(78) Derichs, N. *Eur. Respir. Rev.* **2013**, *22* (127), 58–65.

(79) Bosch, B.; de Boeck, K. *Eur. J. Pediatr.* **2015**, 1–8.

(80) Jih, K.-Y.; Hwang, T.-C. *Physiology* **2012**, *27* (6), 351–361.

(81) Eckford, P. D. W.; Li, C.; Ramjeesingh, M.; Bear, C. E. *J. Biol. Chem.* **2012**, *287* (44), 36639–36649.

(82) Brodlie, M.; Haq, I. J.; Roberts, K.; Elborn, J. S. *Genome Med.* **2015**, *7* (1), 101.

(83) Char, J. E.; Wolfe, M. H.; Cho, H.-J.; Park, I.-H.; Jeong, J. H.; Frisbee, E.; Dunn, C.; Davies, Z.; Milla, C.; Moss, R. B.; Thomas, E. a C.; Wine, J. J. *PLoS One* **2014**, *9* (2), e88564.

(84) MacDonald, K. D.; McKenzie, K. R.; Zeitlin, P. L. *Pediatr. Drugs* **2007**, *9* (1), 1–10.

(85) Quon, B. S.; Rowe, S. M. *BMJ* **2016**, *352*, i859.

(86) Pasyk, S.; Molinski, S.; Yu, W.; Eckford, P. D. W.; Bear, C. E. *Curr. Pharm. Des.* **2012**, *18* (5), 628–641.

(87) Pedemonte, N.; Lukacs, G. L.; Du, K.; Caci, E.; Zegarra-moran, O.; Galietta, L. J. V; Verkman, A. S. *J. Clin. Invest.* **2005**, *115* (9), 2564–2571.

(88) Hall, J. D.; Wang, H.; Byrnes, L. J.; Shanker, S.; Wang, K.; Efremov, I. V.; Chong, P. A.; Forman-Kay, J. D.; Aulabaugh, A. E. *Protein Sci.* **2016**, *25* (2), 360–373.

(89) Ren, H. Y.; Grove, D. E.; De La Rosa, O.; Houck, S. a; Sopha, P.; Van Goor, F.; Hoffman, B. J.; Cyr, D. M. *Mol. Biol. Cell* **2013**, *24* (19), 3016–3024.

(90) Loring, H. S.; ElMallah, M. K.; Flotte, T. R. *Hum. Gene Ther. Methods* **2016**, *27* (2), 49–58.

(91) Griesenbach, U.; W.F.W. Alton, E. *Curr. Pharm. Des.* **2012**, *18* (5), 642–662.

(92) Alton, E. W. F. W.; Armstrong, D. K.; Ashby, D.; Bayfield, K. J.; Bilton, D.; Bloomfield, E. V.; Boyd, A. C.; Brand, J.; Buchan, R.; Calcedo, R.; Carvelli, P.; Chan, M.; Cheng, S. H.; Collie, D. D. S.; Cunningham, S.; Davidson, H. E.; Davies, G.; Davies, J. C.; Davies, L. A.; Dewar, M. H.; Doherty, A.; Donovan, J.; Dwyer, N. S.; Elgmati, H. I.; Featherstone, R. F.; Gavino, J.; Gea-Sorli, S.; Geddes, D. M.; Gibson, J. S. R.; Gill, D. R.; Greening, A. P.; Griesenbach, U.; Hansell, D. M.; Harman, K.; Higgins, T. E.; Hodges, S. L.; Hyde, S. C.; Hyndman, L.; Innes, J. A.; Jacob, J.; Jones, N.; Keogh, B. F.; Limberis, M. P.; Lloyd-Evans, P.; Maclean, A. W.; Manvell, M. C.; McCormick, D.; McGovern, M.; McLachlan,

G.; Meng, C.; Montero, M. A.; Milligan, H.; Moyce, L. J.; Murray, G. D.; Nicholson, A. G.; Osadolor, T.; Parra-Leiton, J.; Porteous, D. J.; Pringle, I. A.; Punch, E. K.; Pytel, K. M.; Quittner, A. L.; Rivellini, G.; Saunders, C. J.; Scheule, R. K.; Sheard, S.; Simmonds, N. J.; Smith, K.; Smith, S. N.; Soussi, N.; Soussi, S.; Spearing, E. J.; Stevenson, B. J.; Sumner-Jones, S. G.; Turkkila, M.; Ureta, R. P.; Waller, M. D.; Wasowicz, M. Y.; Wilson, J. M.; Wolstenholme-Hogg, P. *Lancet Respir. Med.* **2015**, *3* (9), 684–691.

(93) Prickett, M.; Jain, M. *Transl. Res.* **2013**, *161* (4), 255–264.

(94) Murphy, M. P.; Caraher, E. *Drugs R. D.* **2016**, *16* (1), 1–17.

(95) Pellagatti, A.; Dolatshad, H.; Yip, B. H.; Valletta, S.; Boultwood, J. *Adv. Biol. Regul.* **2016**, *60*, 122–134.

(96) Schwank, G.; Koo, B. K.; Sasselli, V.; Dekkers, J. F.; Heo, I.; Demircan, T.; Sasaki, N.; Boymans, S.; Cuppen, E.; Van Der Ent, C. K.; Nieuwenhuis, E. E. S.; Beekman, J. M.; Clevers, H. *Cell Stem Cell* **2013**, *13* (6), 653–658.

(97) Patel, S.; Sinha, I. P.; Dwan, K.; Echevarria, C.; Schechter, M.; Southern, K. W. In *Cochrane Database of Systematic Reviews*; Southern, K. W., Ed.; John Wiley & Sons, Ltd: Chichester, UK, 2015.

(98) Solomon, G. M.; Marshall, S. G.; Ramsey, B. W.; Rowe, S. M. *Pediatr. Pulmonol.* **2015**, *50* (S40), S3–S13.

(99) Becq, F.; Mall, M. a; Sheppard, D. N.; Conese, M.; Zegarra-Moran, O. *J. Cyst. Fibros.* **2011**, *10 Suppl 2*, S129-45.

(100) Flores, A. M.; Casey, S. D.; Felix, C. M.; Phuan, P. W.; Verkman, A. S.; Levin, M. H. *FASEB J.* **2016**, *30* (5), 1789–1797.

(101) Esposito, S.; Tosco, A.; Villella, V. R.; Raia, V.; Kroemer, G.; Maiuri, L. *Mol. Cell. Pediatr.* **2016**, *3* (1), 13.

(102) Luciani, A.; Villella, V. R.; Esposito, S.; Gavina, M.; Russo, I.; Silano, M.; Guido, S.; Pettoello-Mantovani, M.; Carnuccio, R.; Scholte, B.; De Matteis, A.; Maiuri, M. C.; Raia, V.; Luini, A.; Kroemer, G.; Maiuri, L. *Autophagy* **2012**, *8* (11), 1657–1672.

(103) Melis, N.; Tauc, M.; Cougnon, M.; Bendahhou, S.; Giuliano, S.; Rubera, I.; Duranton, C. *Br. J. Pharmacol.* **2014**, *171* (15), 3716–3727.

(104) Phuan, P.-W.; Veit, G.; Tan, J.; Roldan, A.; Finkbeiner, W. E.; Lukacs, G. L.; Verkman, a S. *Mol. Pharmacol.* **2014**, *86* (1), 42–51.

(105) Rowe, S. M.; Accurso, F.; Clancy, J. P. *Proc. Am. Thorac. Soc.* **2007**, *4* (4), 387–398.

(106) Boyle, M. P.; Bell, S. C.; Konstan, M. W.; McColley, S. A.; Rowe, S. M.; Rietschel, E.; Huang, X.; Waltz, D.; Patel, N. R.; Rodman, D. *Lancet Respir. Med.* **2014**, *2* (7), 527–538.

(107) Cholon, D. M.; Quinney, N. L.; Fulcher, M. L.; Esther, C. R.; Das, J.; Dokholyan, N. V; Randell, S. H.; Boucher, R. C.; Gentzsch, M. *Sci. Transl. Med.* **2014**, *6*, 246ra96.

(108) Okiyoneda, T.; Veit, G.; Dekkers, J. F.; Bagdany, M.; Soya, N.; Xu, H.; Roldan, A.;

Verkman, A. S.; Kurth, M.; Simon, A.; Hegedus, T.; Beekman, J. M.; Lukacs, G. L. *Nat. Chem. Biol.* **2013**, *9* (7), 444–454.

(109) Bell, S. C.; De Boeck, K.; Amaral, M. D. *Pharmacol. Ther.* **2015**, *145*, 19–34.

(110) Veit, G.; Avramescu, R. G.; Perdomo, D.; Phuan, P.-W.; Bagdany, M.; Apaja, P. M.; Borot, F.; Szollosi, D.; Wu, Y.-S.; Finkbeiner, W. E.; Hegedus, T.; Verkman, A. S.; Lukacs, G. L. *Sci. Transl. Med.* **2014**, *6* (246), 246ra97-246ra97.

(111) Balfour-Lynn, I. M. *Paediatr. Respir. Rev.* **2014**, *15 Suppl 1*, 2–5.

(112) Robertson, S. M.; Luo, X.; Dubey, N.; Li, C.; Chavan, A. B.; Gilmartin, G. S.; Higgins, M.; Mahnke, L. *J. Clin. Pharmacol.* **2015**, *55* (1), 56–62.

(113) Stanojevic, S.; Ratjen, F. *J. Cyst. Fibros.* **2016**, 1–8.

(114) Lin, W.-Y.; Yu, Y.-C. *Ann. Transl. Med.* **2015**, *3* (6), 75.

(115) Van Goor, F.; Straley, K.; Cao, D.; Gonzalez, J.; Hadida, S.; Hazlewood, A.; Joubran, J.; Knapp, J.; Makings, L. R.; Miller, M.; Neuberger, T.; Olson, E.; Panchenko, V.; Rader, J.; Singh, A.; Stack, J. H.; Tung, R.; Grootenhuis, P. D. J.; Negulescu, P. *Am J Physiol Lung Cell Mol Physiol* **2006**, *290*, 1117–1130.

(116) Van Goor, F.; Hadida, S.; Grootenhuis, P. In *Topics in Medicinal Chemistry: Ion Channels*; 2008; pp 91–120.

(117) Van Goor, F.; Hadida, S.; Grootenhuis, P. D. J.; Burton, B.; Cao, D.; Neuberger, T.; Turnbull, A.; Singh, A.; Joubran, J.; Hazlewood, A.; Zhou, J.; McCartney, J.; Arumugam, V.; Decker, C.; Yang, J.; Young, C.; Olson, E. R.; Wine, J. J.; Frizzell, R.; Ashlock, M.; Negulescu, P. *Proc. Natl. Acad. Sci.* **2009**, *106* (44), 18825–18830.

(118) Binch, H.; Hurley, D.; Fanning, L. T. D.; Grootenhuis, P. D. J.; Botfield, M.; Van Goor, F. Modulators of cystic fibrosis transmembrane conductance regulator. US20100168094, 2010.

(119) Brewington, J. J.; McPhail, G. L.; Clancy, J. P. *Expert Rev. Respir. Med.* **2016**, *10* (1), 5–17.

(120) Kirby, E. F.; Heard, A. S.; Wang, X. R. *J. Pharmacol. Clin. Toxicol.* **2013**, *1* (1), 1007.

(121) Wainwright, C. E.; Elborn, J. S.; Ramsey, B. W.; Marigowda, G.; Huang, X.; Cipolli, M.; Colombo, C.; Davies, J. C.; De Boeck, K.; Flume, P. a; Konstan, M. W.; McColley, S. a; McCoy, K.; McKone, E. F.; Munck, A.; Ratjen, F.; Rowe, S. M.; Waltz, D.; Boyle, M. P. *N. Engl. J. Med.* **2015**, 1–12.

(122) Eckford, P. D. W.; Ramjeesingh, M.; Molinski, S.; Pasyk, S.; Dekkers, J. F.; Li, C.; Ahmadi, S.; Ip, W.; Chung, T. E.; Du, K.; Yeger, H.; Beekman, J.; Gonska, T.; Bear, C. E. *Chem. Biol.* **2014**, *21* (5), 666–678.

(123) He, L.; Kota, P.; Aleksandrov, A. A.; Cui, L.; Jensen, T.; Dokholyan, N. V.; Riordan, J. R. *FASEB J.* **2013**, *27* (2), 536–545.

(124) Loo, T. W.; Bartlett, M. C.; Clarke, D. M. *Biochem. Pharmacol.* **2013**, *86* (5), 612–619.

(125) Hanrahan, J. W.; Sampson, H. M.; Thomas, D. Y. *Trends Pharmacol. Sci.* **2013**, *34* (2), 119–125.

(126) Zhang, W.; Fujii, N.; Naren, A. P. *Future Med. Chem.* **2012**, *4* (3), 329–345.

(127) Schultz, B. D.; Singh, A. K.; Devor, D. C.; Bridges, R. J. *Physiol. Rev.* **1999**, *79* (1 Suppl), S109–S144.

(128) De Boeck, K.; Munck, A.; Walker, S.; Faro, A.; Hiatt, P.; Gilmartin, G.; Higgins, M. *J. Cyst. Fibros.* **2014**, *13* (6), 674–680.

(129) Kapoor, H.; Koolwal, A.; Singh, A. *J. Clin. Diagnostic Res.* **2014**, *8* (11), SE01-SE05.

(130) Kotha, K.; Clancy, J. P. *Ther. Adv. Respir. Dis.* **2013**, *7* (5), 288–296.

(131) Ramsey, B. W.; Davies, J.; McElvaney, N. G.; Tullis, E.; Bell, S. C.; Dřevínek, P.; Griese, M.; McKone, E. F.; Wainwright, C. E.; Konstan, M. W.; Moss, R.; Ratjen, F.; Sermet-Gaudelus, I.; Rowe, S. M.; Dong, Q.; Rodriguez, S.; Yen, K.; Ordoñez, C.; Elborn, J. S. *N. Engl. J. Med.* **2011**, *365* (18), 1663–1672.

(132) Pettit, R. S.; Fellner, C. *Pharm. Ther.* **2014**, *39* (7), 500–511.

(133) Clancy, J. P. *Sci. Transl. Med.* **2014**, *6*, 246fs27-246fs27.

(134) Liu, X.; Dawson, D. C. D. *Biochemistry* **2014**, *53* (35), 5613–5618.

(135) Pasyk, S.; Li, C.; Ramjeesingh, M.; Bear, C. E. *Biochem. J.* **2009**, *418* (1), 185–190.

(136) Csanády, L.; Töröcsik, B. *J. Gen. Physiol.* **2014**, *144* (4), 321–336.

(137) Smith, E.; Collins, I. *Future Med. Chem.* **2015**, *7* (2), 159–183.

(138) Lahti, J. L.; Tang, G. W.; Capriotti, E.; Liu, T.; Altman, R. B. *J. R. Soc. Interface* **2012**, *9* (72), 1409–1437.

(139) Mehmood, S.; Domene, C.; Forest, E.; Jault, J.-M. *Proc. Natl. Acad. Sci. U. S. A.* **2012**, *109* (27), 10832–10836.

(140) Wales, T. E.; Engen, J. R. *Mass Spectrom. Rev.* **2006**, *25* (1), 158–170.

(141) Pirrone, G. F.; Iacob, R. E.; Engen, J. R. *Anal. Chem.* **2015**, *87* (1), 99–118.

(142) Zheng, X.; Gan, L.; Wang, E.; Wang, J. *AAPS J.* **2013**, *15* (1), 228–241.

(143) Ziarek, J. J.; Peterson, F. C.; Lytle, B. L.; Volkman, B. F. *Methods Enzymol.* **2011**, *493*, 241–275.

(144) MacKinnon, A.; Taunton, J. *Curr. Protoc. Chem. Biol.* **2009**, *1* (415), 55–73.

(145) Hashimoto, M.; Hatanaka, Y. *European J. Org. Chem.* **2008**, *2008* (15), 2513–2523.

(146) Dubinsky, L.; Krom, B. P.; Meijler, M. M. *Bioorg. Med. Chem.* **2012**, *20* (2), 554–570.

(147) Blencowe, A.; Hayes, W. *Soft Matter* **2005**, *1*, 178–205.

(148) Brunner, J. *Annu. Rev. Biochem.* **1993**, *62*, 483–514.

(149) Mehmood, S.; Domene, C.; Forest, E.; Jault, J.-M. *Proc. Natl. Acad. Sci. U. S. A.* **2012**, *109* (27), 10832–10836.

(150) Ghosh, B.; Jones, L. H. *Med. Chem. Commun.* **2014**, *5* (3), 247–254.

(151) Brunner, J.; Richards, F. M. *J. Biol. Chem.* **1980**, *255* (8), 3313–3318.

(152) Hashimoto, M.; Kato, Y.; Hatanaka, Y. *Tetrahedron Lett.* **2006**, *47* (20), 3391–3394.

(153) Wang, L.; Murai, Y.; Yoshida, T.; Ishida, A.; Masuda, K.; Sakihama, Y.; Hashidoko, Y.; Hatanaka, Y.; Hashimoto, M. *Org. Lett.* **2015**, *17* (3), 616–619.

(154) Kelly, C. B.; Mercadante, M. A.; Leadbeater, N. E. *Chem. Commun.* **2013**, *49*, 11133–11148.

(155) Sevenard, D. V.; Vorobyev, M.; Sosnovskikh, V. Y.; Wessel, H.; Kazakova, O.; Vogel, V.; Shevchenko, N. E.; Nenajdenko, V. G.; Lork, E.; Röschenthaler, G. V. *Tetrahedron* **2009**, *65* (36), 7538–7552.

(156) Guiles, J. W. *Synlett* **1995**, *1995* (2), 165–166.

(157) Alkhouri, B.; Denning, R. a; Kim Chiaw, P.; Eckford, P. D. W.; Yu, W.; Li, C.; Bogojeski, J. J.; Bear, C. E.; Viirre, R. D. *J. Med. Chem.* **2011**, *54* (24), 8693–8701.

(158) Cheng, H.; Pei, Y.; Leng, F.; Li, J.; Liang, A.; Zou, D.; Wu, Y.; Wu, Y. *Tetrahedron Lett.* **2013**, *54* (33), 4483–4486.

(159) Kosemura, S.; Emori, H.; Yamamura, S.; Anai, T. *Tetrahedron Lett.* **1997**, *38* (12), 2125–2128.

(160) Ettinger, R. *J. Chem. Phys.* **1964**, *40* (6), 1693.

(161) Kumar, N. S.; Young, R. N. *Bioorg. Med. Chem.* **2009**, *17* (15), 5388–5395.

(162) Hatanaka, Y.; Hashimoto, M.; Kanaoka, Y. *J. Am. Chem. Soc.* **1998**, *120* (2), 453–454.

(163) DeMattei, J.; Looker, A.; Neubert-Langille, B.; Truedeau, M.; Roeper, S.; Ryan, M. P.; Dahrika, M.; Guerette, Y.; Krueger, B. R.; Grootenhuis, P. D. J.; Van Goor, F.; Botfield, M.; Zlokarnik, G. Process for making modulators of cystic fibrosis transmembrane conductance regulator. U.S. Patent 8,835,639 B2, September 16, 2014.

(164) Binch, H.; Hurley, D.; Fanning, L. T. D.; Grootenhuis, P. D. J.; Botfield, M.; Van Goor, F. Modulators of cystic fibrosis transmembrane conductance regulator. U.S. Patent 2010/0168094 A1. July 1, 2010.

(165) Ishimoto, K.; Fukuda, N.; Nagata, T.; Sawai, Y.; Ikemoto, T. *Org. Process Res. Dev.* **2014**, *18* (1), 122–134.

(166) Nagaki, A.; Kim, H.; Yoshida, J. *Angew. Chemie* **2009**, *121* (43), 8207–8209.

(167) Hashimoto, M.; Murai, Y.; Holman, G. D.; Hatanaka, Y. Selective Hydrogenation and Transfer Hydrogenation for Post-Functional Synthesis of Trifluoromethylphenyl Diazirine Derivatives for Photoaffinity Labelling. In *Hydrogenation*; Karamé, I., Eds.; InTech, 2012; pp 121–136.

(168) Hatanaka, Y.; Hashimoto, M.; Kurihara, H.; Nakayama, H.; Kanaoka, Y. *J. Org. Chem.* **1994**, *59* (2), 383–387.

(169) Hatanaka, Y.; Hashimoto, M.; Nakayama, H.; Kanaoka, Y. *Chem. Pharm. Bull. (Tokyo).* **1994**, *42* (4), 826–831.

(170) Grivas, J. C.; Taurins, A. *Can. J. Chem.* **1961**, *39* (3), 414–419.

(171) Grivas, J. C.; Taurins, A. *Can. J. Chem.* **1968**, *39* (1961), 2–5.

(172) Kopple, K. D.; Katz, J. J. *J. Org. Chem.* **1959**, *24* (12), 1975–1977.

(173) Takuwa, T.; Minowa, T.; Onishi, J. Y.; Mukaiyama, T. *Bull. Chem. Soc. Jpn.* **2004**, *77* (9), 1717–1725.

(174) Yamabe, S.; Tsuchida, N.; Yamazaki, S. *J. Org. Chem.* **2005**, *70* (26), 10638–10644.

(175) Tschirret-Guth, R. A.; Medzihradszky, K. F.; Ortiz de Montellano, P. R. *J. Am. Chem. Soc.* **1999**, *121* (20), 4731–4737.

(176) Kosemura, S.; Emori, H.; Yamamura, S. **1997**, *38* (12), 2125–2128.

(177) Routier, S.; Saugé, L.; Ayerbe, N.; Coudert, G.; Mérour, J. Y. *Tetrahedron Lett.* **2002**, *43* (4), 589–591.

(178) Moss, R. A. *Acc. Chem. Res.* **2006**, *39* (4), 267–272.

(179) Seixas, R.; Silva, A.; Cavaleiro, J. *Synlett* **2010**, No. 15, 2257–2262.

(180) Schneider, E. K.; Huang, J. X.; Carbone, V.; Baker, M.; Azad, M. A. K.; Cooper, M. A.; Li, J.; Velkov, T. *J. Mol. Recognit.* **2015**, *28* (6), 339–348.

(181) Gottlieb, H. E.; Kotlyar, V.; Nudelman, A. *J. Org. Chem.* **1997**, *62* (21), 7512–7515.

(182) Sheldrick, G. M. *Acta Crystallogr. Sect. A Found. Crystallogr.* **2015**, *71* (1), 3–8.

(183) Sheldrick, G. M. *Acta Crystallogr. Sect. C Struct. Chem.* **2015**, *71* (1), 3–8.

(184) Hübschle, C. B.; Sheldrick, G. M.; Dittrich, B. *J. Appl. Crystallogr.* **2011**, *44* (6), 1281–1284.

(185) Farrugia, L. J. *J. Appl. Crystallogr.* **2012**, *45* (4), 849–854.

(186) Fenn, T. D.; Ringe, D.; Petsko, G. A. *J. Appl. Crystallogr.* **2003**, *36* (3 II), 944–947.